QUANTUM MONTE CARLO STUDIES OF THE POPULATION IMBALANCED FERMI GAS

MARTA JOANNA WOLAK

NATIONAL UNIVERSITY OF SINGAPORE

2012

Quantum Monte Carlo studies of the population imbalanced Fermi Gas.

MARTA JOANNA WOLAK

(MSc, Cardinal Stefan Wyszyński University, Warsaw)

A THESIS SUBMITTED

FOR THE DEGREE OF DOCTOR OF PHILOSOPHY

CENTRE FOR QUANTUM TECHNOLOGIES

NATIONAL UNIVERSITY OF SINGAPORE

2012

DECLARATION

I hereby declare that the thesis is my original work and it has been written by me in its entirety. I have duly acknowledged all the sources of information which have been used in the thesis.

This thesis has also not been submitted for any degree in any university previously.

Marta Wolak

3 August 2012

人皆知有用之用
而莫知无用之用也

庄子

Everybody knows the use of
the useful, but nobody knows
the use of the useless.

Zhuangzi

Acknowledgements

First and foremost I would like to thank my supervisor Berthold-Georg Englert for welcoming me in Singapore with great hospitality and for his continuous support during my studies. I wish to express my gratitude and appreciation to my advisor George Batrouni for the invaluable scientific supervision and a great dose of optimism about this project. I thank Benoit Grémaud for crucial guidance while I was in Singapore. For creating the multiple possibilities for me to work in INLN I thank Christian Miniatura. I wish to express my appreciation to Frederic Hébert for being ready to answer my questions anytime. For welcoming me in Davis and many useful scientific exchanges I am grateful to Richard Scalettar. I wish to thank also Prof. K. Rzążewski, who first mentioned Singapore to me, for pointing me in this great direction.

On the more personal side, I wish to thank all the friends that I found during my studies, for making it a great experience. Andrej - thank you for endless kopi and conversations that made me stay in Singapore and for immense amount of fun and psychological support throughout the years. Nicole, meeting you gave a whole new dimension to the years in Singapore. Thank you for your patience as my chinese teacher and for all the great moments as a friend. Lynette and Marc - thanks for providing the essential nutritional balance by feeding me extremely well and that I could always count on you.

Thanks to all friends from CQT for sticking it out together. Han Rui, thank you for taking great care of me when I first arrived and for introducing me to Rou Jia Mo. Assad it was an honour to share an office with the most positive person I have ever met and to climb with the best climber in Singapore! Julien merci pour une collocation créative, amusante, inspirante et subtile.

Merci a tous les amis de l'INLN de m'avoir acqueilli toujours avec amitié et pour les plus belles moments que on a passé á Mercantour. Florence, merci pour ta énorme motivation à m'apprendre le français et pour ton sense de l'humor inimitable et indispensable. Merci Margherita pour ta joyeuse compagnie et de m'avoir dépanné millier de fois. Merci Fred et la famiglia Vignolo-Gattobigio de m'avoir hébergé pendant la grand finale de cette these.

Hani dziękuję za szczególnie wspierającą przyjaźń długodystansową.

Ponad wszystko dziękuję rodzicom i siostrze za niezawodne wsparcie, niezwykłą ilość zachęty, pigwówki i zaangażowania w tą egzotyczna przygodę.

Contents

Acknowledgements **i**

Contents **iii**

Summary **vii**

List of Publications **ix**

List of Figures **x**

1 Introduction **1**

1.1 Pairing of Fermions 1

1.2 FFLO phase and Breached Pairing 4

1.3 Experiments 9

1.4 Thesis structure 13

2 Methods **15**

2.1 Introduction 15

2.2 Hubbard model 16

2.3 Determinant Quantum Monte Carlo algorithm 19

2.3.1 Measurements 25

2.3.2 Implementation of DQMC 29

2.4 Stochastic Green function and canonical Worm algorithms . . 30

2.4.1 World-line representation 30
2.4.2 Stochastic Green Function 35
2.4.3 Canonical Worm algorithm 40
2.5 Canonical vs Grand Canonical 43
2.6 Summary 45

I One dimensional system 47

3 Low temperature properties of the system in 1D 49
3.1 Introduction 49
3.2 System without the trap 53
3.2.1 Unpolarized mixture of Fermions 53
3.2.2 Polarized mixture of fermions 56
3.3 System in a harmonic trap 62
3.4 Summary 68

4 Finite temperature study of the system in 1D 69
4.1 Introduction 69
4.2 Uniform system 70
4.2.1 Phase diagram 72
4.3 Trapped system 83
4.4 Interaction strength 87
4.5 Summary 89

5 Mass imbalanced system in 1D 93
5.1 Introduction 93
5.2 Heavy Majority: $t_1 > t_2$ 95

5.3 Heavy Minority: $t_1 < t_2$ 111
5.4 Summary 113

II Two dimensional system 115

6 Introduction to population imbalanced systems in 2D 117
6.1 2D Hubbard model 121
6.2 Mean-field 125

7 Translationally invariant system in 2D 129
7.1 Phase Diagram 132
7.2 System around half filling 137
7.3 Summary 141

8 Harmonically confined system in 2D 143
8.1 Harmonic level basis 143
8.2 System at low filling 155
8.3 System around half filling: Mean-Field study 160
8.4 Summary 165

9 Conclusions and outlook 167

Bibliography 173

Summary

In this work Quantum Monte Carlo (QMC) techniques are used to provide an approximation-free investigation of the phases of the one- and two-dimensional attractive Hubbard Hamiltonian in the presence of population imbalance. This thesis can be naturally divided into two parts:

In the first part we present the results of the studies of the one dimensional system. First we look at the pairing in the system at low temperature. We show that the "Fulde-Ferrell-Larkin-Ovchinnikov" (FFLO) pairing is the mechanism governing the properties of the ground-state of the system. Furthermore the effects of finite temperature and mass imbalance are investigated.

The temperature at which the FFLO phase is destroyed by thermal fluctuations is determined as a function of the polarization. It is shown that the presence of a confining potential does not dramatically alter the FFLO regime, and that recent experiments on trapped atomic gases likely lie just within the stable temperature range.

Furthermore we study the case of mass imbalance between the populations. We present an exact Quantum Monte Carlo study of the effect of unequal masses on pair formation in Fermionic systems with population imbalance loaded into optical lattices. We have considered three forms of the attractive interaction and find in all cases that the system is unstable and collapses as the

mass difference increases and that the ground state becomes an inhomogeneous collapsed state. We also address the question of canonical *vs* grand canonical ensemble and its role, if any, in stabilizing certain phases.

In the second part, we investigate the population imbalanced gas in two dimensions. Pairing in a population imbalanced Fermi system in a two-dimensional optical lattice is studied using Determinant Quantum Monte Carlo (DQMC) simulations. The approximation-free numerical results show a wide range of stability of the FFLO phase. Contrary to claims of fragility with increased dimensionality we find that this phase is stable across wide range of values for the polarization, temperature and interaction strength. Both homogenous and harmonically trapped systems display pairing with finite center of mass momentum with clear signatures either in momentum space or real space, which could be observed in cold atomic gases loaded in an optical lattice. We also use the harmonic level basis in the confined system and find that pairs can form between particles occupying different levels which can be seen as the analog of the finite center of mass momentum pairing in the translationally invariant case. Finally, we perform mean field calculations for the uniform and confined systems and show the results to be in good agreement with QMC. The mean field calculations allow us to study a 2D system at half filling and provide a simple picture of the pairing mechanism with oscillating order parameter.

List of Publications

- G. G. Batrouni, M. J. Wolak, F. Hébert, V. G. Rousseau, *Pair formation and collapse in imbalanced Fermion populations with unequal masses*, Europhysics Letters **8**6, 47006 (2009).

- M.J. Wolak, V.G. Rousseau, C. Miniatura, B. Grémaud, R.T. Scalettar and G.G. Batrouni, *Finite temperature QMC study of the one-dimensional polarized Fermi gas*, Physical Review **A82**, 013614 (2010).

- M.J. Wolak, V. G. Rousseau, and G.G. Batrouni, *Pairing in population imbalanced Fermion systems*, Computer Physics Communications 182, 2021(2011).

- M.J. Wolak,, B. Grémaud, R. T. Scalettar, and G. G. Batrouni *Pairing in a two-dimensional Fermi gas with population imbalance.* Accepted for publication in PRA (2012) and available at http://arxiv.org/abs/1206.5050

List of Figures

1.1 BCS and FFLO pairing schematic 4

1.2 Breached pairing schematic 6

2.1 Checkerboard representation of the world-lines 32

2.2 Partition function and extended partition function 36

2.3 Comparison of canonical and grand canonical ensembles 44

3.1 Momentum distributions for $U = 0$. 53

3.2 Momentum distributions for different U at $P = 0$. 55

3.3 Pair momentum distributions for different U at $P = 0$ 55

3.4 Pair Green function $G_{\text{pair}}(|i - j|)$ 57

3.5 Momentum distributions for different U at $P = 0.125$ 58

3.6 Finite size scaling in balanced populations 59

3.7 Pair momentum distributions for different P and $U = -9$ . . . 60

3.8 Kinetic energy 61

3.9 Pair momentum distribution for different P in a trap 64

3.10 Density profiles at low T and low P 65

3.11 Density profiles for different P 66

3.12 Local magnetization for different P. 66

3.13 Density profiles at low T and $P = 0.56$ 67

4.1 Pair momentum distribution of Cooper pairs as a function of T 70

4.2 Pair Green function of Cooper pairs as a function of T 71

4.3 Chemical potential versus density at finite T 73

4.4 Pair momentum distribution with increasing T 75

4.5 Pair Green function with increasing T 76

4.6 Double occupancy at finite T in 1D 77

4.7 Polarization *vs.* temperature phase diagram of a 1D system . . 79

4.8 Phase diagram of a 1D system from MF method 81

4.9 Density histograms for $L = 30$ and $L = 60$ 82

4.10 Density histograms for varying chemical potentials 82

4.11 Density profiles at low P and finite T. 84

4.12 Pair momentum distribution for $P = 0.05$ and finite T 85

4.13 Density profiles and pair momentum distribution for $P = 0.56$ 86

4.14 Experiment *vs.* simulations 88

4.15 Pair momentum distribution for different U at $P = 0.25$ 90

4.16 Pair momentum distribution and magnetization for different U 91

5.1 Momentum distributions with unequal masses 95

5.2 Pair momentum distribution with unequal masses 96

5.3 Density profiles for collapsed system 97

5.4 Quantifying collapse by δn vs $t_2/|U|$ 98

5.5 Momentum distributions with $V > 0$ 100

5.6 Pair momentum distribution with $V > 0$ 102

5.7 Density profiles with $V > 0$ 103

5.8 Delayed collapse due to $V > 0$ 103

5.9 Pair momentum distribution and density profiles with $V_{12} < 0$ 104

5.10 Momentum distributions with $V_{12} < 0$ 105

5.11 Momentum distributions with $V_{12} > 0$ 106

5.12 Pair momentum distribution with $V_{12} > 0$ 107

5.13 Density profiles with weak $V_{12} > 0$ 108

5.14 Density profiles with strong $V_{12} > 0$ 110

5.15 Delayed collapse due to $V_{12} > 0$ 111

5.16 Collapse and charge density wave with heavy minority 112

6.1 Fermi surface in 2D 118

7.1 Momentum distributions when $\rho_1 = \rho_2$ in 2D 130

7.2 Momentum distributions when $\rho_1 \neq \rho_2$ in 2D 131

7.3 Double occupancy at finite T in 2D 134

7.4 Polarization *vs.* temperature phase diagram of a 2D system . . 134

7.5 Pairing susceptibility 136

7.6 Pairing around half filling 138

7.7 Momentum distributions around half-filling (MF) 140

7.8 Momentum distributions around half-filling (QMC) 141

8.1 Green function in the harmonic level basis (HLB), $P = 0$ (QMC) 146

8.2 Pair Green function in the HLB, $\rho_1 = \rho_2$ (QMC) 147

8.3 Green functions in the HLB when $\rho_1 = \rho_2$ (MF) 148

8.4 Green functions in the HLB when $P = 0.11$ (QMC) 150

8.5 Green functions in the HLB when $P = 0.22$ (QMC) 151

8.6 Green functions in the HLB when $P = 0.37$ (QMC) 153

8.7 Green functions in the HLB when $P = 0.27$ (MF) 154

8.8 Momentum distributions for $\rho_1 = \rho_2$ in a trap in 2D 156

8.9 Momentum distributions for $\rho_1 \neq \rho_2$ in a trap in 2D 157

8.10 Density profiles and local magnetization in a trap in 2D 159

8.11 Local magnetization in a trap in 2D using MF and QMC . . . 160

8.12 Mean field parameter for $P = 0.13$ 161

8.13 Mean field parameter for $P = 0.43$ 162

8.14 Mean field parameter for $P = 0.48$ 163

8.15 Mean field parameter for $P = 0.66$ 164

Chapter 1

Introduction

1.1 Pairing of Fermions

The discovery of electric conduction without resistance by Heike Kamerlingh Onnes in 1911 marked the beginning of an exciting era in Physics. The progress made in low temperature physics opened the door to discoveries of many new phenomena some of the most interesting of which are those involving the interplay between quantum mechanics and statistical physics (systems with many particles). Since then, remarkable progress has been made in the microscopic understanding of the fascinating subject of superconductivity which can be thought of as charged superfluidity. The discovery of the superfluid transition in bosonic ^{4}He at 2.17K and the connection between superfluidity and Bose-Einstein Condensation suggested by London inspired ideas linking superconductivity and fermions forming bosonic pairs. Building on many theoretical developments, John Bardeen, Leon Neil Cooper and John Robert Schrieffer [1] proposed a microscopic theory which successfully explained superconductivity as being due to the formation of Cooper pairs [2] coupled by attractive

interaction stemming from lattice vibrations. Cooper pairs form between two fermions with opposite spin and equal but opposite momenta. The pairing occurs in momentum space (as opposed to real space pairing of strongly bound molecules) and the pair has zero center-of-mass momentum, zero angular momentum (s-wave pairing) and zero total spin (singlet state). The proposed BCS state is a wavefunction of overlapping pairs of fermions which are correlated and thus lead to a superconducting order parameter. The theory gained wide acclaim as it agreed quantitatively with a body of experimental results available at that time, and in 1972 the authors were awarded a Nobel prize in Physics. The same year at temperature three orders of magnitude smaller than ^{4}He the superfluidity of the fermionic ^{3}He was observed. This provided a strong hint that this transition is due to the bosonic character of the participating pairs of fermions. Since then pair formation between fermions has been a very active, fruitful and often very surprising field of research in condensed matter systems. Apart from its realization in the superconducting state it appears in various contexts such as for example the interior of neutron stars [3] or exciton formation in quantum well structures [4].

The question of pairing in polarized superconducting systems, that is, when the populations of the two spin states are imbalanced, came to the fore soon after the development of the BCS theory. Initially the question was motivated by the interest in the nature of superconductivity in the presence of a magnetic field, which can induce spin polarization. The magnetic field then would couple to the electronic magnetic moment and induce a difference in the spin populations by creating a disparity between the chemical potentials. As is well known, superconductivity is destroyed at a critical magnetic field. The reason for that is a strong coupling of the field to the orbital degrees of freedom

rather than to the spin, in which we are interested. The metal goes back to a normal state as the superconducting state is not energetically favorable in the presence of the supercurrents induced by the magnetic field. The manner in which the superconducting materials go through this transition marks the difference between type I superconductors and type II superconductors [5]. In the superconductors of type I with increased magnetic field the system goes directly to a normal state through a first order phase transition. In the case of type II superconductors, from the Meissner state at low magnetic field, the system transitions first to a mixed state where the magnetic field flux can partially penetrate the sample and vortices are present. Then, when the magnetic field is increased further, the superconductivity is destroyed and the system goes to a normal state. In this case both these transitions are of continuous type (second-order). It has been shown that in quasi two-dimensional systems the appearance of the supercurrents can be avoided and thus the critical fields become much higher. The geometry of a stack of conducting planes with very small tunnelling between the planes is realized in some high-T_C cuprate superconductors. The investigations into the physics of this system have obviously high practical interest.

Apart from superconductors, other instances of systems where such a mechanism can appear have become of interest recently. In the astrophysical community, it is believed that at extreme conditions of pressure, for example, in the interior of supermassive stars, quark matter forms and pairing between the quarks could lead to color superconductivity, which means formation of pairs between quarks of different colors [6]. Another situation of major current experimental interest is in systems of confined ultra-cold fermionic atoms such as ^{6}Li or ^{40}K.

1.2 FFLO phase and Breached Pairing

Fulde and Ferrel in 1964 [7] and independently Larkin and Ovchinnikov in 1965 [8] proposed similar but not identical pairing mechanisms where in the system with spin population imbalance the fermions would form pairs with finite center-of-mass momentum. In the balanced case the Cooper pairs form between fermions with momenta, for example k_{F1} and $-k_{F2}$, but in that case $k_{F1} = k_{F2}$ and the center-of mass momentum of the pair is zero. This is illustrated in Fig. 1.1 (left panel). When the populations of the two fermion

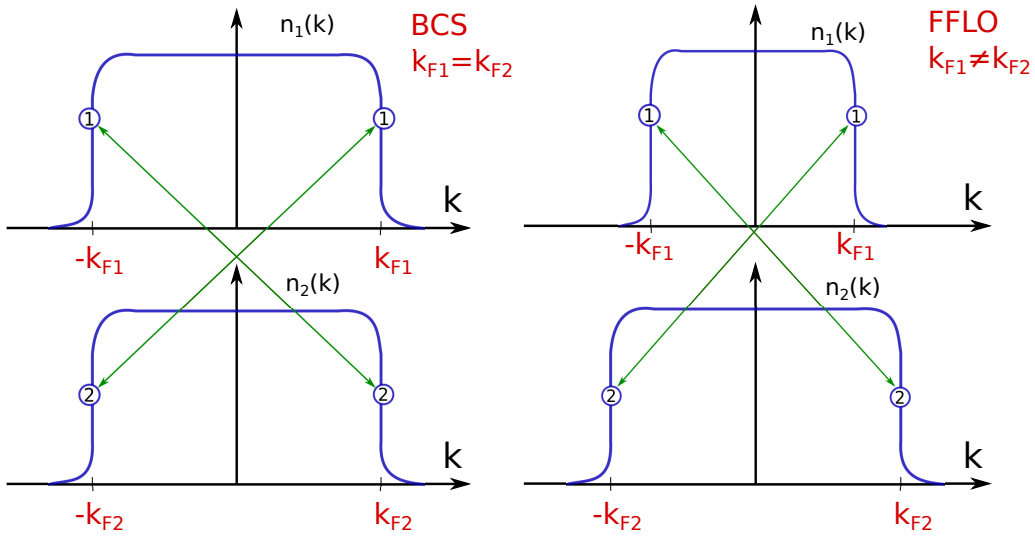

Figure 1.1: BCS pairing schematic (Left panel) and FFLO pairing schematic (right panel). Pairing happens between fermions (1) and (2) from the Fermi surfaces of each species. In the balanced case the momenta of the particles forming a pair are equal but opposite (left panel) and thus the pair has zero center-of mass momentum. In the imbalanced case and FFLO-type pairing the pair will have a non-zero center-of-mass momentum equal to the difference in the Fermi momenta of each species.

species are different, we call the system polarized and define the polarization as $P = \frac{|N_1 - N_2|}{N_1 + N_2}$. Since the Fermi momentum depends on the number of particles, the Fermi momenta of each species are unequal $k_{F1} \neq k_{F2}$ in the case of non-

zero polarization. In the FFLO scenario, the pairs still form between particles from respective Fermi surfaces as shown in Fig. 1.1 (right panel) but since the momenta are unequal the pair has a finite center-of mass momentum equal to the difference in the Fermi momenta of the two populations, $k_{pair} = |k_{F1} - k_{F2}|$. As a result the pairing order parameter is not homogenous but oscillates with the wave vector given by $|k_{F1} - k_{F2}|$. Consequently in real space the system consists of regions that are rich in pairs separated by pair-depleted regions where the excess of majority particles reside. The translational invariance of the system is broken. In other words, in the FFLO mechanism, the momentum distribution of pairs $n_{\rm pair}(k)$ has its peak at a momentum equal to the difference between the two Fermi momenta $k_{\rm peak} = k_{\rm pair} = |k_{F1} - k_{F2}|$. The peak at non-zero momentum in the momentum distribution will be the signature that we will use in this study to identify the FFLO phase. One can understand the energetical advantage of forming pairs with non-zero momentum from the following qualitative argument [9]. Compared to a simple Fermi sea at $T = 0$, forming Cooper pairs causes a cost in kinetic energy as the particles participating in the pairing need to be excited above the Fermi momentum. Pairing as close as possible to the Fermi momenta will minimize the kinetic energy cost but also implies pairing at non-zero momentum, which creates additional kinetic energy cost. Obviously the formation of pairs is the source of important interaction energy gain. Surely a quantitative calculation is essential to decide on the energetically most favorable phase.

Another scenario proposed by Sarma in Ref. [10] is referred to as Breached Pairing (BP). Here the majority fermions whose momenta are higher than the Fermi momentum of the minority species are promoted to higher momentum levels thus forming a deformation (breach) in the Fermi distribution of the ma-

jority population as shown in Fig. 1.2. Since at this interaction limit the pairing

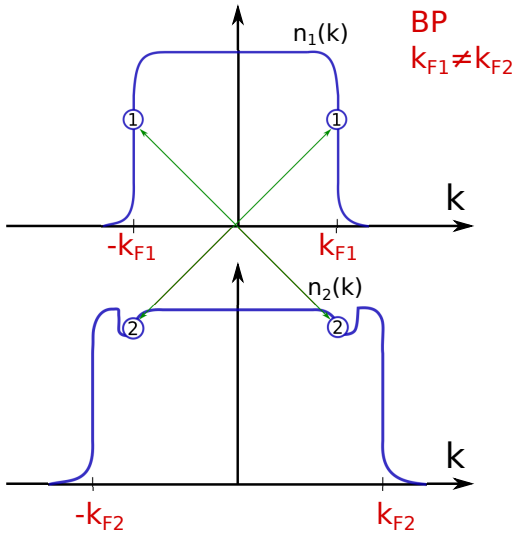

Figure 1.2: Breached pairing (Sarma phase) schematic. Pairing happens between fermion (1) from the Fermi surface of the minority and fermion (2) from the breach in the Fermi surface of the majority. As a result the respective momenta are equal but opposite and the pair has a zero center-of-mass momentum.

can only happen at the Fermi surface not inside the Fermi sea, this breach allows majority fermions with momentum equal to the Fermi momentum of the minority to pair up with the minority fermions near their Fermi momentum. In this way, pairs that are formed have zero center-of mass momentum with a pair momentum distribution which is peaked at zero momentum ($k_{\text{peak}} = 0$). The system in this scenario remains uniform and is a homogenous mixture of pairs and unpaired majority particles. It appears that the pairs and excess particles form a collective state in which the excitations are not gapped as opposed to the case in the FFLO pairing. From the energy balance point of view, in this case there is a cost of kinetic energy from promoting many particles to higher momenta in order to form the breach while the pairing obviously brings gain in the interaction energy.

In order to distinguish between the possible pairing states more quantitatively we need to study more closely the interaction term of the Hubbard Hamiltonian that we will use to describe the system and which will be described in more details in the Chapter 2

$$\mathcal{H}_U = U \sum_j \hat{n}_{j\,1} \hat{n}_{j\,2} = U \sum_j c^\dagger_{j\,1} c^\dagger_{j\,2} c_{j\,2} c_{j\,1}. \tag{1.1}$$

The interaction term is quartic in the fermionic operators and so to decouple it one can use, for example, Mean-Field theory in which an operator can be written as its average and the fluctuations around it: $\hat{A} =< \hat{A} > +\delta\hat{A}$. Neglecting the second order fluctuation term, we can write down the interaction term as

$$\mathcal{H}_U^{\mathrm{MF}} = U \sum_j \left(c^\dagger_{j\,1} c^\dagger_{j\,2} < c_{j\,2} c_{j\,1} > + < c^\dagger_{j\,1} c^\dagger_{j\,2} > c_{j\,2} c_{j\,1} - < c^\dagger_{j\,1} c^\dagger_{j\,2} >< c_{j\,2} c_{j\,1} > \right). \tag{1.2}$$

Where the mean-field order parameter is given by $\Delta = U \sum_j \langle c^\dagger_{j\,1} c^\dagger_{j\,2} \rangle$. With the use of Fourier transform, the Hamiltonian can be written in momentum space and the interaction term takes the form:

$$\mathcal{H}_U = \frac{U}{L} \sum_{k,k',q} c^\dagger_{1\,k+\frac{q}{2}} c^\dagger_{2\,-k+\frac{q}{2}} c_{2\,-k'+\frac{q}{2}} c_{1k'+\frac{q}{2}}. \tag{1.3}$$

In the mean-field approximation:

$$\mathcal{H}_U^{\mathrm{MF}} = \frac{1}{\sqrt{L}} \sum_{k,q} c^\dagger_{1\,k+\frac{q}{2}} c^\dagger_{2\,-k+\frac{q}{2}} \Delta_q + \frac{1}{\sqrt{L}} \sum_{k',q} c_{2\,-k'+\frac{q}{2}} c_{1\,k'+\frac{q}{2}} \Delta^\dagger_q - \frac{1}{U} \sum_q \Delta^\dagger_q \Delta_q$$

where we introduced the pairing amplitude in momentum space:

$$\Delta_q^\dagger = \sqrt{L} \cdot U \sum_k \left\langle c^\dagger_{1\,k+\frac{q}{2}} c^\dagger_{2-k+\frac{q}{2}} \right\rangle . \tag{1.4}$$

The plane-wave ansatz for the pairing amplitude $\Delta_q = \Delta_0 e^{iqj}$ was suggested by Fulde and Ferrel [7]. Larkin and Ovchinnikov [8] proposed the order parameter in the form $\Delta_q = \Delta_0 \cos(qj)$. The plane wave ansatz suggested in the paper by Fulde and Ferrel implies a net current flow of the superconducting electron pairs, and they argue that in parallel an equal and opposite direction current flow of the unpaired electrons is observed. It is thus a state which breaks the time-reversal symmetry. On the other hand the solution of Larkin and Ovchinnikov is a standing wave, and can be seen as a combination of counterpropagating waves. This solution breaks the translational symmetry and is found in general to be more stable [11]. The two possibilities are usually referred to as one scenario with oscillating order parameter and called FFLO or LOFF phase. It is a widely accepted practice to call the state FFLO or LOFF even though most of the time one means the LO standing pair density wave solution.

In order to find the ground-state solution one needs to diagonalize the Hamiltonian using the Bogoliubov transformation and then look for Δ_0 and q which minimize the free energy of the system. In the balanced case we know that $q = 0$ is the minumum energy solution and corresponds to the usual BCS solution. We can see in Eq. 1.4 that this corresponds to pairing between particles with equal but opposite momenta. In the case of imbalanced populations getting $q \neq 0$ as the solution with minimal free energy means that pairs form with $q \neq 0$ center of mass momentum, and consequently, the ground

state is FFLO. In the case of breached pairing, the solution giving the minimum free energy would be for $q = 0$ for the system with imbalanced populations.

Furthermore not only the imbalance between the populations of Fermions is of great interest but also the case of unequal masses between the two species participating in the pairing. Naturally, with growing expertise in the cold-atom experiments, mixtures of fermions from different atomic species, for example ^{6}Li and ^{40}K, can be studied at low temperatures [12] and possible phase diagrams have been recently reviewed in [13]. The interest in mixtures of different types of fermions is fueled by hope that they might open a door to better understanding of some high-temperature superconductors. Another motivation for these investigations comes from the astrophysical community where, in the case of cold dense quark matter, the quarks participating in the pairing can have masses that significantly differ from each other.

1.3 Experiments

Distinguishing these two scenarios experimentally proved to be difficult. The observation of the FFLO phase in solids turned out to be very challenging and was only achieved relatively recently with indirect measurements by Radovan *et. al.* [14]. They have studied a heavy-fermion material $CeCoIn_5$ which has a crystalline structure of quasi two-dimensional layers. With the use of penetration depth experiments, formation of the FFLO state was demonstrated. Penetration depth is sensitive to the density of superconducting electrons, which changes when the system enters a state characterized by the oscillating order parameter. It is the unusually big coupling of the field to the electron spins in this material that allows for new superconducting phase to appear, as

the coupling to the electron orbits is comparatively weaker. They report on a second order transition from the uniform superconducting to FFLO state in the case of the magnetic field aligned parallel to the planes, as this suppresses the orbital effects that quench the superconductivity.

The recent experimental realization of trapped ultra-cold fermionic atoms with tunable attractive interactions has created a new experimental system in which the effects of polarization on pairing of fermions could be studied. Ultra-cold atoms confined in traps where two hyperfine states of fermionic atoms play the role of up and down spins provide a very clean and highly controllable experimental setup as compared to condensed matter experiments. In superconductors only very limited control over the fermion density can be achieved by doping, while there is no control over the interactions [15]. Similarly in nuclear physics and astrophysics there is almost no control over the parameters of interest. The unprecedented control of the interactions achieved in experiments with cold-atoms through Feshbach resonances makes them a favorite laboratory tool to study strongly correlated systems. These systems are seen as the quantum emulators of condensed matter systems and models that cannot be solved theoretically. With the application of optical lattices to these experiments, crystallographic arrangements can be mimicked and an optical lattice loaded with cold bosons or fermions can realize the physics of Bose- or Fermi- Hubbard models with the hope of shedding more light on the holy Grail of condensed matter physics which is the high-T_c superconductivity.

First experiments reporting Bose Einstein Condensates of strongly bound fermion molecules were done in 2003 using ^{6}Li in [16, 17] and ^{40}K in [18]. Using magnetically-driven Feshbach resonance the interactions between the fermions can be tuned and become attractive, playing the role of the phonon induced

effective attractive interaction in the BCS theory. When the fermions pair up, tuning the interaction between strong and weak attraction across the unitarity regime brings the system from a state of strongly bound molecules through a regime of strongly interacting pairs to a state made of loosely bound and overlapping Cooper pairs. This carries the name of BCS-BEC crossover and has been realized experimentally in systems of cold fermionic atoms as reported in [19, 20]. These ultracold atomic systems provide an ideal experimental opportunity to study the physics of attractive Fermi gases with population imbalance. Such experiments using ^{6}Li have now reported the presence of pairing in the case of unequal populations in the group at MIT [21, 22] and Rice University [23] in three-dimensional cigar shaped traps. In these system the role of two species of fermions is played by the populations of distinct hyperfine levels. In the system of ^{6}Li the two lowest hyperfine states are used. In order to have control on the polarization of the system, a scheme has been devised in which appropriate use of RF pulses can transfer particles from one state to another. This way, an impressive level of control over the relative populations of the two states has been achieved. In Ref. [21] the MIT group studied the influence of the population imbalance on the vortex lattice both in the BEC and BCS regimes. In both regimes they demonstrated that the superfluidity persist in the polarized systems up to a critical polarization P_c, when the disappearance of vortices and thus breakdown of superfluidity was observed. In the BCS regime of loosely bound pairs, the normal time-of-flight imaging techniques fail to provide information about the system, as the pairs can easily dissociate and what is imaged is no longer a paired state of fermions. In the above experiment, a trick is used in which a rapid switch of the magnetic field to the BEC side of the Feshbach resonance is applied and thus Cooper

pairs are "projected" onto tightly bound molecules, which can then be imaged. The results obtained by the two main experimental groups working on the subject have stirred up controversy. The group at Rice University [23] claimed observation of a quantum phase transition from a homogenous paired superfluid to a phase separated state. The phase separation happening between a superfluid core of the cloud which is fully paired and excess particles located in the outer shell. The results at MIT [22] have been shown to exhibit the phase separation even for a very weak polarization and argued against the observation of a phase transition. It was shown that possibly the large difference in the aspect ratios of the cigar shaped traps (MIT - 5.6 and Rice - 48.6 being a much more elongated confinement) used in those experiments contributed to the discrepancies [24]. More recently Liao *et. al.* at Rice have reported the observation of pairing between fermions in one-dimensional traps [25]. Ultracold fermionic atoms of ^{6}Li were confined in arrays of one-dimensional tubes and the polarization of the clouds can be controlled thus allowing for studies over a wide range of polarizations. The imaging of the densities of the species is done in-situ. At a very low imbalance the density profiles exhibit a fully paired region located at the wings of the cloud. The core of the system is partially polarized and consists of both pairs and excess particles. At a critical polarization P_c a change in the density profiles occurs and the wings of the cloud become fully polarized (consisting of only majority particles) while the core of the cloud maintains its partially polarized character. These experimental results are discussed in greater detail in Chapter 3 where we perform simulations in a parameter regime close to the experimental one. The experimental observations in an imbalanced Fermi gas in one dimension suggest that the behavior is significantly different from the situation in three dimensions. There

have been speculations about a possibility of a dimensionally=driven crossover from 1D where for low P the fully paired phase is observed in the wings of the lattice to 3D where it is believed to occur at the core of the cloud. As one can see, experimental progress in this field has been immense. However, the precise nature of the pairing in the imbalanced Fermi gases has not yet been elucidated experimentally. It requires tools that allow for measuring the momentum space signatures of the cloud (such as the pair momentum distribution) and a lot of experimental effort is focused on implementing such tools. New schemes have been proposed, for example to make use of measurements of noise correlations to find a signature of the FFLO phase [26].

As mentioned earlier, experiments with mixtures of fermions such as ^{6}Li and ^{40}K create exciting opportunities to study mixtures of fermions with unequal masses. These experiments are of great interest to a wide community of nuclear physicists and astrophysicists. In the experiment by Taglieber *et. al.* [12], the quantum degenerate regime was reached for the ^{6}Li and ^{40}K mixture. The existence of the Feshbach resonances for this system that allows for interaction control is reported in [29].

1.4 Thesis structure

The main motivation of this thesis is to study the system of a mixture of Fermions with imbalanced populations and imbalanced masses. There has been an enormous amount of theoretical effort put into understanding of the pairing mechanism. The stability of the phases was studied with many different methods and it is impossible to mention all the results. Calculations using mean field theory [30]-[41], effective Lagrangian [42], Bethe ansatz [43, 44]

studies have been performed for the uniform system, with extensions to the trapped system using the local density approximation (LDA). Simple many-body approaches such as polaron physics and Fermi-liquid theory has been also used to study the population imbalanced system [45]. The specific literature relevant to our work will be reviewed in respective chapters. We contribute to the body of research on this topic by performing approximation-free numerical calculations using Quantum Monte Carlo techniques which are described in Chapter 2. In Part 1 of this thesis we present results concerning the one-dimensional system. In Chapter 3 we present results which establish that the FFLO phase is the ground state of the population imbalanced system of fermions. The stability of this phase at finite temperatures remains an open question and a very important one for the experimental community. This is the focus of Chapter 4. The Sarma phase was not detected yet in the above mentioned numerical work but it was suggested that it could be stabilized in systems with mass imbalance. We address this issue in Chapter 5. Another interesting question is the stability of this phase in higher dimensions. Lack of exact numerical studies of the 2D system motivated us to study it using both Quantum Monte Carlo as well as Mean-Field theory and we present the results in Part 2.

Chapter 2

Methods

2.1 Introduction

In this chapter we present the model and numerical methods that we have used to study a mixture of fermions interacting attractively with imbalanced populations on a lattice. It is of practical value to employ the "second quantization" formalism to describe systems of many interacting identical particles. We used Quantum Monte Carlo methods (QMC) in order to simulate the system according to the probability distribution given by:

$$\mathcal{P} = \frac{1}{\mathcal{Z}} e^{-\beta \mathcal{H}} \tag{2.1}$$

where the partition function $\mathcal{Z}$ is defined as follows:

$$\mathcal{Z} = \mathrm{Tr}\left(e^{-\beta \mathcal{H}}\right) = \sum_i \left\langle \psi_i | e^{-\beta \mathcal{H}} | \psi_i \right\rangle \tag{2.2}$$

where $|\psi_i\rangle$ are the basis states, $\beta = 1/(k_B T)$ is the inverse temperature and $k_B = 1$ is used in all our calculations.

We present a concise introduction to the Stochastic Green Function algorithm (SGF) and Determinant Quantum Monte Carlo (DQMC) both used to study the ground state and finite temperature effects in a one-dimensional system. The investigations into the behavior of the system on a two-dimensional lattice were carried out using only DQMC. The Continuous imaginary time Worm algorithm (CW) used to study the mass imbalanced system is described.

2.2 Hubbard model

The aim of our study of a mixture of fermions interacting attractively is to gain insight into the physics of a mixture of spin up and down electrons in a superconducting material. In cold atom experiments what is used to realize this system is a two-component Fermi gas consisting of atoms in two different hyperfine sublevels of a ground state of an atom (for example ^{6}Li). This pseudo spin-1/2 system of atomic fermions can be loaded into an optical lattice in the tight-binding regime that mimics a regular lattice of fixed nuclear positions in a solid state material. This system can then be described by the Hubbard Hamiltonian with two fermionic species, as was shown for bosons by Jaksch *et al.* [46]. The Hubbard model was introduced originally in [47] in order to study the behavior of electrons in solids and the transition between metallic and insulating phases. Since then it has been extensively used in the investigations of many condensed matter systems. Despite its simplicity the model has brought an abundance of insight into the physics of strongly correlated electronic systems. A practical introduction to the physics of the model

can be found in [48]. The simplest Hubbard Hamiltonian is given by:

$$\mathcal{H} = -t \sum_{<i,j>\sigma} (c^{\dagger}_{i\,\sigma} c_{j\,\sigma} + c^{\dagger}_{j\,\sigma} c_{i\,\sigma}) + U \sum_{i} \hat{n}_{i\,1} \hat{n}_{i\,2} - \mu \sum_{i} (\hat{n}_{i\,1} + \hat{n}_{i\,2}) \quad (2.3)$$

which due to its structure can be also written in a more concise way as

$$\mathcal{H} = \mathcal{H}_K + \mathcal{H}_U + \mathcal{H}_\mu. \quad (2.4)$$

Where $\mathcal{H}_K$ is the kinetic term, $\mathcal{H}_U$ interaction term and $\mathcal{H}_\mu$ chemical potential term. In the "second quantization" formalism $c^{\dagger}_{i\,\sigma}$ and $c_{i\,\sigma}$ are fermion creation and annihilation operators on lattice site i satisfying the usual anticommutation relations: $\{c_{i\,\sigma}, c^{\dagger}_{j\,\sigma'}\} = \delta_{i,j}\delta_{\sigma,\sigma'}$. The fermionic species are labeled by $\sigma = 1, 2$ but we will use it alternately with $\sigma = +, -$ or $\sigma = \uparrow, \downarrow$ and it is to be understood as describing the same system. The $\hat{n}_{i\,\sigma} = c^{\dagger}_{i\,\sigma} c_{i\,\sigma}$ is the corresponding number operator. Due to the Pauli principle it can take only values 0 or 1 so at each lattice site we can find at most two particles, one from each species.

The first term in the Hamiltonian ($\mathcal{H}_K$) is the kinetic energy term and governs how particles hop from one site to neighboring one. The hopping parameter "t" sets the energy scale of the system. Its origin is the overlap of the wavefunctions of the electrons, and since these die off exponentially, we take into account only the hopping between nearest neighboring sites. This is denoted with the symbol $< i, j >$ which means that "i" and "j" are adjacent sites. In all our studies we apply periodic boundary conditions.

The second term ($\mathcal{H}_U$) is the interaction energy term. It is zero when there is no or one particle at a site and has a strength "U" when there are

two particles at a site. Only on site interaction is taken into account here motivated by the physical situation of electrons interacting via a screened Coulomb potential where the dominant interaction is when both atoms are at the same spatial position. This is also the case relevant to the cold-atoms experiments where atoms of different species only interact when they are at the same lattice site. One can also include longer range interactions in the model which is usually referred to as extended Hubbard model. The original Hubbard model considers the repulsive interaction ($U > 0$) as is the case for interacting electrons but we will study the case of attractive interaction ($U < 0$) since the focus of our studies is the pair formation due to effective attraction between fermions and because attractive interactions are realized in cold atomic systems experimentally.

The last term ($\mathcal{H}_\mu$) is the chemical potential term that tunes the filling of the lattice in the grand-canonical ensemble. An important density regime is half-filling of the lattice where the density at each site is $\rho = 1$. In this formulation this occurs for the chemical potential $\mu = U/2$. Since the half-filling of the lattice is an important regime in our studies it is convenient to shift the chemical potential μ by $U/2$ so that $\mu = 0$ then corresponds to $\rho = 1$ per site and there is a slight change to the interaction term of the Hamiltonian. The energy of the system is also shifted as a result by a constant $U/4$. The equivalent Hamiltonian then takes the form:

$$\mathcal{H} = -t \sum_{<i,j>\sigma} (c^\dagger_{i\sigma} c_{j\sigma} + c^\dagger_{j\sigma} c_{i\sigma}) + U \sum_i \left(\hat{n}_{i1} - \frac{1}{2}\right)\left(\hat{n}_{i2} - \frac{1}{2}\right) - \mu \sum_i (\hat{n}_{i1} + \hat{n}_{i2}) \qquad (2.5)$$

Since we are interested in imbalanced populations of Fermions, independent chemical potentials need to be introduced for each species and the chemical potential part of the Hamiltonian can be written as:

$$\mathcal{H}_\mu = -\sum_i \left(\mu_1 \hat{n}_{i\,1} + \mu_2 \hat{n}_{i\,2}\right). \tag{2.6}$$

The more specific one- and two-dimensional models that have been used in the course of this research project are presented in the chapters dealing with simulations of 1D and 2D systems.

2.3 Determinant Quantum Monte Carlo algorithm

One can think about Monte Carlo methods as numerical experiments. Equations which underlie the simulations make sure that the generated configurations follow the desired probability distribution. We describe here the determinant QMC algorithm that we used to generate samples which follow the probability distribution of interest. We follow the derivation as formulated in [49]. The aim of our simulations is to calculate the expectation values of physical observables. The Hamiltonian of interest can be written as in Eq. 2.4. Denoting the observable of interest as $\mathcal{A}$, its expectation value is given by:

$$\langle \mathcal{A} \rangle = \mathrm{Tr}\left(\mathcal{A}\mathcal{P}\right) \tag{2.7}$$

Where $\mathcal{P}$ is the probability distribution operator defined in Eq. 2.1. The trace is taken over the Hilbert space of the basis states. In all algorithms used in

this work, the most convenient representation is the basis of occupation states, so its dimension is 4^N where N is the number of sites. There are four possible occupation states of every lattice site due to Pauli principle and these are: $|\cdot\rangle$, $|\uparrow\rangle$, $|\downarrow\rangle$ and $|\uparrow\downarrow\rangle$.

Since $\mathcal{H}$ is an operator, one needs first to use a transformation to find a computable approximation of the probability distribution operator $\mathcal{P}$. In order to do this, we need to cast $\mathcal{P}$ into a real number so we can use it as a weight of a configuration in our simulations.

One treats β as an imaginary time variable, since the evolution operator in real time is $e^{-it\mathcal{H}}$. This introduces an additional dimension to the problem (the lower the temperature T the bigger the β and the additional dimension). We start by writing the exponential as:

$$e^{-\beta\mathcal{H}} = e^{-\tau\mathcal{H}}e^{-\tau\mathcal{H}}e^{-\tau\mathcal{H}}\dots e^{-\tau\mathcal{H}}. \tag{2.8}$$

where one divides β into L_τ subintervals $\tau = \beta/L_\tau$ called time slices. This well-known mapping of D dimensional quantum systems (or quantum path integral) to D+1 dimensional classical systems (classical path integral) [50, 51] lies at the base of all QMC algorithms used in this thesis.

The Suzuki-Trotter decomposition states that for small τ we can rewrite the exponential of an operator as:

$$e^{-\tau(\mathcal{A}+\mathcal{B})} = e^{-\tau A}e^{-\tau B} + \mathcal{O}\left(\tau^2\right) \tag{2.9}$$

and by taking the τ to be small we can minimize the so called Trotter error.

The partition function takes the form :

$$\mathcal{Z} = \mathrm{Tr}\left(e^{-\tau L_\tau \mathcal{H}}\right) = \mathrm{Tr}\left(e^{-\sum_{l=1}^{L_\tau}\tau\mathcal{H}}\right) = \mathrm{Tr}\left(\prod_{l=1}^{L_\tau} e^{-\tau\mathcal{H}}\right) \tag{2.10}$$

Using the Trotter-Suzuki decomposition and the fact that our Hamiltonian consists of three terms we can expand the exponential further:

$$\mathcal{Z} = \mathrm{Tr}\left(\prod_{l=1}^{L_\tau} e^{-\tau\mathcal{H}_K} e^{-\tau\mathcal{H}_U} e^{-\tau\mathcal{H}_\mu}\right) + \mathcal{O}\left(\tau^2\right) \tag{2.11}$$

The kinetic energy part consists of independent terms for each species so we can write it down as follows:

$$e^{-\tau\mathcal{H}_K} = e^{-\tau\mathcal{H}_{K\uparrow}} e^{-\tau\mathcal{H}_{K\downarrow}}. \tag{2.12}$$

As a result both parts of the kinetic term can be written in bilinear form:

$$\mathcal{H}_{K\uparrow} = -t \sum_{<i,j>} (c^\dagger_{i\uparrow} c_{j\uparrow} + c^\dagger_{j\uparrow} c_{i\uparrow}) = -t \boldsymbol{c}^\dagger_\uparrow K \boldsymbol{c}_\uparrow \tag{2.13}$$

where

$$\boldsymbol{c}_\uparrow = \begin{bmatrix} c_{1\uparrow} \\ c_{2\uparrow} \\ \vdots \\ c_{N\uparrow} \end{bmatrix}, \boldsymbol{c}^\dagger_\uparrow = \begin{bmatrix} c^\dagger_{1\uparrow}, c^\dagger_{2\uparrow}, \cdots, c^\dagger_{N\uparrow} \end{bmatrix}, K = \begin{bmatrix} 0 & 1 & 0 & \cdots & 1 \\ 1 & 0 & 1 & \cdots & 0 \\ 0 & 1 & 0 & \cdots & 0 \\ \vdots & \vdots & \vdots & \ddots & \vdots \\ 1 & 0 & 0 & \cdots & 0 \end{bmatrix} \tag{2.14}$$

and analogously for $\mathcal{H}_{K\downarrow}$.

The interaction term is the most problematic, as it is quartic in the fermionic

operators. We rewrite the interaction term in Eq. 2.5 as

$$e^{-\tau\mathcal{H}_U} = e^{-\tau U\sum_i\left(\hat{n}_{i\uparrow}-\frac{1}{2}\right)\left(\hat{n}_{i\downarrow}-\frac{1}{2}\right)} = \prod_i e^{-\tau U\left(\hat{n}_{i\uparrow}-\frac{1}{2}\right)\left(\hat{n}_{i\downarrow}-\frac{1}{2}\right)}. \tag{2.15}$$

We use the discrete Hubbard-Stratonovich transformation [53, 54] to express the interaction term in quadratic form at the expense of introducing an auxiliary field h. For $U<0$, this takes the form

$$e^{-\tau U\left(\hat{n}_{i\uparrow}-\frac{1}{2}\right)\left(\hat{n}_{i\downarrow}-\frac{1}{2}\right)} = A\cdot \mathrm{Tr}_h e^{ah_i\left(\hat{n}_{i\uparrow}+\hat{n}_{i\downarrow}-1\right)} \tag{2.16}$$

where $\cosh(a) = e^{-\frac{\tau U}{2}}$ and $A=\frac{1}{2}e^{\frac{\tau U}{4}}$. The h_i introduced here is the site-dependent H-S field. The trace over the H-S variable is a sum over all configurations $\{h_i=\pm 1\}$. There will be a configuration of those H-S variables for each time slice so we add another index l and write the auxiliary field as h_{il}.

As a result we can write down the partition function as

$$\mathcal{Z} = A^{NL_\tau}\mathrm{Tr}_h e^{-\mathrm{Tr}V_l(h)}\mathrm{Tr}\left(\prod_{l=1}^{L_\tau} e^{-\tau\mathcal{H}_{K\uparrow}}e^{\mathcal{H}^l_{U\uparrow}}e^{-\tau\mathcal{H}_{\mu\uparrow}}\right)\mathrm{Tr}\left(\prod_{l=1}^{L_\tau} e^{-\tau\mathcal{H}_{K\downarrow}}e^{\mathcal{H}^l_{U\downarrow}}e^{-\tau\mathcal{H}_{\mu\downarrow}}\right) \tag{2.17}$$

where $\mathcal{H}_{K\uparrow,\downarrow}$ is as shown in Eq. 2.13. One can write the H-S field for a given time slice in matrix form as $V_l(h) = a\cdot\mathrm{diag}(h_{1l}\ldots h_{Nl})$ so then the interaction part of the Hamiltonian can be written in a billinear form $\mathcal{H}^l_{U\uparrow} = \boldsymbol{c}^\dagger_\uparrow V_l(h)\,\boldsymbol{c}_\uparrow$ and analogously for $\downarrow$. As opposed to the kinetic energy term that is the same for all time slices, $V_l(h)$ is different for each time slice. We take the Hamiltonian to have separate chemical potentials for each species $\mu_\uparrow$ and $\mu_\downarrow$ so that $\mathcal{H}_{\mu\uparrow} = -\boldsymbol{c}^\dagger_\uparrow\mu_\uparrow\mathrm{I}\boldsymbol{c}_\uparrow$ where I is the identity matrix.

Having transformed all parts of the Hamiltonian into quadratic forms of fermionic operators one can now use the central identity of this algorithm that

allows us to evaluate the trace. It was introduced by Blackenbecker et. al. [55] and proved in an alternative way by Hirsch in [56].

If $\mathcal{H}_l$ are operators which are quadratic forms of fermionic operators *i.e.*

$$\mathcal{H}_l = \sum_{ij} c_i^\dagger \left(H_l\right)_{ij} c_j \tag{2.18}$$

where H_l are matrices of real numbers. Then,

$$\mathrm{Tr}\left(e^{-\mathcal{H}_1} e^{-\mathcal{H}_2} \ldots e^{-\mathcal{H}_{L_\tau}}\right) = \det\left(I + e^{-H_{L_\tau}} e^{-H_{L_\tau - 1}} \ldots e^{-H_1}\right). \tag{2.19}$$

This identity allows us to write the partition function as a product of determinants of real matrices so it is readily computable.

$$\mathcal{Z}_h = A^{NL_\tau} \mathrm{Tr}_h e^{-\mathrm{Tr} V_l(h)} \det\left[M_\uparrow\left(h\right)\right] \det\left[M_\downarrow\left(h\right)\right] \tag{2.20}$$

where $M_\sigma\left(h\right) = I + B_{L,\sigma}\left(h_L\right) B_{L-1,\sigma}\left(h_{L-1}\right) \cdots B_{1,\sigma}\left(h_1\right)$ are the fermion matrices for $\sigma = (\uparrow, \downarrow)$ and $B_{l\sigma}\left(h_l\right) = e^{\tau t K} e^{V_l(h_l)} e^{\tau \mu_\uparrow}$. We thus have a determinant of a real matrix to calculate for each species, in this way the partition function of the quantum problem is translated in to a classical Monte Carlo task where one has to sum over all possible realizations of the variables $h_{i,l}$. One must generate the H-S variables with the probability which is the product of the two determinants:

$$\mathcal{P} = \frac{1}{Z_h} \det\left[M_\uparrow\left(h\right)\right] \det\left[M_\downarrow\left(h\right)\right]. \tag{2.21}$$

We introduce the weights for configurations as:

$$\mathrm{P}(h) = \det\left[M_{\uparrow}\left(h\right)\right]\det\left[M_{\downarrow}\left(h\right)\right]. \tag{2.22}$$

Although the matrices are real, in general there is no guarantee that the determinant is positive. Furthermore the two determinants are not equal in general. Consequently the weight $\mathrm{P}(h)$ can become negative leading to the infamous "fermion sign problem". In this case we can write the weight as $\mathrm{P}(h) = sgn * |\mathrm{P}(h)|$ and use the absolute value as the probability while keeping track of the sign. The average value of a physical quantity, for *e.g.* $\mathcal{A}$, is then calculated as:

$$\langle\mathcal{A}\rangle = \frac{\sum_h \mathcal{A}_h sgn * |\mathrm{P}(h)|}{\sum_h sgn * |\mathrm{P}(h)|} = \frac{\langle\mathcal{A} * sgn\rangle'}{\langle sgn\rangle'} \tag{2.23}$$

where $\langle\cdots\rangle'$ is the average calculated with the weight $|\mathrm{P}(h)|$. The sign problem is absent for some specific situations. For example, in the case of attractive interaction the two determinants are identical when $\mu_{\uparrow} = \mu_{\downarrow}$ making $P > 0$. Since we are interested mostly in the situation when the populations of fermions are imbalanced we will have a sign problem in our simulations. However, in the cases we studied, this problem was manageable with $\langle sgn\rangle \gtrsim 0.7$ so that we were able to obtain good statistics for our measurements.

This algorithm allowed us to study imbalanced mixtures of fermions at very low temperatures $\beta t = 32$ in one dimension and $\beta t = 12$ in two dimensions on lattices of up to 400 sites. The algorithm and the first results for a two-dimensional Hubbard model can be found in Ref. [57].

2.3.1 Measurements

In order to gain insight into the behavior of our system one needs to measure several physical quantities. The single particle Green's function is very useful to calculate many quantities of interest. It is given by:

$$\tilde{G}_\sigma(i,j) = \langle c_{i\,\sigma} c^\dagger_{j\,\sigma} \rangle = \left(M_\sigma(h)\right)^{-1}_{ij}. \tag{2.24}$$

Later, in the results section, we will mostly use the distance averaged Green function $\tilde{G}(l)$ (with periodic boundary condition the largest distance in the system is half the system size) which is more practical to characterize a translationally invariant system and is defined as:

$$\tilde{G}_\sigma(l) = \frac{1}{N}\sum_i \langle c^\dagger_{i+l\,\sigma} c_{i\,\sigma} \rangle = \frac{1}{N}\sum_i \begin{cases} 1 - \left(M_\sigma(h)\right)^{-1}_{ii} & \text{if } l = 0 \\ -\left(M_\sigma(h)\right)^{-1}_{i,i+l} & \text{if } l \neq 0 \end{cases} \tag{2.25}$$

where the maximum distance is $l = N/2$ due to periodic boundary conditions. The average particle density on a site is given by

$$\langle n_{i\sigma} \rangle = \langle c^\dagger_{i\,\sigma} c_{i\,\sigma} \rangle = 1 - \langle c_{i\,\sigma} c^\dagger_{i\,\sigma} \rangle = 1 - \left(M_\sigma(h)\right)^{-1}_{ii} \tag{2.26}$$

and when averaged over all sites (average particle density) is equal to $\tilde{G}_\sigma(0)$. The double occupancy of each site is

$$\langle n_{i\uparrow} n_{i\downarrow} \rangle = \langle c^\dagger_{i\uparrow} c_{i\uparrow} c^\dagger_{i\downarrow} c_{i\downarrow} \rangle = \left(1 - \left(M_\uparrow(h)\right)^{-1}_{ii}\right)\left(1 - \left(M_\downarrow(h)\right)^{-1}_{ii}\right). \tag{2.27}$$

The central quantity to our studies is the pair Green function and is given by:

$$\begin{aligned} G_{\text{pair}}(i,j) &= \langle \Delta_i^\dagger \, \Delta_j \rangle = \langle c_{i\uparrow}^\dagger c_{i\downarrow}^\dagger \, c_{j\downarrow} c_{j\uparrow} \rangle = \\ &= \begin{cases} \left(1 - (M_\uparrow(h))_{ji}^{-1}\right)\left(1 - (M_\downarrow(h))_{ji}^{-1}\right) & \text{if } i = j \\ (M_\uparrow(h))_{ji}^{-1} \, (M_\downarrow(h))_{ji}^{-1} & \text{if } i \neq j \end{cases} \end{aligned} \tag{2.28}$$

Again it is useful to calculate a distance averaged version:

$$\begin{aligned} G_{\text{pair}}(l) &= \frac{1}{N}\sum_i \langle \Delta_i^\dagger \, \Delta_{i+l} \rangle = \frac{1}{N}\sum_i \langle c_{i\uparrow}^\dagger c_{i\downarrow}^\dagger \, c_{i+l\downarrow} c_{i+l\uparrow} \rangle = \\ &= \frac{1}{N}\sum_i \begin{cases} \left(1 - (M_\uparrow(h))_{i+l,i}^{-1}\right)\left(1 - (M_\downarrow(h))_{i+l,i}^{-1}\right) & \text{if } l = 0 \\ (M_\uparrow(h))_{i+l,i}^{-1} \, (M_\downarrow(h))_{i+l,i}^{-1} & \text{if } l \neq 0 \end{cases} \end{aligned} \tag{2.29}$$

In two dimensions one can write the single particle Green function in the following form:

$$G_\sigma(\boldsymbol{l}) = \frac{1}{N}\sum_{\boldsymbol{r}} \langle c_{\boldsymbol{r}+\boldsymbol{l}}^\dagger \, c_{\boldsymbol{r}} \rangle \tag{2.30}$$

and the pair Green function as

$$G_{\text{pair}}(\boldsymbol{l}) = \frac{1}{N}\sum_{\boldsymbol{r}} \langle \Delta_{\boldsymbol{r}}^\dagger \, \Delta_{\boldsymbol{r}+\boldsymbol{l}} \rangle \tag{2.31}$$

where $\boldsymbol{r} = \{x, y\}$, x and y being the coordinates of a lattice site.

The Fourier transform of the single particle and pair Green function yields the respective momentum distributions. In 1D this takes the form

$$n_\sigma(k) = \frac{1}{L}\sum_l G_\sigma(l) e^{ikl} \qquad n_{\text{pair}}(k) = \frac{1}{L}\sum_l G_{\text{pair}}(l) e^{ikl}. \tag{2.32}$$

It is important to comment on the error analysis in the algorithm we are using [58, 59]. The only source of systematic errors in the DQMC algorithm,

which is discrete in time, comes from the Trotter decomposition and can be reduced by decreasing the imaginary time interval. The order of this error is the order of the commutator of the operators, in our case $\sim \tau^2 t|U|$. We need to choose the imaginary time step for our simulations such that this error is minimized. In practice, as mentioned in Ref. [52], one needs to make sure that $\tau^2 t|U| < 0.1$. The size of τ obviously depends on the interaction strength U and, for example, in a case most prevalent in this work $|U| = 3.5$ taking $\tau = 0.125$ so the Trotter error is of the order of ~ 0.05.

By construction a Monte Carlo method performs statistical averaging of quantities and, as such, the results will have a statistical error that needs to be calculated. The simplest way to calculate the error on a statistical sample is to evaluate the standard deviation. For example in case one wants to measure the physical quantity x per site in a lattice one follows the standard procedure calculating

$$\langle x \rangle = \frac{1}{N_m} \sum_{i=0}^{N_m} x_i \qquad \text{and} \qquad \langle x^2 \rangle = \frac{1}{N_m} \sum_{i=1}^{N_m} x_i^2 \tag{2.33}$$

and the error as

$$\langle \sigma \rangle = \sqrt{\frac{\langle x^2 \rangle - \langle x \rangle^2}{N_m - 1}}. \tag{2.34}$$

However the formula for the standard error assumes that the measured values are independent. Since in a simulation, configurations are generated one from the previous one, they are correlated with a finite decorrelation number of Monte Carlo steps (or decorrelation time). The longer one waits between successive measurements the less correlated the outcomes. In this way the outcomes are dependent on the time step we take between the measurements. In order not to waste time to make the measurements when the data are correlated one introduces a waiting time between the measurements which is

longer than the correlation time τ_{cor}. Additional approach that is used is called "binning" of the data. The whole time series of the measurement is divided into $L_b = N_m/M$ "bins" where N_m is the total number of measurements and M is the size of the bin. Then the data in each bin are averaged:

$$m_j = \frac{1}{M} \sum_{i=M*(j-1)+1}^{M*j} x_i \tag{2.35}$$

where the bins are labelled with j. These values are treated as independent measurements and one can calculate the error on these measurements:

$$\langle x \rangle = \frac{1}{L_b} \sum_{j=0}^{L_b} m_j \qquad \langle x^2 \rangle = \frac{1}{L_b} \sum_{j=1}^{L_b} m_j^2 \tag{2.36}$$

and

$$\langle \sigma \rangle = \sqrt{\frac{\langle x^2 \rangle - \langle x \rangle^2}{L_b - 1}}. \tag{2.37}$$

If the bin size is too small the measurements will still be correlated and the error bars underestimated. As the bin size increases the σ increases as well and reaches an asymptotic value before it drops again when the bins are too big and one doesn't have enough measurements to estimate the error. We use the binning method to calculate errors for the measurements taken during a simulation. A reliable strategy, stemming from years of experience in using the algorithm, is to perform a relatively long simulation, measure the quantities of interest every 10 or 15 Monte Carlo step, and bin the data into $L_b = 10$ bins. In practice this strategy works well and when, there appears a suspicion that the errors are under(over)estimated, we perform a longer run to check if the measured values have changed or if only the error bars decreased.

2.3.2 Implementation of DQMC

We now present a brief description of the implementation of this algorithm. The first step is to initialize the Hubbard-Stratonovich field by filling in the array h_{il} with randomly drawn values ± 1 as well as initializing the kinetic K and interaction $V_l(h)$ matrices then computing the Green's function for both species. The main task is in doing the so called sweeps of the lattice. This means that one suggests a change in the H-S field for each spatial site for the particular time slice so $h'_{i,l} = -h_{il}$. The change is accepted or rejected according to the Metropolis algorithm. One calculates the Metropolis ratio:

$$r_{il} = \frac{\det\left[M_\uparrow(h')\right]\det\left[M_\downarrow(h')\right]}{\det\left[M_\uparrow(h)\right]\det\left[M_\downarrow(h)\right]} \tag{2.38}$$

and by comparing it to a random number r drawn uniformly from $[0,1]$ accepts the flip if $r \leq \min\{1, r_{il}\}$. If the change is accepted the Green's function needs to be updated. The Green function corresponding to the configuration h is defined by:

$$G_\sigma(h) = M_\sigma^{-1}(h). \tag{2.39}$$

Suggesting the changes in H-S field continues through all the spatial sites of the lattice. After finishing a particular time slice,*e.g.* $l = L_\tau$, one needs to wrap the Green's functions

$$\tilde{G}_\sigma = \left[e^{\tau t K} e^{V_{L_\tau}(h_{l_\tau})} e^{\tau\mu_\uparrow}\right] \tilde{G}_\sigma \left[e^{\tau t K} e^{V_{L_\tau}(h_{l_\tau})} e^{\tau\mu_\uparrow}\right]^{-1}. \tag{2.40}$$

One continues with the next time slice and completes the updates for the whole space-time lattice. This is called a sweep of the lattice. After a few sweeps one performs the measurements of the operators of interest. In practice in order

to let the system equilibrate from the initial starting point, one preforms first the "warm-up" sweeps without measurement.

We have used DQMC to study the 1D and 2D systems. Its advantage is that the convergence rates are rather fast. For a one-dimensional system a typical simulation for $L = 50$ sites and $\beta = 30$ with an imaginary time step $\Delta\tau = 0.1$ runs for about 4 to 5 days on a desktop computer and yields error bars of the order of 0.5% for the peak of the pair momentum distribution, a central quantity of interest in this work. In two dimensions the typical simulations of the harmonically confined system at low temperature took about two weeks on a 3 GHz processor. One inconvenience of this algorithm is that in order to perform simulations at a fixed particle number, the chemical potentials need to be tuned.

2.4 Stochastic Green function and canonical Worm algorithms

2.4.1 World-line representation

As mentioned before, the mapping of a D dimensional quantum system to a D+1 dimensional classical system with the additional dimension being the imaginary time is the foundation for the numerical methods we are using. One of the first algorithms developed to simulate the one-dimensional system of fermions or bosons was the world-line algorithm [60]. The world-line algorithm is the base of a whole family of algorithms to simulate quantum spins, bosons and fermions on a lattice. After mapping the quantum system to the classical one, the degrees of freedom correspond to the eigenvalues of

the number operator. The evolution of these variables is mapped out by the world-lines and thus offers an intuitive picture of the simulated system [61]. We take a closer look at this representation in the case of one dimension. The Hamiltonian in Eq. 2.3 can be broken up to a sum of two-site operators:

$$\mathcal{H} = \mathcal{H}_1 + \mathcal{H}_2 \tag{2.41}$$

where we choose

$$\mathcal{H}_1 = \sum_{i\,\text{odd}} \mathcal{H}_{i,i+1} \tag{2.42}$$

and

$$\mathcal{H}_2 = \sum_{i\,\text{even}} \mathcal{H}_{i,i+1} \tag{2.43}$$

so that the problem becomes a product of two-site problems and is easy to handle. Similarly as in DQMC, here one makes use of the Suzuki-Trotter decomposition:

$$e^{-\tau(\mathcal{H}_1+\mathcal{H}_2)} = e^{-\tau\mathcal{H}_1}e^{-\tau\mathcal{H}_2} + \mathcal{O}\left(\tau^2\right). \tag{2.44}$$

The standard recipe for the path integral as mentioned before is dividing the imaginary time span $[0, \beta]$ into L_τ subintervals $\tau = \beta/L_\tau$. By inserting a complete set of occupation states at each time slice one can represent the partition function as:

$$\mathcal{Z} = \sum_{i_1,\ldots,i_{2L_\tau}} \langle i_1|U_1|i_{2L_\tau}\rangle\langle i_{2L_\tau}|U_2|i_{2L_\tau-1}\rangle \times \langle i_{2L_\tau-1}|U_1|i_{2L_\tau-2}\rangle \cdots \langle i_2|U_2|i_i\rangle \tag{2.45}$$

where

$$U_{1(2)} = e^{-\tau\mathcal{H}_{1\,(2)}} = \prod_{i\,\text{odd (even)}} e^{-\tau\mathcal{H}_{i,i+1}}. \tag{2.46}$$

This decomposition leads to a checkerboard representation shown in Fig. 2.1 where within each time interval τ (or $\Delta\tau$ in the picture) both operators U_1 and U_2 are applied once.

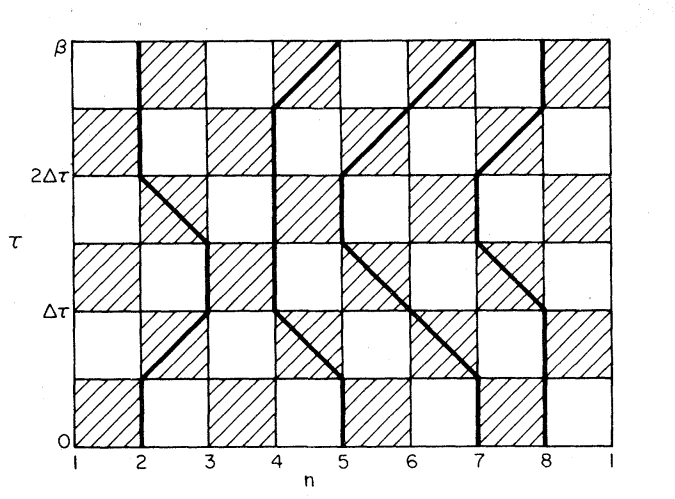

Figure 2.1: The shaded plaquettes of the space-imaginary time lattice denote the sites at which the operators $\mathcal{H}_{1\,(2)}$ act. At alternate half time-slices the hopping operators act either only between odd and even or even and odd sites. This is called checkerboard decomposition and the hopping is only allowed via the shaded plaquettes. Examples of allowed world-lines for fermions are drawn with thick lines. Figure taken from [60].

When the problem is cast into a classical one, what is left is to use the classical Monte Carlo machinery. Calculating the sum stochastically in Eq. 2.45 involves randomly generating fermion configurations using importance sampling and then accepting or rejecting them according to an algorithm of choice (for *e.g.* Metropolis or heat-bath). This representation was a big step towards modern QMC methods but it is strongly limited by the update scheme which is local. In addition, some observables cannot be measured in the world-line algorithm such as correlation functions represented by broken world-lines, *e.g.* the Green function. These limitations were dealt with in the algorithms that

introduce discontinuities into the world-lines, which will be discussed later.

In the case of fermions the many-body wave function is antisymmetric thus changes sign when two particles are exchanged. In the world-line formulation, this corresponds to the crossing of the world-lines which causes negative statistical weights to appear and the sign problem arises in the simulations of fermionic systems. In this case one is not able to perform the measurements since the averages are calculates as in Eq. 2.23 and when average sign is small the division of two small numbers is unstable numerically. The fermionic sign problem in algorithms based on world-lines is much more severe than in DQMC. Consequently, these algorithms are used only when there is no sign problem.

Further development of the world-line formulation led to the introduction of the continuous time algorithms where the Trotter error due to the imaginary time discretization is eliminated. In this case the useful decomposition of the partition function is related to the evolution operator in the interaction representation, see for *e.g.* [62]. First, one divides the Hubbard Hamiltionian into two parts: diagonal $\mathcal{V}$ (for example terms depending on number operator) and non-diagonal $\mathcal{T}$ (for example nearest neighbor hopping).

$$\mathcal{H} = \mathcal{V} + \mathcal{T} \tag{2.47}$$

Then, following Ref. [66] the partition function can be expanded in the form:

$$\mathcal{Z}(\beta) = \mathrm{Tr} \sum_{n=0}^{+\infty} \int_{0<\tau_1<\cdot<\tau_n<\beta} e^{-\beta\mathcal{V}} \mathcal{T}(\tau_n) \cdot \mathcal{T}(\tau_2)\mathcal{T}(\tau_1) d\tau_1 \cdot d\tau_n, \tag{2.48}$$

where $\mathcal{T}(\tau) = e^{\tau\mathcal{V}} \mathcal{T} e^{-\tau\mathcal{V}}$. Complete sets of occupation states $I = \sum_\Psi |\Psi\rangle\langle\Psi|$

need to be introduced between all operators $\mathcal{T}$. The partition function takes the form:

$$\begin{aligned}\mathcal{Z}(\beta) &= \sum \int_{0<\tau_1<\cdots<\tau_n<\beta} \langle\Psi_0|e^{-\beta\mathcal{V}}\mathcal{T}(\tau_n)|\Psi_{n-1}\rangle\langle\Psi_{n-1}|\mathcal{T}(\tau_{n-1})|\Psi_{n-2}\rangle \\ &\cdots \langle\Psi_k|\mathcal{T}(\tau_k)|\Psi_{k-1}\rangle\cdots\langle\Psi_2|\mathcal{T}(\tau_2)|\Psi_1\rangle\langle\Psi_1|\mathcal{T}(\tau_1)|\Psi_0\rangle d\tau_1\cdots d\tau_n,\end{aligned} \tag{2.49}$$

where the sum is over all possible configurations of the time indices τ and states $\{|\Psi_k\rangle\}$. The matrix elements can be written as:

$$\langle\Psi_k|\mathcal{T}(\tau)|\Psi_l\rangle = e^{\tau \mathrm{V}_k}\langle\Psi_k|\mathcal{T}|\Psi_l\rangle e^{-\tau \mathrm{V}_l} \tag{2.50}$$

where V_k is the eigenvalue of $\mathcal{V}$ in the eigenstate $|\Psi_k\rangle$ since we use the occupational basis which is the eigen basis for the diagonal operator $\mathcal{V}$. We can look at this representation as world-lines in the continuous imaginary time. We take here the example of one species on a one-dimensional lattice in a model where $\mathcal{T}$ is just the nearest-neighbor hopping. In Fig. 2.2 (left) a graphical representation is shown for a particular configuration. At imaginary time $\tau = 0$ one starts with a state $|\Psi_0\rangle$ (chosen randomly) and this state evolves according to the operator $e^{\tau_1 \mathrm{V}_0}$. When the first time slice τ_1 is reached the $\mathcal{T}$ operator acts on the state and creates a sum of few states. However only the state $|\Psi_1\rangle$ will give a non-zero matrix element and thus survives. This state is now the new state and evolves according to $e^{-(\tau_2-\tau_1)\mathrm{V}_1}$ until it reaches the time slice τ_2. This procedure continues until the time β is reached. One can see that the world-lines are periodic in the imaginary time direction with period β which comes from the appearance of the trace in the formula. In

this representation the partition function is expressed as a "path integral" and consists of a sum over all possible deformations of N world-lines if the system consists of N particles.

2.4.2 Stochastic Green Function

The general goal for the numerical methods we describe here is to sample the partition function given in Eq. 2.49. Different algorithms have been developed to achieve this. The worm algorithm was introduced first by Prokof'ev and Svistunov in [63, 64]. Then a canonical worm algorithm was developed by Van Houcke, Rombouts and Pollet [65]. Based on the Canonical Worm algorithm, the Stochastic Green Function (SGF) algorithm was derived by V. G. Rousseau [66, 67]. We start with the Stochastic Green Function algorithm because its formulation is very general.

In order to sample the partition function one introduces a Green operator $\mathcal{G}$ at an imaginary time slice τ.

$$\mathcal{Z}(\beta,\tau) = \mathrm{Tr}\,\left(e^{-(\beta-\tau)\mathcal{H}}\mathcal{G}e^{-\tau\mathcal{H}}\right) \tag{2.51}$$

As a result an extended partition function can be written as follows:

$$\begin{aligned}\mathcal{Z}(\beta,\tau) = \sum \int_{0<\tau_1<\cdots<\tau_n<\beta} & \langle\Psi_0|e^{-\beta\mathcal{V}}\mathcal{T}(\tau_n)|\Psi_{n-1}\rangle\langle\Psi_{n-1}|\mathcal{T}(\tau_{n-1})|\Psi_{n-2}\rangle \\ \cdots\ & \langle\Psi_{L+1}|\mathcal{T}(\tau_L)|\Psi_L\rangle\langle\Psi_L|\mathcal{G}(\tau)|\Psi_R\rangle\langle\Psi_R|\mathcal{T}(\tau_R)|\Psi_{R-1}\rangle \\ \cdots\ & \langle\Psi_2|\mathcal{T}(\tau_2)|\Psi_1\rangle\langle\Psi_1|\mathcal{T}(\tau_1)|\Psi_0\rangle d\tau_1\cdots d\tau_n.\end{aligned} \tag{2.52}$$

The states directly before and after the insertion of the Green operator are

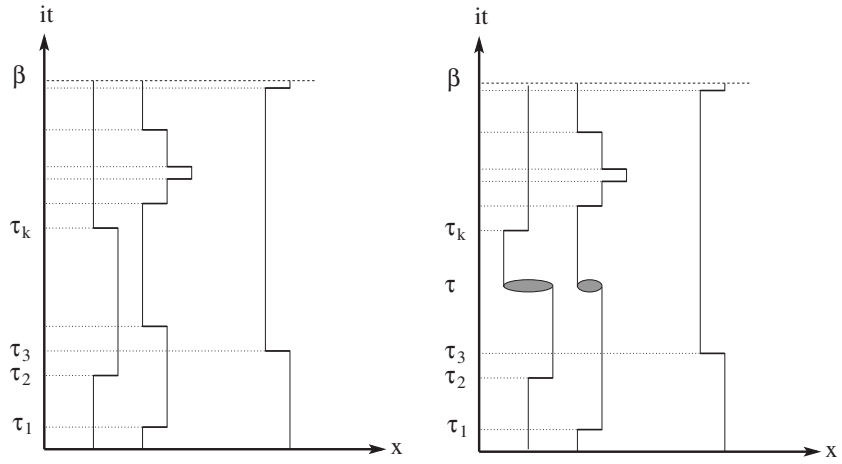

Figure 2.2: Particular set of time indices τ_i and states $|\Psi_k\rangle$ for the partition function (left) and the extended partition function (right). Figure taken from [66].

called $|\Psi_R\rangle$ (to the right of $\mathcal{G}$) and $|\Psi_L\rangle$ (to the left of $\mathcal{G}$). Similarly τ_R and τ_L is the time slice to the right and to the left of the Green operator when $\mathcal{T}$ acts. The time-dependent Green operator is $\mathcal{G}(\tau) = e^{\tau\mathcal{V}}\mathcal{G}e^{-\tau\mathcal{V}}$. The Green operator is used to sample the partition function by updating its configurations. To define this operator one needs the normalized creation and annihilation operators:

$$\mathcal{A}^\dagger = a^\dagger \frac{1}{\sqrt{\hat{n}+1}} \qquad \text{and} \qquad \mathcal{A} = \frac{1}{\sqrt{\hat{n}+1}} a \tag{2.53}$$

which create or annihilate one particle without changing the norm of the state

$$\mathcal{A}^\dagger|n\rangle = |n+1\rangle \quad , \quad \mathcal{A}|n\rangle = |n-1\rangle \quad \text{and specifically} \quad \mathcal{A}|0\rangle = 0. \tag{2.54}$$

The Green operator is taken to have the following form:

$$\mathcal{G} = \sum_{p=0}^{+\infty}\sum_{q=0}^{+\infty} g_{pq} \sum_{\{i_p|j_q\}} \prod_{k=1}^{p} \mathcal{A}_{i_k}^\dagger \prod_{l=1}^{q} \mathcal{A}_{j_l}, \tag{2.55}$$

where g_{pq} is the martix that defines the Green operator. The state $|\Psi_L\rangle$ is created by the application of the $\mathcal{G}$ on $|\Psi_R\rangle$ in such a way that on sites $\{i_p\}$ p particles are created and on sites $\{j_q\}$ q particles are annihilated. The notation $\{i_p|j_q\}$ makes sure that there are no cancellations between the anihilation and creation operators as it denotes two subsets of site indices with the condition that all indices i_p are different from all j_p. An example of the insertion of the Green operator is illustrated in Fig. 2.2 (right) where two particles jump, without restriction to only nearest neighboring sites.

The updates are done according to the following general outline. First the direction of propagation of the $\mathcal{G}$ is chosen with some probability $P(\rightarrow)$ or $P(\leftarrow)$. Then with probability $P^{\dagger}_{\rightarrow}(\tau)$ and $P^{\dagger}_{\leftarrow}(\tau)$ a new operator $\mathcal{T}$ is inserted to the right or to the left of the Green operator and if the move is accepted there appears an intermediate state $|\psi\rangle$ with probability $P(\psi)$.

In order to measure physical quantities which are diagonal operators in this representation, the Green operator has to reach a diagonal configuration where $|\Psi_L\rangle = |\Psi_R\rangle$. On the other hand, measurements of the Green functions are performed when the configurations are not diagonal. In this case the measurement is finished when the system goes to the diagonal configuration. The matrix g_{pq} is chosen to ensure that the Green operator goes back to a diagonal configuration. To this end g_{pq} has to decrease sufficiently fast with increasing p and q so that the state $|\Psi_L\rangle$ is not too different from $|\Psi_R\rangle$. Depending on the measurement one is interested in making during the simulation, the appropriate choice for g_{pq} can be made. For example in our situation we are interested in measuring the pair Green functions, a choice of g_{pq} that provides

good statistics for this measurement is

$$g_{pq} = \begin{cases} 1 & \text{if } p+q \leq 4 \\ e^{-4(4-p-q)^2} & \text{if } p+q > 4 \end{cases} \tag{2.56}$$

The partition function is calculated by performing the sum over the states stochastically. The Monte Carlo now consists of making the updates, accepting or rejecting and satisfying the detailed balance. Take the probability of initial (final) configuration to be $P_i\,(P_f)$ and the probability of the transition from initial to final configuration $S_{i\to f}$ (analogously $S_{f\to i}$ for the reverse transition). Acceptance rate for the transition from initial to final is denoted by $A_{i\to f}$ and $A_{f\to i}$ for the reverse. Using this notation, detailed balance is described by

$$P_i S_{i\to f} A_{i\to f} = P_f S_{f\to i} A_{f\to i}. \tag{2.57}$$

The Metropolis solution [68] is chosen to determine the acceptance rate:

$$A_{i\to f} = \min(1, q) \qquad \text{where} \qquad q = \frac{P_f S_{f\to i}}{P_i S_{i\to f}} \tag{2.58}$$

Detailed balance is ensured by the choice of the acceptance ratios for the suggested updates. The details of the choice of the acceptance rates are beyond the scope of this thesis, for more details refer to [66]. A more efficient directed update scheme was devised and described in [67].

As the Green operator is sampled stochastically and measurements are performed on randomly selected Green functions this algorithm was given the name Stochastic Green Function. The generality of this algorithm can cause it to be slower than other methods when applied to simpler models, however

the generality is also its main advantage. It has been formulated in a way that can be applied to different Hubbard Hamiltonians including for *e.g.* mixtures of atoms and molecules and with conversion terms from atoms to molecules. Its main advantage is the possibility to measure n-body Green functions easily, since when $\mathcal{G}$ is in some configuration the corresponding Green function can be measured.

The SGF algorithm can be used both in the grand canonical or canonical modes. From its definition, the Green operator contains terms that do not conserve the number of particles. However if the Hamiltonian commutes with the operator that measures the total number of particles, $\hat{\mathcal{N}}$, for example the Hamiltonian in Eq. 2.5, then only conservative terms of $\mathcal{G}$ have non vanishing contributions since the trace imposes the same number of particles both at the begining and the end of the operator string. As a consequence, the number of particles remains strictly constant and the SGF algorithm works in the canonical ensemble by nature. However, a simple trick can be used in order to simulate exactly the grand-canonical ensemble. The idea is to add a non conservative part $\hat{\mathcal{H}}_{\text{nc}}$ to the Hamiltonian,

$$\hat{\mathcal{H}}_{\text{nc}} = \gamma \sum_j \left(c_j^\dagger + c_j\right), \tag{2.59}$$

where γ is an optimization parameter, and allows the Green operator to insert at most one $\hat{\mathcal{H}}_{\text{nc}}$ operator in the string. This allows the number of particles to fluctuate, while the addition of the usual term $-\mu\hat{\mathcal{N}}$ to the Hamiltonian determines the mean number of particles via the chemical potential μ. When measuring physical quantities, ignoring configurations in which the operator string contains a $\hat{\mathcal{H}}_{\text{nc}}$ operator, corresponds to integrating over these config-

urations the probability of going from a given configuration with N particles and no $\hat{\mathcal{H}}_{\rm nc}$ to another one with M particles and no $\hat{\mathcal{H}}_{\rm nc}$, via intermediate configurations with $\hat{\mathcal{H}}_{\rm nc}$. This integrated probability corresponds exactly to the probability of going from one configuration with N particles to another one with M particles. As a result, the configurations of the grand-canonical partition function Tr $e^{-\beta(\hat{\mathcal{H}}-\mu\hat{N})}$ are generated with the correct Boltzmann weight.

To use this algorithm to simulate fermions in one dimension, we first use the Jordan-Wigner transformation (see for *e.g.* [69]) to map the system onto a system of hard core bosons. Consequently, this algorithm does not suffer from the sign problem but, clearly, it cannot be used in higher dimensions where the Jordan-Wigner transformation fails to solve the sign problem. This transformation has the effect that the number of fermionic particles we can simulate is limited to odd numbers. We used this algorithm in the canonical ensemble mainly for the confined system where it is very convenient to control the populations directly rather than tune the chemical potentials. A typical simulation for $L = 120$ and $\beta = 32$ runs for about 5 days on a desktop computer and yields an error of the order of 0.5% for the peak of the pair momentum distribution.

2.4.3 Canonical Worm algorithm

The Green operator is in fact a generalization of the Worm operator introduced in the Worm algorithm [63]. It is based on the idea of inserting two world-line discontinuities (worm's head and worm's tail) and propagating them to change

the configurations. The extended partition function in this case has the form:

$$\mathcal{Z}(\beta,\tau) = \mathrm{Tr}\,\left(W^{\dagger}e^{-\tau\mathcal{H}}We^{-(\beta-\tau)\mathcal{H}}\right) \tag{2.60}$$

we can see that the operators W and $W^{\dagger}$ can be separated by an imaginary time interval. When after some Markov steps the discontinuities are removed ("head of the worm bites its tail") then such a configuration contributes to the sampling as one knows that is was generated according to the distribution $\mathrm{Tr}(e^{-\beta\mathcal{H}})$. Since this algorithm is non-local in imaginary time one can imagine a situation in which the worm head makes the loop in the imaginary time with respect to the tail and this results with insertion or removal of a particle.

As mentioned before a canonical version of this algorithm was introduced by Van Houcke, Rombouts and Pollet in [65]. In this case the worm operator is local in imaginary time and samples the partition function keeping the particle number fixed (canonical ensemble). Inserting the worm operator at time τ leads to the extended partition function:

$$\mathcal{Z}(\beta,\tau) = \mathrm{Tr}\,\left(e^{-\tau\mathcal{H}}\mathcal{A}e^{-(\beta-\tau)\mathcal{H}}\right). \tag{2.61}$$

Here $\mathcal{A}$ the worm operator updates the configurations while sampling the extended partition function. The worm operator is inserted at imaginary time τ and suggests a creation of operator $\mathcal{T}$. One constraint on the generality of this algorithm is that the worm operator $\mathcal{A}$ has to be chosen in such a way that it commutes with the non-diagonal part of the Hamiltonian $[\mathcal{A},\mathcal{T}] = 0$. There will thus exist different choices for the form of the worm operator depending on the non-diagonal term in the Hamiltonian.

For example to study a system of ultra-cold bosons on an optical lattice

described by the Bose-Hubbard model where

$$\mathcal{V} = \frac{U}{2}\sum_i n_i(n_1 - 1) \qquad \text{and} \qquad \mathcal{T} = t\sum_{<i,j>} b_i^\dagger b_j \tag{2.62}$$

the worm operator used has the following form:

$$\mathcal{A} = \frac{1}{N}\sum_i n_i + \sum_{i\neq j} b_i^\dagger b_j \tag{2.63}$$

where N is the total number of particles. If the worm operator is chosen with constant diagonal terms (*i.e.* $\langle\Psi_k|\mathcal{A}|\Psi_k\rangle = const.$ for all $|\Psi_k\rangle$) then the canonical partition function with particle-number projected trace $\mathrm{Tr}_N\left(e^{-\beta\mathcal{H}}\right)$ is proportional to the sum of the weights of the diagonal configurations. By sampling those configurations the canonical ensemble is sampled, thus the name of the algorithm: Canonical Worm.

The fact that in the worm algorithm only one discontinuity is introduced to the world-line allows only for 1-body Green functions to be measured. We have however used this algorithm to simulate the imbalanced mixtures of fermions with different masses in 1D and calculate pair Green functions. In the case of two species there are two worm operators introduced and propagated, one for each species. The pair Green function (2-body Green function) can thus be measured. Thanks to the fact that the algorithm is local in imaginary time *i.e.* the worm head and tail are propagated simultaneously the measurements of equal-time Green functions are very efficient. It is however not possible to measure the Green functions separated in imaginary time and thus to study dynamics (by performing the $i\tau \to t$ rotation). Analogously to the situation in SGF one can study systems of fermions in 1D while simulating hard-core

bosons and making use of the Jordan-Wigner transformation. In the case of the CW algorithm is has been shown in [70] that it can be applied to a system of hard-core bosons.

We used this algorithm to study the mixture of fermions with different masses in one dimension. Typical run took a day on a desktop computer.

2.5 Canonical vs Grand Canonical

Finally, we consider the question of canonical versus grand canonical ensembles. It has been suggested [71, 40] that the stability of BCS, FFLO or BP phases can depend on whether one fixes the populations or the chemical potentials. It is important to compare the results obtained using canonical and grand-canonical ensembles since in our work we use both depending on the algorithm of choice for the given problem. During our work on the mass imbalance system [72] we used the canonical Worm algorithm for the one-dimensional system, where N_1 and N_2 are kept strictly fixed. In finite temperature studies of 1D system [73] we worked in both ensembles and used the grand-canonical DQMC as well as both canonical and grand-canonical versions of SGF algorithm. The study of the 2D system [74] was done in the grand-canonical ensemble where the populations are fixed by choosing the chemical potential.

We compare in Fig. 2.3 typical results for the momentum distributions obtained with the CW and the DQMC algorithms with μ_1 and μ_2 chosen to give average fillings corresponding to the fixed fillings in the canonical case. There is no disagreement between the two; in particular, the signature of the FFLO phase, a peak in the pair momentum distrubution at $k \neq 0$, is seen

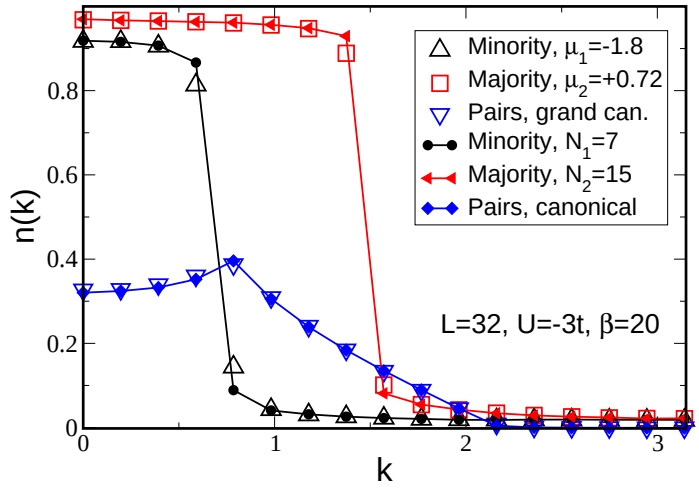

Figure 2.3: Momentum distributions for the minority, majority and pair populations using canonical and grand canonical QMC with $t_1 = t_2$. In the grand canonical case, $\langle N_1 \rangle = 6.996\,(\mu_1 = -1.8)$, $\langle N_2 \rangle = 14.949\,(\mu_2 = +0.72)$.

to be stable whether one fixes the populations or the chemical potentials. Whatever $\langle N_1 \rangle$ and $\langle N_2 \rangle$ one has obtained by fixing μ_1 and μ_2, one will obtain the same physics in the canonical ensemble by fixing the populations to the corresponding values, as seen in Fig. 2.3. One is free to study these phases and their stability in either ensemble.

As part of our code verification, the grand canonical SGF and DQMC were compared for the same parameters and found to yield the same results within the error bars. Furthermore, we verified that DQMC and grand canonical SGF both agreed with the canonical SGF when the chemical potentials in the grand canonical cases were tuned to give the same populations as the canonical cases.

The results we have obtained for the one-dimensional system were obtained with these three algorithms; the choice being dictated by the specific measurement we were after. Because of the equivalence of the three algorithms, we do not comment on which results were obtained with which algorithm. The study of the 2D system was carried out exclusively using DQMC.

2.6 Summary

In this chapter we have introduced the numerical methods used in this thesis. We study the Hubbard model and thus restrict ourselves to lattice systems. The Determinant Quantum Monte Carlo algorithm that we used both in one and two dimensions is presented with the Hubbard-Stratonovich field decoupling the interaction term in the Hamiltonian. The algorithms based on the world-line formulation such as Canonical Worm and Stochastic Green Function are briefly introduced, as they have been used to study the one-dimensional system of fermions. Finally we compare the results obtained using the grand-canonical and canonical ensembles to find that they are equivalent.

Part I

One dimensional system

Chapter 3

Low temperature properties of the system in 1D

3.1 Introduction

One-dimensional systems have been the focus of intense theoretical studies as they can exhibit exotic phenomena due to strong correlations, quantum fluctuations, nesting of Fermi surfaces, *etc.* In this part of the thesis we study the one-dimensional system of a population imbalanced Fermi gas on a lattice. At the time when this thesis work was initiated, the consensus had not yet been reached about the actual ground state of a imbalanced populations Fermi mixture with attractive interaction. The discussions revolved around the question of which pairing mechanism would be realized in the system: Breached Pairing or FFLO? Another important issue being debated was the question of stability of those phases for example with respect to temperature and dimensionality. Calculations based on mean-field theory performed for uniform and trapped systems using local density approximation [37, 41] showed that the

FFLO phase dominates the phase diagram for the untrapped case and that phase separation appears when system is confined. In a quasi-one-dimensional system studied using bosonisation techniques, Yang [75] found that a 1D analog of the FFLO state is the ground state of a Fermi gas interacting attractively with imbalanced spin population. An exact analytical solution using the Bethe ansatz was found by Orso [43] for a system in a trap, where he also discovered a superfluid core in the cloud exhibiting FFLO-type pairing. In the meantime extensive exact numerical work for the 1D system using Quantum Monte Carlo (QMC) [76, 77] and the Density Matrix Renormalization Group (DMRG) [78, 26, 79, 80, 81] and approximate numerical work using variants of Dynamical Mean Field Theory (DMFT) [82] have demonstrated that, in the ground state, population imbalance leads to a robust FFLO phase over a very wide range of polarization and interaction strengths. In addition, it was shown to be stable in quasi-one dimensional geometries, *i.e.* in the case of an elongated trap [83, 84].

In this chapter we focus on low temperature studies of pairing in a one dimensional system when the populations of Fermions are imbalanced. To begin with, we look at the case without harmonic confinement, also called in this thesis the uniform or homogenous case. We then follow with a discussion of the system in a harmonic trap. The main result here is that FFLO-type pairing is very robust and according to our results the dominant pairing mechanism. It is shown that the pair Green function exhibits oscillations in real space characteristic of the pair density wave. As a result the pair momentum distribution exhibits a peak at non-zero momentum which corresponds to the difference between the Fermi momenta of each species.

The lower the temperature of interest, the larger the value of β and, conse-

quently, the longer the imaginary time direction gets. In practice this means that one dimension of the system becomes very large and this can cause difficulties in simulations due to increased cost in computational power. As a rule of thumb gained from experience in QMC simulations when $\beta = 2L$ the temperature is low enough for the system to sample predominantly the ground state. We follow this rule, yet we still verify it occasionally by doing simulations at lower temperatures and comparing the results. The results shown here for the uniform system were published in [76] and [85].

In our studies of a one-dimensional system we looked at the mixture of two species of fermions on a lattice. The focus of our studies was the situation when the populations of the two species are unequal. To describe the system we use the Hubbard model with different chemical potentials for each species (μ_1 and μ_2) and by changing their ratio the imbalance is tuned. This is the case in the grand-canonical formulation. In the canonical ensemble there is no chemical potential term in the Hamiltonian. To provide insight into an experimentally realizable setup we also studied harmonically confined system.

The Hubbard Hamiltonian of such a lattice system in one dimension is:

$$\begin{aligned}\mathcal{H} = -t\sum_{i\,\sigma}(c^{\dagger}_{i\,\sigma}c_{i+1\,\sigma} + c^{\dagger}_{i+1\,\sigma}c_{i\,\sigma}) - \sum_{i}(\mu_1\hat{n}_{i\,1} + \mu_2\hat{n}_{i\,2}) \\ +U\sum_{i}\left(\hat{n}_{i\,1} - \frac{1}{2}\right)\left(\hat{n}_{i\,2} - \frac{1}{2}\right) \\ +V_T\sum_{i}\left(x_i - \frac{L}{2}\right)^2(\hat{n}_{i\,1} + \hat{n}_{i\,2})\,. \qquad (3.1)\end{aligned}$$

The energy scale is set by taking the hopping parameter $t = 1$. The contact interaction strength U is negative since we are interested in pair formation in the attractive model. The last term describes the harmonic trap which is

centered at the midpoint, $L/2$, of the L-site lattice. By setting $V_T = 0$ one can still study a translationally invariant system. In all our studies we apply periodic boundary conditions. Lattice spacing is equal to unity by which the momentum space lattice spacing is set to $\frac{2\pi}{L}$. Since we are studying mainly the systems where the number of particles of each species are not equal, one can treat it as introducing polarization in the system. Polarization is then defined by,

$$P = \frac{N_1 - N_2}{N_1 + N_2}, \tag{3.2}$$

where N_1 (N_2) is the majority (minority) population and $N = N_1 + N_2$ is the total number of particles.

The Fermi momentum that can be calculated from the non-interacting description of the system is a useful quantity also in the interacting case of interest. In 1D where $\frac{2\pi}{L}$ is the reciprocal lattice spacing the Fermi momentum is:

$$k_{F\sigma} = \frac{N_\sigma - 1}{2} \cdot \frac{2\pi}{L} \tag{3.3}$$

and in the case of large particle number can be approximated to $k_{F\sigma} = \frac{N_\sigma \pi}{L}$. The Fermi energy and Fermi temperature are found from the equation

$$E_F = t k_F^2 = k_B T_F. \tag{3.4}$$

We will take $k_B = 1$ and we usually calculate T_F for balanced system where $N_\sigma = N_{tot}/2$.

In the harmonically trapped system the non-interacting Fermi momentum is calculated from the distribution of the Fermions over the harmonic levels with energies $E_n = \hbar\omega(n + \frac{1}{2})$. The trapping frequency can be calculated from

$\frac{1}{2}m\omega^2 = V_T$ using $m = \frac{\hbar^2}{2t}$ to get $\omega = \frac{2}{\hbar}\sqrt{V_T t}$. The Fermi energy is then given by:

$$E_F = \hbar\omega(N + \frac{1}{2}) \tag{3.5}$$

where N can be taken as N_σ or $N_{tot}/2$.

3.2 System without the trap

3.2.1 Unpolarized mixture of Fermions

To set the stage we look at a balanced mixture of fermions without interactions. The Green function and its Fourier transform are calculated for $T = 0$ to get the momentum distribution shown in Fig. 3.1.

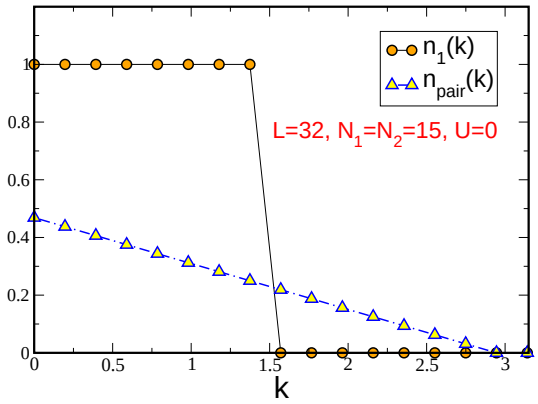

Figure 3.1: Momentum distribution of particles and pairs in the mixture of fermions without interaction and when number of particles of each species is equal.

It is useful to recall the definitions of the Green functions here. The single particle Green function is given by:

$$G_\sigma(i,j) = \langle c_{i\,\sigma} c^\dagger_{j\,\sigma} \rangle \tag{3.6}$$

and the pair Green function by:

$$G_{\text{pair}}(i-j) = \langle \Delta_i^\dagger \, \Delta_j \rangle \tag{3.7}$$

where the pair creation operator is $\Delta_i^\dagger = c_{i\uparrow}^\dagger c_{i\downarrow}^\dagger$.

One can see in Fig. 3.1 the famous Fermi distribution of the particles denoted with circles. Since there is no interaction there is no pairing in the system, however the pair momentum distribution (triangles) has a residual non-zero value which is easy to understand. In the non-interacting system the pair Green function factorizes:

$$\begin{aligned} G_{\text{pair}}(|i-j|) &= \langle c_{i\downarrow}^\dagger c_{i\uparrow}^\dagger c_{j\uparrow} c_{j\downarrow} \rangle = \langle c_{j\downarrow} c_{i\downarrow}^\dagger c_{j\uparrow} c_{i\uparrow}^\dagger \rangle = \langle c_{j\downarrow} c_{i\downarrow}^\dagger \rangle \langle c_{j\uparrow} c_{i\uparrow}^\dagger \rangle \\ &= G_\downarrow(i-j) \cdot G_\uparrow(i-j). \end{aligned} \tag{3.8}$$

We use the known convolution theorem and the fact that the momentum distribution of free Fermions at zero temperature in 1D is a Fermi step:

$$\begin{aligned} n_{\text{pair}}(k) &= \mathcal{FT}\left(G_{\text{pair}}(i-j)\right) = \mathcal{FT}\left(G_\downarrow(i-j) \cdot G_\uparrow(i-j)\right) \\ &= \mathcal{FT}\left(G_\downarrow(i-j)\right) * \mathcal{FT}\left(G_\uparrow(i-j)\right) = n_\downarrow(k) * n_\uparrow(k) \\ &= \Theta(k-k_{F\downarrow}) * \Theta(k-k_{F\uparrow}). \end{aligned} \tag{3.9}$$

The Fermi momentum in 1D is $k_{\text{F}} = \frac{N-1}{2}\frac{2\pi}{L}$ where N is the number of particles in the species and L is the number of sites of the lattice. A convolution of two Heaviside step fuctions with the same width gives exactly the function depicted with triangles in Fig. 3.1.

In order to study the effect of interactions on the basic quantities that characterize the system, we first examine the balanced population mixture

with attractive on-site interactions between different species. In figures 3.2 and 3.3 the Fourier transforms of the Green functions are shown for different interaction strengths. The single particle Green function in momentum

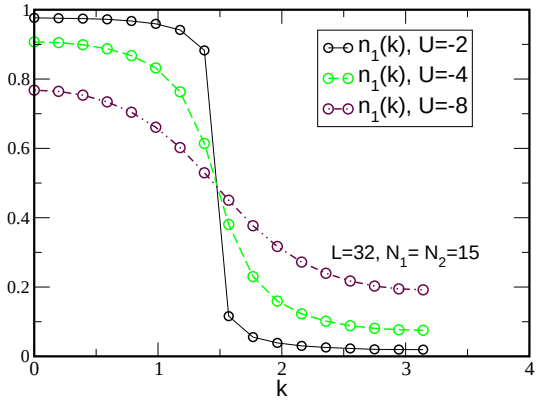

Figure 3.2: Momentum distribution of fermions for several attractive interaction strengths U.

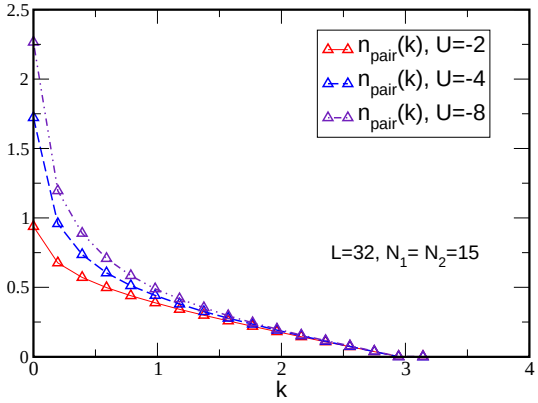

Figure 3.3: Momentum distribution of pairs in the mixture of fermions with equal number of particles in each species for several attractive interaction strengths U.

space, *i.e.* the momentum distribution of fermions, $n_1(k)$ in Fig. 3.2 exhibits a sharp Fermi surface for low interaction. Increased interaction strength U has a rounding effect, which is very similar to the effect of increasing the temperature. One should also notice the depletion of the Fermi "sea", by which we

mean that with increasing interaction the filling drops much below $n_1(k) = 1$ for $k \leq k_{F1}$. In this situation, interactions among particles inside the Fermi "sea" are allowed. The pair momentum distribution exhibits a peak at $k = 0$ (Fig. 3.3) which signals formation of pairs whose center of mass is at rest. With increasing interaction strength $|U|$, the pairs are more tightly bound and their number increases illustrated by the peak becoming higher. This peak at $k = 0$ momentum is characteristic of BCS pairing and corresponds to a quasi-condensate of pairs, since, as it is well known, the condensation does not happen in one-dimensional systems.

3.2.2 Polarized mixture of fermions

We now turn to study a mixture of unequal number of fermions in each species in one dimension and at a low temperature. The pair Green function in real space shown in Fig. 3.4 reveals oscillations as a function of distance, which are characteristic of the FFLO-type pairing that occurs in the system. One observes that in the balanced populations case ($P = 0$) the correlations decay monotonically but when the system is polarized ($P \neq 0$) oscillations appear. The modulations signal the appearance of spatial inhomogeneities in the system in the form of regions that are rich in pairs neighboring regions depleted in pairs but rich in the excess majority population. It has been shown that when the order parameter oscillates, the excess particles are mostly found in its nodal regions [86]. What is observed is that imbalance in populations causes mismatch in Fermi momenta and leads to pairing with finite center of mass momentum the consequence of which are the oscillations in the pairing amplitude. It is clear from Fig. 3.4 that the larger the polarization, thus the mismatch between the Fermi momenta ($|k_{F1} - k_{F2}|$), the shorter the os-

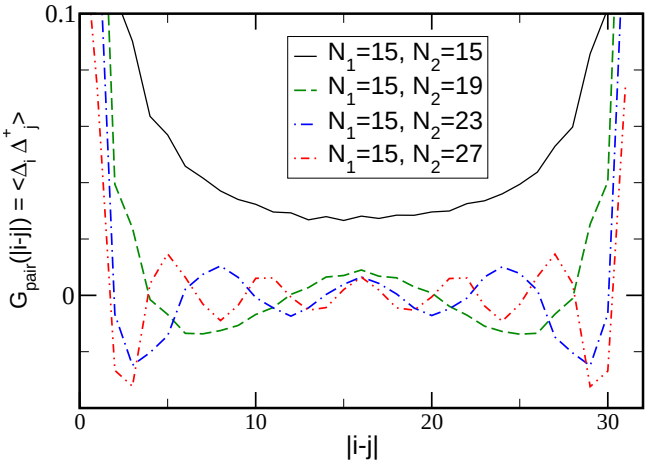

Figure 3.4: Pair Green function $G_{\text{pair}}(|i-j|)$ in the real space of balanced and imbalanced populations of a Fermi mixture with $U = -8$. Figure from [76].

cillation period T. One can see that the pair Green function oscillates with period $T = \frac{2\pi}{|k_{F1}-k_{F2}|}$ *i.e.* wavelength $\lambda = \frac{2\pi}{|k_{peak}|}$. The modulations follow the form presented by Larkin and Ovchinnikow in [8] where the order parameter oscillates according to $\Delta(r) = \Delta 2\cos(\mathrm{k}\cdot\mathrm{q})$ as a function of position r with $q = \pm|k_{F1} - k_{F2}|$.

In momentum space, the oscillations show up as a peak in the pair momentum distribution at a non-zero momentum ($k_{peak} \neq 0$)as can be seen in Fig. 3.5. It is important to notice that $n_{pair}(k)$ has always a peak at $\pm|k_{F1} - k_{F2}|$ for the two different interaction strength considered. With increased interaction (right panel), both the pairing at $k \neq 0$ and $k = 0$ increase. The momentum at which the pair momentum distribution is peaked is the momentum of the center of mass of the majority of pairs formed. Interestingly the Fermi surfaces are much more sharply defined than their $P = 0$ counterparts (see Fig. 3.2) for similar interaction strength. Additionally a deformation of the momentum distribution of the majority population develops in the form of a bump in $n_2(k)$ for $k > k_{F1}$. It seems that as U becomes more attractive and pairing

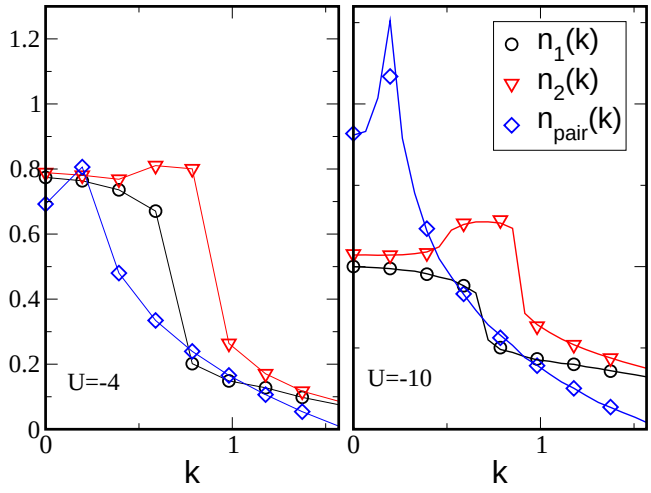

Figure 3.5: Single particle ($n_1(k)$ and $n_2(k)$) and pair momentum distributions ($n_{\text{pair}}(k)$) in an imbalanced system with polarization $P = 0.125$ shown for different interaction strength $U = -4$ (left) and $U = -10$ (right) for two different system sizes $L = 32$, $\beta = 64$ (symbols) and $L = 96$, $\beta = 192$ (lines). Only $k > 0$ is shown since the figures are symmetric.

is allowed in the Fermi sea. the minority and majority Fermi surfaces begin to try to match with each other. The excess particles are pushed out to the states with momenta higher than the Fermi momentum of the minority, but are still trying to minimize the kinetic energy by occupying the lowest possible momentum states thus forming a bump in the $n_2(k > k_{F1})$. This feature is very robust at high negative U and is not a finite size effect. In order to rule out the finite size effects another simulation was done for a $L = 96$ and the results are displayed with a continuous line. One can observe in Fig. 3.5 the increase in the height of the peak which signals the increase in the population in the quasi-condensate of pairs.

In order to better characterize the phase of the system, we studied the finite size scaling of the height of the peak of the pair momentum distribution. To see that the peak is a signature of a quasi-condensate of pairs, we simulate

the system at fixed densities but bigger lattices. For the balanced case at half-filling we plot the quasi-condensate fraction - in our case the height of the peak normalized by the total number of particles $n_{pair}(k=0)/N_{tot}$. Data shown in Fig. 3.6 indicate that the height of the peak is decreasing slowly towards zero and that it appears to follow a power law. Since in order to study the ground state β must be increased as the system size increases, it becomes very difficult to obtain reliable numerical results for large systems. This makes it hard to determine this exponent accurately. We also tried to look at the scaling with

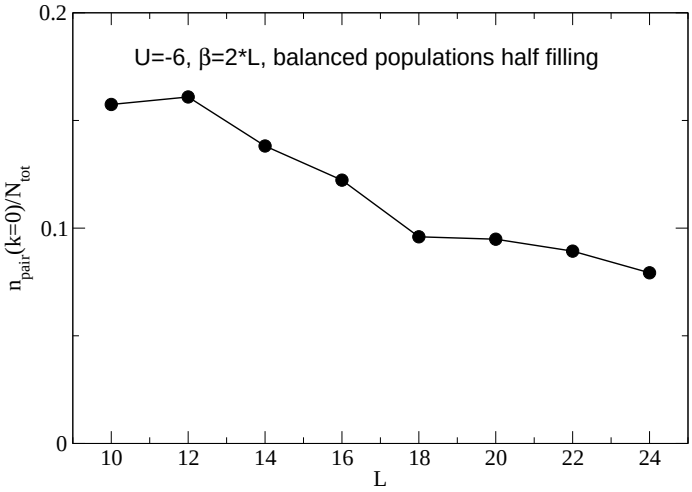

Figure 3.6: Finite size scaling of the fraction of the quasi-condensate of pairs as a function of the increasing system size L, at $\beta = 2L$ and $U = -6$.

the system size of the FFLO peak in the case of imbalanced populations. From the data we have acquired from the grand-canonical algorithm by tuning the chemical potentials to maintain constant densities for different sizes, we find that the quasi-condensate fraction decreases as expected, however we were not able to get good enough data to determine accurately the exponent. The simulations are hard with the canonical algorithm since we can only simulate odd numbers of particles, thus scaling with system size quickly requires simulations

of lattice sizes that we cannot handle.

To underline the robustness of the FFLO pairing, we present the pair momentum distribution for a range of polarizations as shown in Fig. 3.7. The

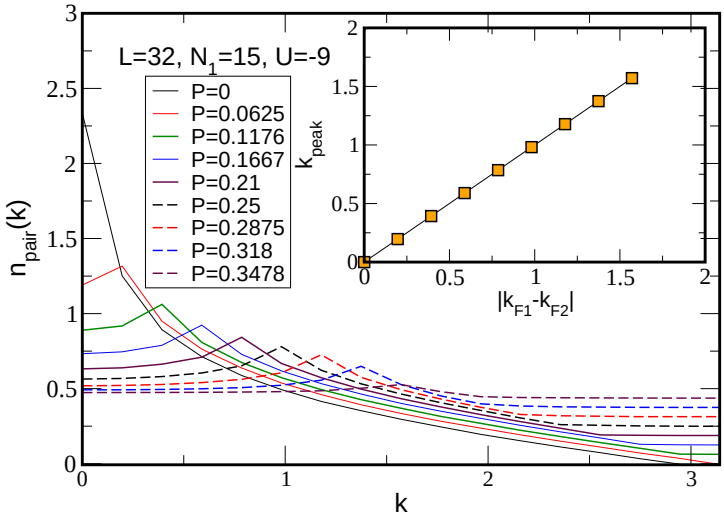

Figure 3.7: Pair momentum distributions ($n_{\text{pair}}(k)$) for several polarizations P and $U = -9$. The inset shows that the position of the FFLO peak is equal to $|k_{F1} - k_{F2}|$.

main observation is that with increasing polarization, the FFLO peak shifts to higher momenta. In other words the bigger the imbalance between the Fermi species the higher the center of mass momentum of the pair. It is clear from the inset that the location of the peak is equal to $k_{peak} = |k_{F1} - k_{F2}|$ as predicted in the FFLO scenario. Even for the highest polarizations the FFLO peak is still present which leads us to conclude that we have not found the Clogston-Chandrasekhar limit [87, 88] at which the external magnetic field polarizes the system to the point of complete destruction of the superconducting state. This could be related to the fact that in our calculations presented in this part of the thesis, we have a fixed number of particles and we do not include any term that could mimic the effect of magnetic field. It is important to report that

the peak forms at $k \neq 0$ even for the smallest $|U|$ we used in the simulations. For example, for the case of $P = 0.125$ in Fig. 3.5, FFLO pairing is observed for attraction as low as $U = -0.5$.

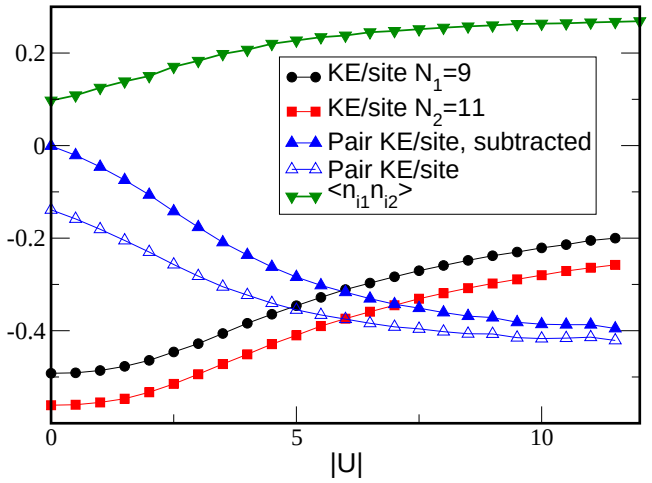

Figure 3.8: Kinetic energy per site for each species and for the pairs as a function of $|U|$ and double occupancy.

Further insight into the subject of pairing is gained by looking at the energy. For each species, the kinetic energy (KE) per site is the average of the nearest-neighbor hopping calculated as $\langle c^{\dagger}_{i+1\,\sigma} c_{i\,\sigma} \rangle$ and, in the case of pairs, as $\langle \Delta^{\dagger}_{i+1} \Delta_i \rangle$. It is also useful to show the pair kinetic energy after subtracting the contribution from the nonpaired particles. We calculate the "KE/site substracted" defined as $\langle \Delta^{\dagger}_{i+1} \Delta_i \rangle - \langle c^{\dagger}_{i1} c_{i1} \rangle \langle c^{\dagger}_{i2} c_{i2} \rangle$. In addition, the double occupancy $\langle n_{i1} n_{i2} \rangle$ allows us to study the degree of pairing in the system. In Fig. 3.8 one can see that as $|U|$ increases the kinetic energy of single particles (circles and squares) decreases in absolute value while kinetic energy of the pairs (up triangles) increases. This indicates that with stronger attractions the particles tend to hop in pairs. This also hints at entering a strongly bound-pairing regime. When looking at the double occupancy (down triangles), one

should keep in mind, that in the non-interacting limit, there is no pairing so the value limiting $\langle n_{i1} n_{i2} \rangle$ from below is just the product of densities $\frac{N_1 N_2}{L^2}$. In the extreme strongly interacting limit, the maximum double occupancy is the density of the minority particles $\frac{N_1}{L}$. In the regime of maximum pairing the system consists of N_1 tightly bound pairs and $N_2 - N_1$ excess majority particles. In the case of Fig. 3.8 the maximum pairing is $\frac{N_1}{L} = 0.28$ and we can see that the double occupancy is approaching this value as the pairing is saturated. Multiplying the double occupancy by $|U|$ gives the average interaction energy (as the interaction considered in the model is only on-site).

3.3 System in a harmonic trap

The principal motivation for the studies of the trapped system is its relevance to the ongoing experiments on ultra cold atoms. In addition, it is of great interest to study how the inhomogeneity in local polarization and density influences the pairing.

Continuing earlier work in higher dimension [21, 22, 23], the Rice group [25] in 2010 reported on experiments in one dimensional confined Fermi systems (^6Li atoms) with imbalanced populations. These experiments were done in the continuum, *i.e.* without an optical lattice, and focused on the behaviour of the system in three polarization regimes by measuring the density profiles of the fermionic species. It was found that the central part of the system is always partially polarized whereas the behaviour of the outlying regions depends on the total polarization. For low polarization, $P = 0.05$, the outlying regions were found to be fully paired in the sense that the density profiles of the two fermion species matched within experimental precision. For intermediate

polarization, $P = 0.15$, the density profiles indicated that the whole system is partially polarized. Finally, for large polarization, $P = 0.59$, the wings were found to be populated exclusively by the excess fermion species and thus were fully polarized.

The experiment [25] consisted of a two-dimensional array of elongated (one-dimensional) tubes. Along the tube, the axial direction, the atoms were confined with a trap frequency $\omega_z = 2\pi \times 200$Hz; in the central tube, the total number of atoms at zero polarization was approximately 250. The pair binding energy, $\epsilon = \hbar^2/ma_{1D}$ (where a_{1D} is the effective one-dimensional scattering length), was estimated to be $\epsilon/\epsilon_F \approx 5.3$ with the Fermi energy calculated assuming a balanced system with a total of 250 particles. The temperature was estimated at $T/T_F \approx 0.1$. It is thus important to study the system at finite temperature in order to be able to make contributions that would be relevant to the experimental progress. The finite temperature behavior of the system was the main motivation for our numerical study and will be presented in Chapter 4.

To set the stage for the finite temperature studies, in this section we present QMC results for the fermionic Hubbard model in 1D in the presence of the confining potential at low temperature. Our ultimate goal is to make contact with the above mentioned experiment in the continuum; to this end we simulate lattice systems that are dilute enough so that the fermions in the center of the trap are far from forming a flat plateau corresponding to a band insulator. We introduce the trapping potential in Eq.(3.1) $V_T = 0.0007t$ which corresponds to $\hbar\omega_z = 2\sqrt{tV_T}$. The total number of particles in our simulations for balanced populations is 78, to be compared with 250 in the experiment. We performed our simulations in the temperature range $0.008 \leq T/T_F \leq 0.25$ which includes

the temperature at which the experiments were performed, $T/T_F = 0.1$. In addition, to place our system in the same coupling parameter regime as the experiments, we present our results for a coupling strength of $U = -10t$. U is the "pair binding energy" and the value we have chosen gives $|U|/\epsilon_F = 4.8$, close to the experimental value.

First we look at the system at low temperature as a function of polarization. As in the homogenous case, the pair momentum distribution exhibits a maximum at $k_{\text{peak}} \neq 0$ (Fig. 3.9) and, as before, k_{peak} increases with growing polarization. Looking at the density profiles one immediately observes that the low and high polarization regimes differ significantly.

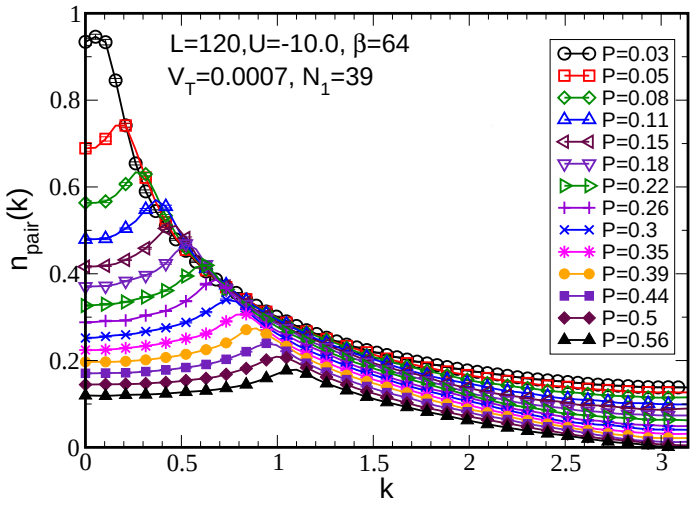

Figure 3.9: Pair momentum distribution in a trapped system for several polarizations. The FFLO peak moves to higher momentum values as P increases as in the uniform system. The majority population is fixed $N_1 = 39$, $T/T_F = 0.008$ in the balanced case $N_1 = N_2 = 39$.

First we look at the low polarization regime. In Fig. 3.10, we show the density profiles at very low temperature, $T/T_F = 0.008$, for a system at very small polarization, $P = 0.05$, corresponding to the open (red) squares in Fig. 3.9. The central region of the system is clearly partially polarized: the profiles

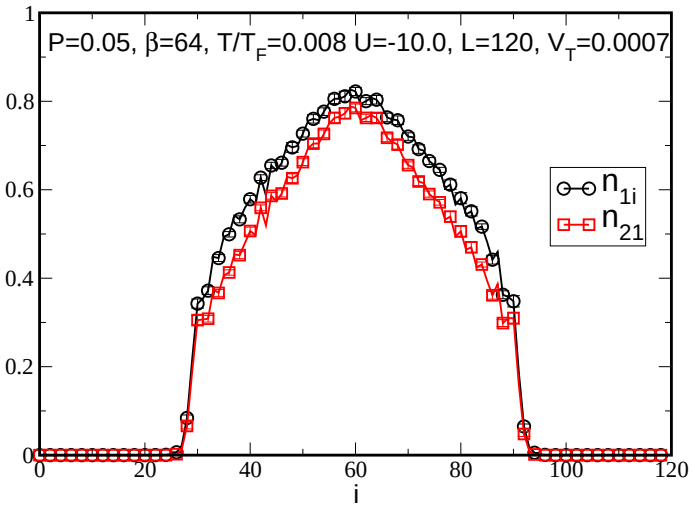

Figure 3.10: Density profiles of the two species for the low temperature and low polarization case. Very narrow fully paired regions are seen at the edges of the cloud. $N_1 = 39$ and $N_2 = 35$.

do not overlap. This partial polarization, *i.e.* population imbalance, causes FFLO pairing to take place as is evidenced by the pair momentum distribution in Fig. 3.9. However, in a very narrow interval at the edges of the system, the density profiles match very closely and the system is fully paired [86, 25]. This fully paired region was studied in the continuum by Casula *et. al.* in [77] using Path Integral Monte Carlo (PIMC) simulations. It was shown that at a polarization $P = 0.04$, the fully paired region exists for $T < 0.025T_F$ and $T < 0.035T_F$ for the two strong couplings studied (the first value corresponds to the smaller coupling). The narrowness of this region on the lattice was studied at $T = 0$ in Ref. [89, 90].

In figure 3.11 we show the evolution of the density profiles and their difference with increasing polarization. One can see that in the case of the lowest polarization $P = 0.03$ (top left) the local magnetization is zero in the center of the trap. One could see it as a fully paired core of the cloud. However we observe it only in this very low polarization case when the difference between

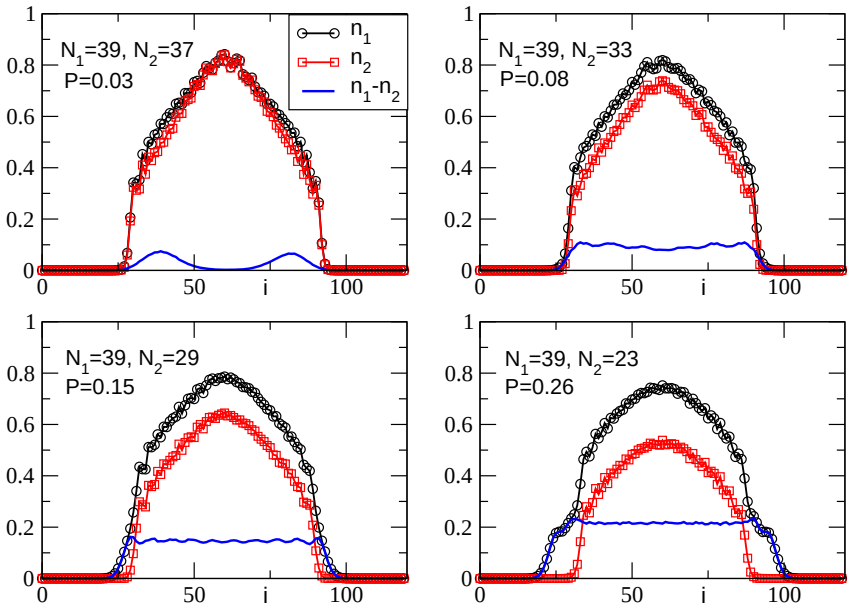

Figure 3.11: Density profiles and local magnetization for different polarizations. $L = 120$, $U = -10$,$V_T = 0.0007$, $\beta = 64$ and so $T/T_F = 0.008$ for the balanced case with $N = 78$ particles.

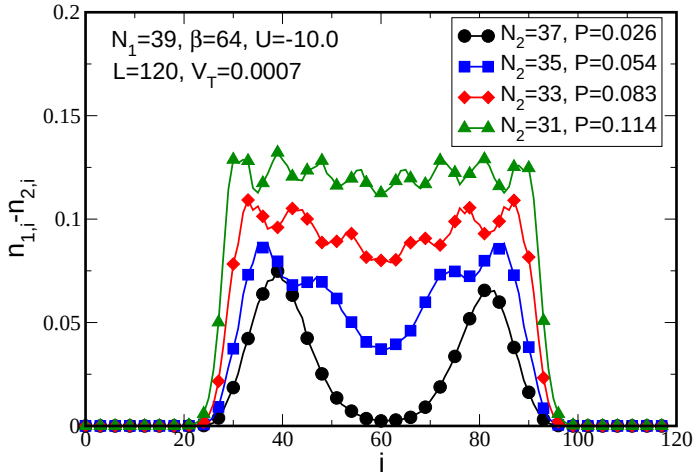

Figure 3.12: Density profile differences (local magnetization) for different polarizations. The oscillations are standing waves showing the pair rich (minima) and pair depleted (maxima) regions in the confined system. $T/T_F = 0.008$ for the balanced case with $N = 78$ particles.

the particles is $N_1 - N_2 = 2$.

The difference in the density profiles, Fig. 3.12, of the two species shows regular oscillations indicating that the partially polarized region is not uniform. Such oscillations have been seen before [78, 80, 76] and correspond to the standing wave of length $\lambda = 2\pi/k_{\text{peak}}$, as can be easily verified from Figs. 3.9 and 3.12. These oscillations describe the length scale at which the system passes from pair-rich to pair-poor regions. This is a striking visual demonstration that the FFLO phase is not uniform.

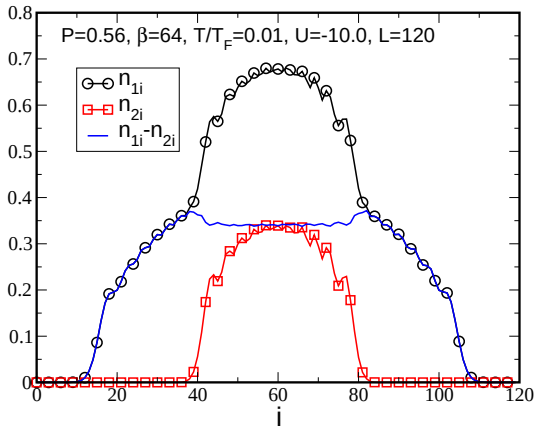

Figure 3.13: Trapped system at low temperature and high polarization. $N_1 = 39, N_2 = 11, L = 120$, $U/t = -10$, $V_t = 0.0007$. T_F is calculated for the total balanced population of $N = 50$. Large fully polarized regions are seen at the boundaries of the system.

We now turn to investigate a highly polarized system at low temperature. Figure 3.13 shows the density profiles in the system with $P = 0.56$ at $\beta = 64$ ($T/T_F = 0.01$). At this large P,it is clear that the central region is partially polarized and the wings are fully polarized, populated only by the majority species as was also observed in [78]. The population difference in the central region of the system in Fig. 3.13 is almost constant but with oscillations, $\lambda = 2\pi/k_{\text{peak}}$, due to the presence of FFLO pairing as shown clearly by the pair momentum distribution in Fig. 3.9 (black triangles).

3.4 Summary

In this chapter the results of our studies of a mixture of fermions with population imbalance interacting attractively and at low temperature are presented. It is found that the FFLO pairing is the mechanism that prevails in this system and is apparent in a wide range of polarizations and coupling strengths. Density profiles of the atomic cloud trapped harmonically are presented. It is shown that in the low temperature regime one can observe very narrow fully paired regions at the edge of the cloud for very weakly polarized system. On the other hand, for a highly polarized system the wings of the cloud are shown to be fully polarized. We do not find the fully paired core of the cloud, apart from a very specific population imbalance case. The core of the system is found in general to be partially polarized and as such is the part of the cloud where the FFLO pairing is realized. The local magnetization measurements provide a direct illustration of the FFLO phase with pair rich and pair depleted regions.

Chapter 4

Finite temperature study of the system in 1D

4.1 Introduction

It is widely accepted now that the FFLO phase of a pair density wave is the ground state of the 1D mixture of fermions with imbalanced populations. with or without a trap. However the stability of the FFLO phase at finite temperatures remains an open question. Mean field calculations [91, 86, 92] possibly shed some light but can be less reliable in low dimension where quantum fluctuations are large. This question is of paramount importance for experiments, especially in trapped atomic systems, since difficulties in cooling fermionic atoms raise concerns about whether the currently attainable temperatures are low enough for a thorough investigation of FFLO physics. Our work aims at providing a contribution to the understanding of the conditions required for the experimental realization of the FFLO phase.

We present in this chapter our investigations into the influence of the finite

temperature on the system. The temperature - polarization phase diagrams that we have calculated are discussed. Of high practical importance to the experimental quantum gases community are our results on the trapped system and the stability of FFLO at finite temperature at which the experiments are inevitably performed. Our key result is that the paired phase can exist up to temperatures of order one tenth of the Fermi energy, when the polarization is sufficiently large, even in the presence of a confining potential. Current experiments on trapped atoms are likely to work in this temperature range.

4.2 Uniform system

We begin with a discussion of the physics at finite temperature in the absence of a confining potential, $V_T = 0$.

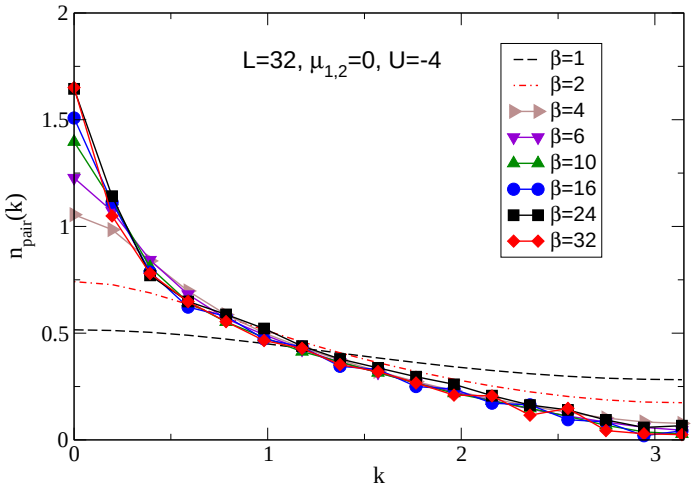

Figure 4.1: Pair momentum distribution for balanced populations at half filling of the lattice as a function of inverse temperature β. The peak disappears at a critical temperature where the pairs no longer form a quasi-condensate. The size of the lattice is 32 sites and $U = -4$.

First, we look at a mixture of balanced populations of fermions that interact

attractively and study their behavior as a function of temperature. In Fig. 4.1 we show that the quasi-condensate peak of BCS pairs at zero momentum disappears with increased temperature.

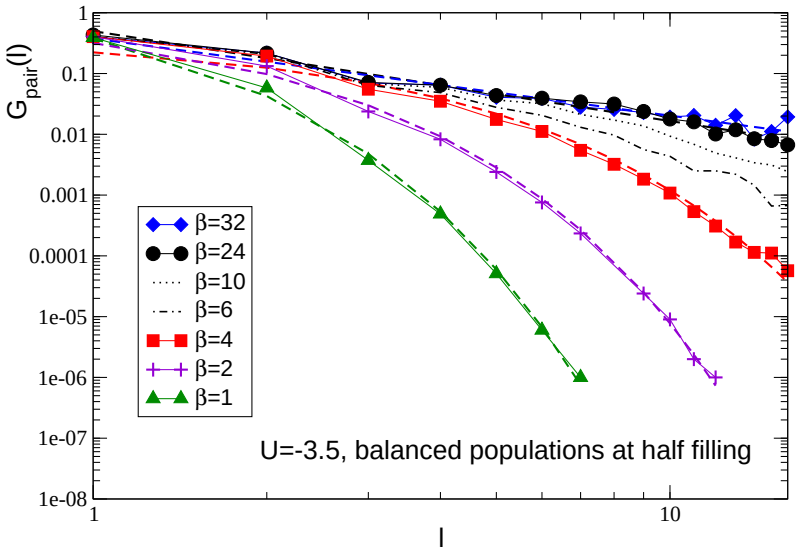

Figure 4.2: Pair Green function as a function of distance and its dependence on the temperature. The data are plotted in the log-log scale and the dashed lines are the fits to the data points. One observes a change in the decay character from a power-law at high β to an exponential decay for low β.

The transition between the quasi-condensed pairs and normal pairs can be seen in the change of the character of the decay of the pair Green function with increasing temperature. One can see in Fig. 4.2 that there is a clear distinction between the low temperature regime where the correlations decay as a power law and the high temperature regime where they decay exponentially. The power-law appears as a straight line in the log-log scale used in this figure, the fits to data points are denoted by dashed lines. In the case of $\beta = 32$ and $\beta = 24$ we can see the decay follows a power-law. When the temperature is increased there is a crossover regime (here for *e.g.* $\beta = 10$ and $\beta = 6$) where it is not clear what kind of decay of correlations is observed. At much higher

temperature the correlations decay exponentially, which is shown for $\beta = 4$, $\beta = 2$ and $\beta = 1$.

4.2.1 Phase diagram

As discussed in the introduction, it is now generally agreed that the ground state of a Fermi system with attractive interactions and imbalanced populations is the FFLO state. The mismatch in the Fermi momenta results in pair formation with nonzero center-of-mass momentum $k = \pm|k_{F_1} - k_{F_2}|$. Consequently the pair momentum distribution, the Fourier transform of the pair Green function, Eq. 6.3, peaks at this value of the momentum. This peak at nonzero momentum serves as the principal signature indicating the presence of the FFLO state [26, 76, 78, 79, 80].

The situation at finite temperature, which is important experimentally, is less clear. Approximate methods, such as mean field, do not always yield the same phase diagram. In this section we will map out the phase diagram in the polarization-temperature plane. To this end, we study, at fixed polarization P, the behaviour of the pair momentum distribution, $n_{\text{pair}}(k)$, as a function of the temperature T.

It is important to mention that, when using a grand-canonical algorithm for the simulations, one needs to find numerically the density as a function of chemical potential and temperature in order to study the system at fixed polarization. For example in the case of balanced populations in Fig. 4.3 (top) we show how the density changes with chemical potential at fixed temperature. It is clear that in our formulation of the Hamiltonian the half filling of the lattice for each species occurs at $\mu_\sigma = 0$ where $\sigma = \{1, 2\}$. Studying the system at finite temperature in the grand-canonical ensemble and with fixed

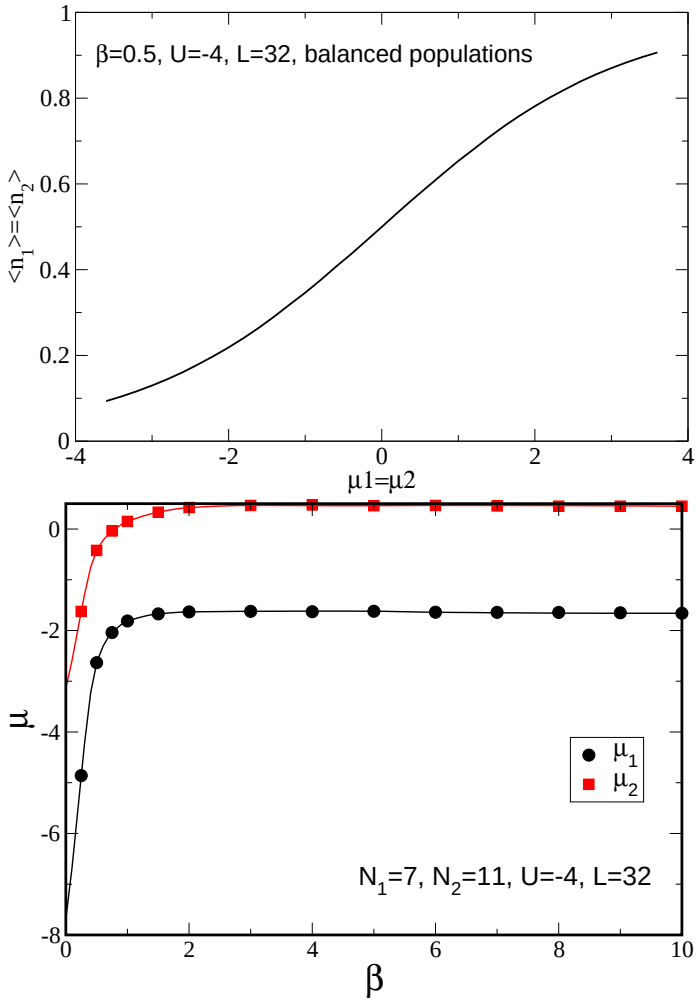

Figure 4.3: Top: Chemical potential versus density in a grand-canonical simulation. Populations of each species are equal, $\beta = 0.5$, $L = 32$, $U = -4$. Bottom: Chemical potentials which yields particular densities of each species and this fixed polarization, here for *e.g.* $P = 0.22$, for different temperatures β.

polarization involves finding the chemical potentials yielding desired densities of species for different temperatures. An example of this mapping can be seen in Fig. 4.3 (bottom). In order to find a phase diagram in the polarization and temperature plane with fixed total density of particles we had to perform this mapping for a wide range of parameters. Once we find the μ_1 and μ_2 which correspond to the desired densities of particles at some temperature we perform long simulations with measurements of the physical quantities that characterize the system, *e.g.* the pair momentum distribution.

For very low T, $n_{\text{pair}}(k)$ peaks at $k \neq 0$ and the system is in the FFLO state. As T is increased, the peak in n_{pair} gets lower and shifts to $k = 0$. The temperature at which the peak in n_{pair} shifts to $k = 0$ is the crossover temperature, T_c. Note that in this one-dimensional system, transitions at finite temperature are not true phase transitions, but rather crossovers. This is illustrated in Fig. 4.4 where we show QMC results for $n_{\text{pair}}(k)$ as a function of k for several values of the inverse temperature β. The simulations were done for fixed populations, $N_1 = 13$ and $N_2 = 7$ on a system with $L = 32$ lattice sites and an attractive interaction $U = -3.5t$. The figure shows clearly that, as β decreases from $\beta = 32$, the height of the FFLO peak decreases and, in fact, shifts to lower k values. The shift to lower k values is made more evident by simulating larger systems since this gives more k grid points. When the peak at nonzero k is equal to $n_{\text{pair}}(0)$ to within 1%, we consider the peak to have shifted to $k = 0$ and the FFLO state to have disappeared. In Fig. 4.4 this happens for $\beta_c \approx 6$. Reducing β further leads to continued decrease of the height of the peak, which remains at $k = 0$.

The peak of $n_{\text{pair}}(k)$ at $k_{\text{peak}} \neq 0$ means that the system is, in fact, not homogenous: The spatial pair Green function, Eq. 6.3, oscillates as a function

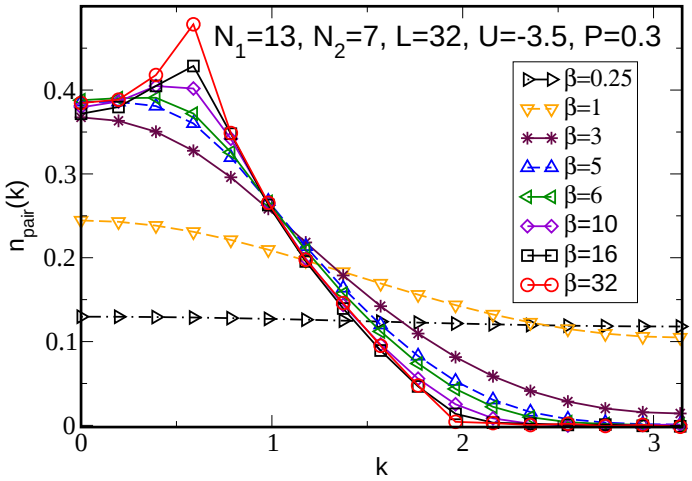

Figure 4.4: The effect of temperature on the pair momentum distribution. A peak at non-zero momentum is a signature of the FFLO state. As β decreases, the peak disappears at a crossover value $\beta_c = 1/T_c$. In this case, $\beta_c \approx 6$. The error bars are of the order of the symbol size.

of distance with a period given by $2\pi/|k_{\text{peak}}|$. These oscillations have been discussed, for example, in the context of mean field theory [11, 41]. Physically, they indicate that the system has regions which are rich in pairs separated by regions poor in pairs but rich in the excess fermion species. Such oscillations are shown in Fig. 4.5 for three values of β. It is seen that as the temperature increases and the height of the FFLO peak decreases, the oscillations decrease in amplitude and eventually disappear as homogeneity is restored in the system.

The question then arises as to the nature of the phase at $T > T_c$. Two possibilities are: (1) At $T > T_c$ the pairs are broken and the system is a mixture of two Fermi liquids or (2) pairs are still present but the system has been homogenized by thermal agitation. A first indication is given by the energy scales involved. The binding energy of the pairs at very low temperature is of the order of $|U|$ and in our system here $|U| = 3.5t$. So, to break the pairs, an

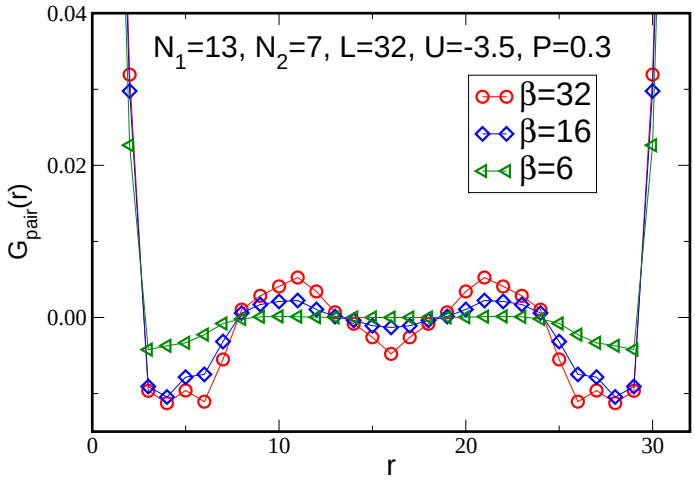

Figure 4.5: Pair Green function calculated at low temperatures where the system is in the FFLO state ($\beta = 32$ and $\beta = 16$) and at the temperature at which FFLO disappears ($\beta = 6$). Note that the oscillations disappear at the higher temperature.

equivalent amount of thermal energy is needed which means $\beta \approx 1/|U|$. For the case discussed in Fig. 4.5, the crossover from FFLO to the uniform phase happens at $\beta_c \approx 6$ not $t/|U| = 0.286$. This means that T_c is more than an order of magnitude smaller than the temperature needed to break the pairs. This, then, favors the conclusion that when FFLO first disappears, the pairs have not yet been broken and the system is in a homogeneous polarized paired phase (PPP). Another piece of evidence is provided by studying the average double occupancy of the sites given by

$$D = \langle n_{i1} n_{i2} \rangle = \langle \Delta_i^\dagger \, \Delta_i \rangle. \tag{4.1}$$

In the absence of pairing, $\langle n_{i1} n_{i2} \rangle = \langle n_{i1} \rangle \langle n_{i2} \rangle = N_1 N_2 / L^2$ while if pairing is perfect, *i.e.* if all the minority particles are paired, $\langle n_{i1} n_{i2} \rangle = N_2/L$. We

define the normalized double occupancy by

$$\mathcal{D} = \frac{D - n_1 n_2}{n_2 - n_1 n_2}, \tag{4.2}$$

where $n_1 = N_1/L$ and $n_2 = N_2/L$ and we recall that $N_2 < N_1$. With this normalization, we have $0 \leq \mathcal{D} \leq 1$.

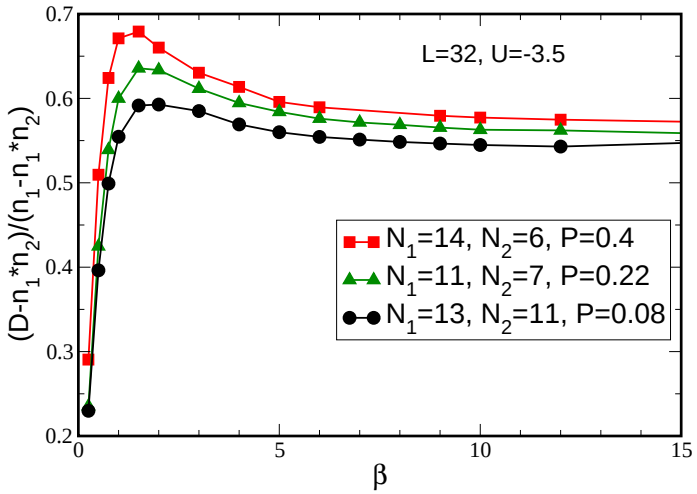

Figure 4.6: Double occupancy versus β for three polarizations exhibits a very sharp drop for $\beta < 1$ indicating that pairs are being broken near $\beta \sim 1/|U|$.

This quantity is shown in Fig. 4.6 for three polarizations. One can see that the pairing drops significantly at rather high temperatures, $\beta \approx 1/U$. Thus we conclude that the pairs are not broken when the FFLO peak disappears but the systems is in a PPP. As one can see, this pairing parameter does not saturate for the case we presented. One could expect it to reach the maximum value at a very strong U limit in the low temperature regime, where thermal fluctuations are absent.

Note in Fig. 4.6 that the double occupancy increases just before it drops signaling the breaking of the pairs. This increase can be understood physically

as follows. As the temperature is increased, the Fermi distribution near the Fermi momentum gets rounded but for $k < k_F$ the distribution remains saturated. This means that pairing can happen only near the Fermi surface while inside the Fermi sea the particles are still blocked by the Pauli exclusion principle. Eventually, as T continues to increase, the occupation of momentum states inside the Fermi sea drops, rather suddenly as shown by our simulations, which makes available for pairing a larger number of particles causing the double occupancy to rise.

We are now ready to apply the above considerations to determine the phase diagram in the (P, T) plane. To this end, we keep the total population, N, constant and for different values of the polarization, P, determine the temperature, T_c, at which the peak in $n_{\text{pair}}(k)$ shifts to $k = 0$. Figure 4.7 shows the resulting phase diagrams for $N = L$ (half filling) and $N = L/2$ (quarter filling). The Fermi temperatures shown in the figure are calculated assuming equal populations using $\epsilon_F = tk_F^2$ where ϵ_F is the Fermi energy. We mention again that the phase boundaries represent a crossover behaviour, not phase transitions since this one-dimensional quantum system does not have phase transitions at finite temperature. The word "phase" which is used in this thesis will hopefully not mislead the reader and will be understood as the "state" and the phase diagram as the diagram of states.

The phase diagrams show clearly that the FFLO phase is quite robust, persisting over a wide range of polarizations and to rather high temperatures. For $N = L$, it persists up to $T/T_F \approx 0.2$ and for $N = L/2$ up to $T/T_F \approx 0.8$. We also see that, in both cases, the crossover temperature increases with the polarization up to a maximum value after which it decreases again. This can be understood physically as follows: When P is small, the Fermi "surfaces" of

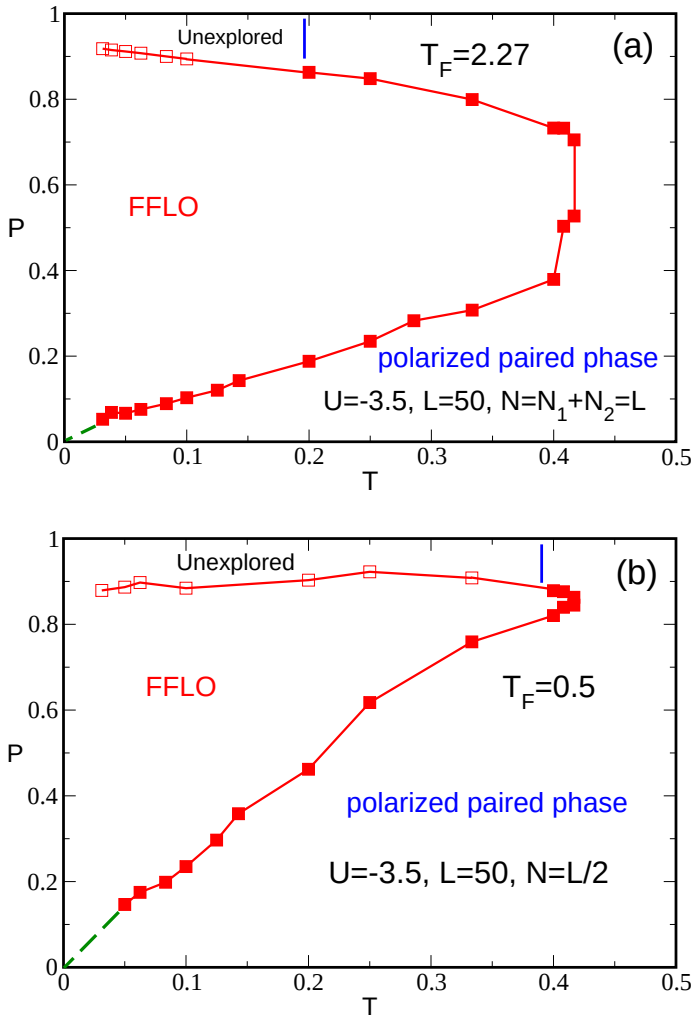

Figure 4.7: Phase diagram in the polarization-temperature plane. (a) the system at $N = L$ (half filling), (b) the system at $N = L/2$ (quarter filling). At P=0 system is in the BCS state. The regions above the open (red) squares and to the left of the vertical (blue) lines are unexplored. Up to the open squares the system is in the FFLO phase. Phase boundaries represent cross-over behaviour not phase transitions. In the FFLO phase, $n_{\text{pair}}(k)$ peaks at $k \neq 0$, in the PPP phase, the peak is at $k = 0$.

the two populations are so close to matching that very little thermal energy is needed to get them to match. Thus even at very low finite temperature, pairing takes place at zero center-of-mass momentum. Therefore, larger polarizations have a stabilizing effect on the FFLO phase.

There are numerical difficulties with the determination of the phase diagram at very low and very high polarizations. At very high polarization, there is a very small number of minority particles, making the FFLO signal difficult to discern clearly. We were therefore not able to examine $P > 0.9$ in our simulations. For that reason, some symbols on the phase boundary at high polarization are open, indicating that up to this polarization, the system is still in the FFLO phase. The solid symbols mark the true boundary between FFLO and PPP.

In addition, at small polarization, very low temperature is needed to observe the FFLO phase but there is a practical limit to our simulations as the lower the temperature the longer the simulation time needed to obtain precise results. However, DMRG calculations at $T = 0$ [26, 78, 79, 80] do, in fact, confirm that the FFLO phase persists all the way to $T = 0$. The dashed (green) line connecting the origin to the first numerical points simply schematizes the expected position of the boundary.

A phase diagram in the (P, T) plane was calculated in Ref. [91] using mean field theory (MFT). The general shape of the FFLO phase obtained there as shown in Fig. 4.8 is similar to what we found here. However there are very important differences. For example, unlike MFT, we have found that there is no direct transition from the FFLO phase to the Fermi liquid phase (broken pairs): The FFLO phase is destroyed at a temperature which is much lower than that required to break the pairs and is replaced by the PPP.

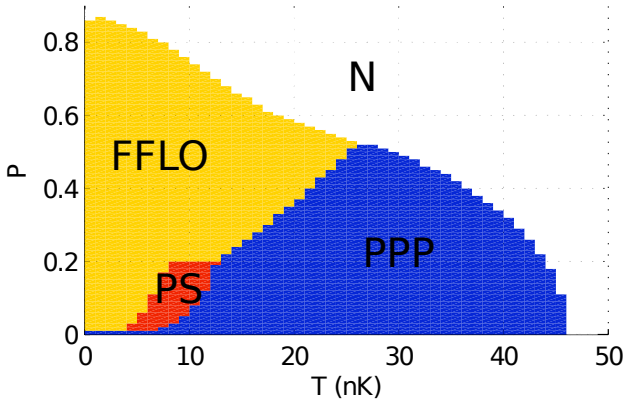

Figure 4.8: Phase diagram in the polarization-temperature plane for a 1D system obtained using mean-field method. Figure taken from Ref. [91]. PS denotes phase separation and N is a normal, unpaired phase.

Reference [91] predicts a phase separation between the FFLO and PPP at low P and T (Fig. 9 in Ref. [91]). In order to examine this possibility, we study the density histograms in the grand canonical ensemble. The idea is as follows: Starting in, say, the PPP, we increase the polarization by tuning the chemical potentials, μ_1 and μ_2. For each choice of μ_1 and μ_2, we accumulate the histograms of the particle populations. If phase separation is present, then as the system approaches the phase separation region, the density histogram of *each* species should develop a double peak structure. If no such structure develops, it means that there is no phase separation as the system crosses from the PPP to the FFLO. We first verify the correct behaviour of the obtained histogram as the size of the system is changed.

In Fig. 4.9 we show the histograms for two system sizes at half filling but with all other parameters fixed. We see that the histograms for the two system sizes agree very well; the main difference is that the larger system size (obviously) allows for a finer grid of densities which redistributes the values a little and exhibits the main peak more clearly. In Fig. 4.10 we show, for fixed inverse temperature $\beta = 16$, the histograms for three cases at half filling: In

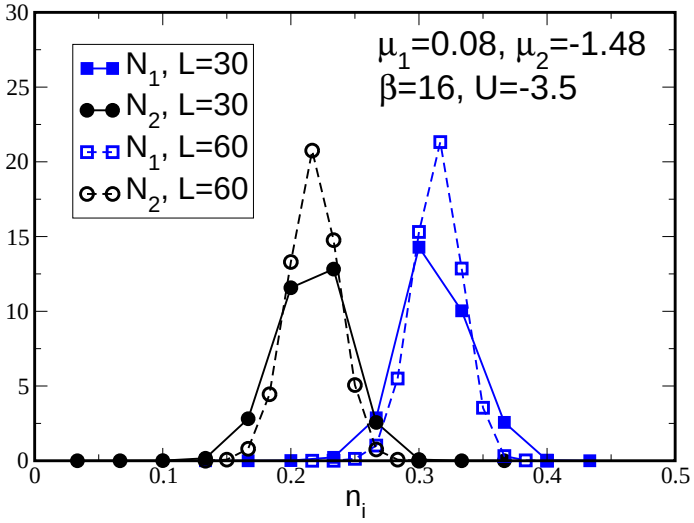

Figure 4.9: Majority (N_1) and minority (N_2) density histograms at the FFLO-PPP boundary for two system sizes. The larger system size offers more grid points and, therefore, a finer resolution of the density fluctuations. A single peak is seen for each population indicating the absence of phase separation.

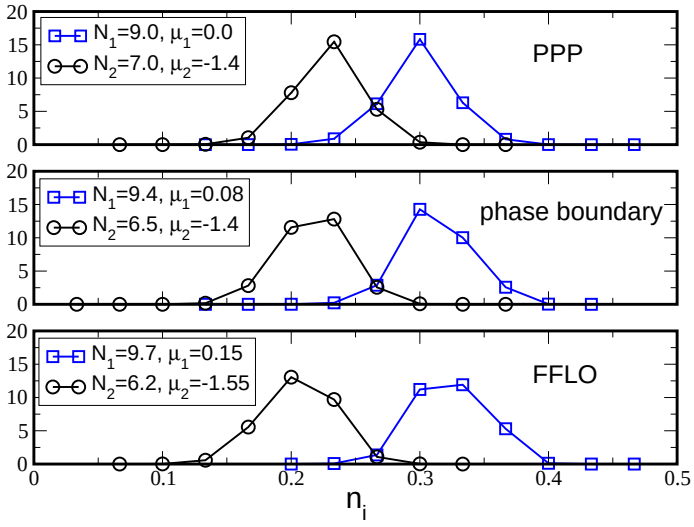

Figure 4.10: Histograms of local densities for $L = 30$, $\beta = 16t$ and $U = -3.5t$. Left peaks correspond to the minority species and right ones to the majority. The peaks move smoothly as μ_1 and μ_2 are tuned to take the system across the boundary between PPP and FFLO. No double peak structure is observed, indicating the absence of phase separation.

the top panel the system is just inside the PPP phase, the middle panel the system is at the PPP-FFLO boundary and the bottom panel the system is just inside the FFLO phase. No double peak structure develops, which leads us to conclude that there is no phase separation. This was done for several temperatures at low polarization.

It is useful here to comment on the algorithm choice for calculating the histograms. Although the DQMC algorithm is grand canonical and thus allows for particle number fluctuations, it is not useful for calculating the density histograms. The reason is that, in DQMC one changes the realization of the auxiliary Hubbard-Stratonovich field; but for each such realization, the fermions have been traced over all their possible configurations. On the contrary, in the grand canonical version of the SGF algorithm, the update is done over the fermion configurations themselves. So, the particle number can be measured configuration by configuration.

4.3 Trapped system

As a continuation of the study of the system in a harmonic trap at low temperature we now turn to examine temperature effects on the system. Similarly to the untrapped system when using a grand-canonical ensemble we need to tune the chemical potential to the densities we are interested in. In particular we will mostly look at the low density regime to minimize the lattice effects and make our results most relevant to the experiment performed in continuum. The simulations are performed in the parameter regime close to the one at which the experiment of Liao *et. al* [25] has been done (as discused in Chapter 3). We have investigated the temperature range $0.008 \leq T/T_F \leq 0.25$

within which lies the experimental temperature $T/T_F = 0.1$.

First we look at a weakly polarized mixture. The system at $\beta = 64$, Fig. 3.10, is now heated to $\beta = 28$ ($T/T_F = 0.016$) and $\beta = 5$ ($T/T_F = 0.1$) as shown in Fig. 4.11 (a) and (b) respectively. As the temperature increases,

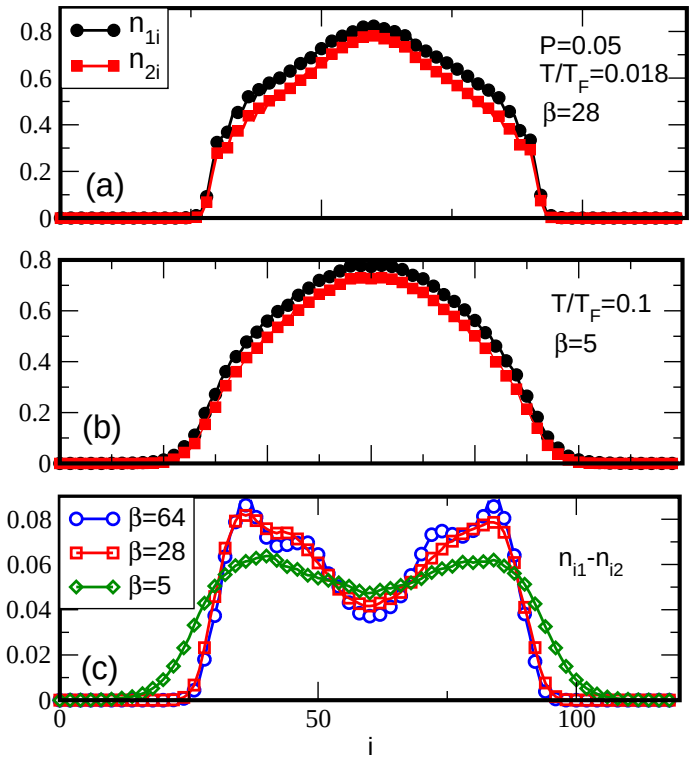

Figure 4.11: Trapped system at finite temperature and low polarization. (a) and (b) density profiles at $T/T_F = 0.016$ and $T/T_F = 0.1$ respectively. (c) density profile difference for different temperatures.

the clouds spread out and the profiles become more rounded. Figure 4.11 (c) shows what happens to the population differences as the temperature rises. As T increases, the population difference vanishes in the wings more gradually than at the lower temperatures. In addition, the oscillations which indicate the presence of FFLO get smoothed out substantially at $\beta = 28$ and have essentially disappeared for $\beta = 5$. This is confirmed by the behaviour of the pair momentum distribution, displayed in Fig. 4.12, which shows the FFLO

peak disappearing as T is increased to $T = 0.016T_F$. This value is smaller than, but consistent with, the phase diagram in Ref. [86] (Fig. 1) which shows that at $P = 0.05$ the FFLO phase disappears for $T > 0.05T_F$. Our value is also consistent with that found in Ref. [77]. This illustrates the fragility of the fully paired paired wings and the FFLO phase at low polarization.

In the previous section, we calculated the phase diagram of the uniform system and showed that the FFLO phase persists to higher temperatures for larger polarization. We now demonstrate the same effect in the trapped system.

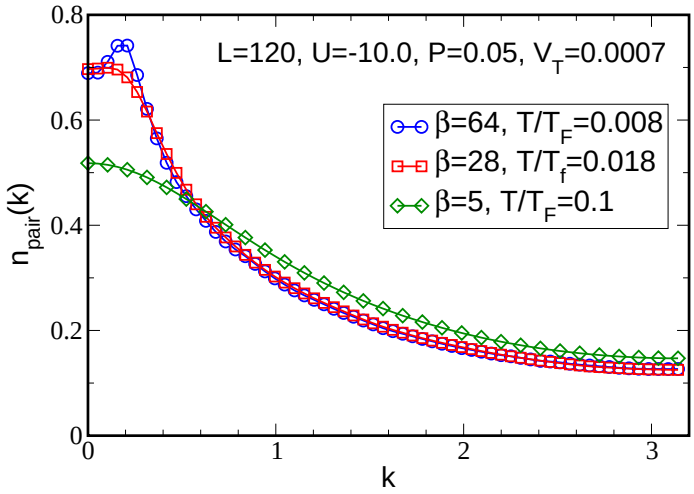

Figure 4.12: Pair momentum distribution of the system at P=0.05 (Fig. 4.11) and increasing temperature. The FFLO peak disappears at $T/T_F = 0.016$.

In Fig. 3.13 the density profiles of a highly polarized system ($P = 0.56$) at low temperature were shown. We observed that the cloud separates into the partially polarized central region and the wings which consist only of majority species. As the temperature is increased, this shell structure, *i.e.* partially polarized core and fully polarized wings, persists, as can be seen in Fig. 4.13 (a) and (b).

However, we observe that the partially polarized core expands in size and

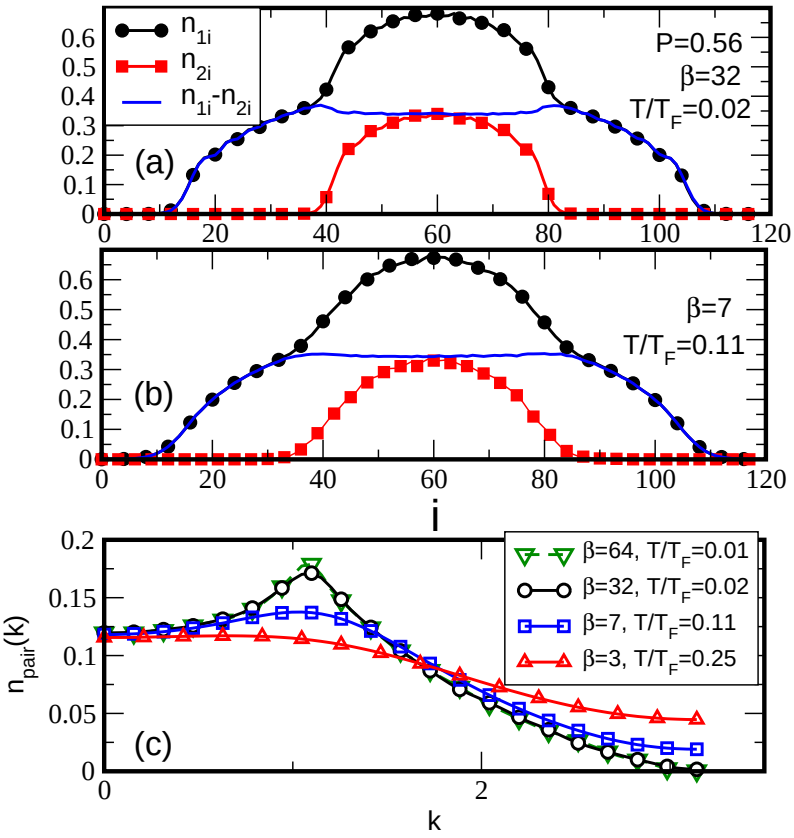

Figure 4.13: Same trapped system as in Fig. 3.13 at higher temperature. $P = 0.56, L = 120$, $U/t = -10$, $V_t = 0.0007t$, $N_1 = 39$, $N_2 = 11$. (a) and (b) show the density profiles and differences for two temperatures. (c) Pair momentum distribution.

the fully polarized population in the wings decreases. We also see that the FFLO phase at this large polarization is stabilized significantly compared with the $P = 0.05$ case (Fig. 4.12). For $P = 0.56$, the FFLO peak persists, albeit weakly, up to $T/T_F = 0.11$, vanishing completely at $T/T_F = 0.25$. This result is encouraging for the experiments [25] which can be done at high polarization and $T/T_F \approx 0.1$. However, at this temperature, the FFLO peak is not very pronounced and might still be difficult to observe experimentally.

We note that, as in the case of the uniform system, the FFLO phase disappears at a temperature which is much lower than the contact potential energy. In the case above, the FFLO phase disappears at $\beta t \approx 3$ while the contact interactions is $U = -10t$. The approximate condition to break the pairs is $\beta U \approx 1$; we see that $\beta t = 3$ is not a high enough temperature to break the pairs. Therefore, as T is increased, the FFLO phase is replaced by the PPP discussed in the previous section and not by the normal state composed of the two unpaired spin populations. Our QMC result is in disagreement with mean field predictions that as T is increased for high polarization, the system passes directly from the FFLO phase to the normal state [86].

It is interesting to see a direct comparison of the experimental and numerical data.The density profiles obtained in the simulations agree qualitatively with those measured in the experiment as shown in Fig. 4.14.

4.4 Interaction strength

The question then arises as to how the FFLO peak behaves as a function of U at fixed β, N_1 and N_2 (and consequently fixed P). We first look at the system without a trap. Clearly, for $U = 0$ there is no pairing and no FFLO peak.

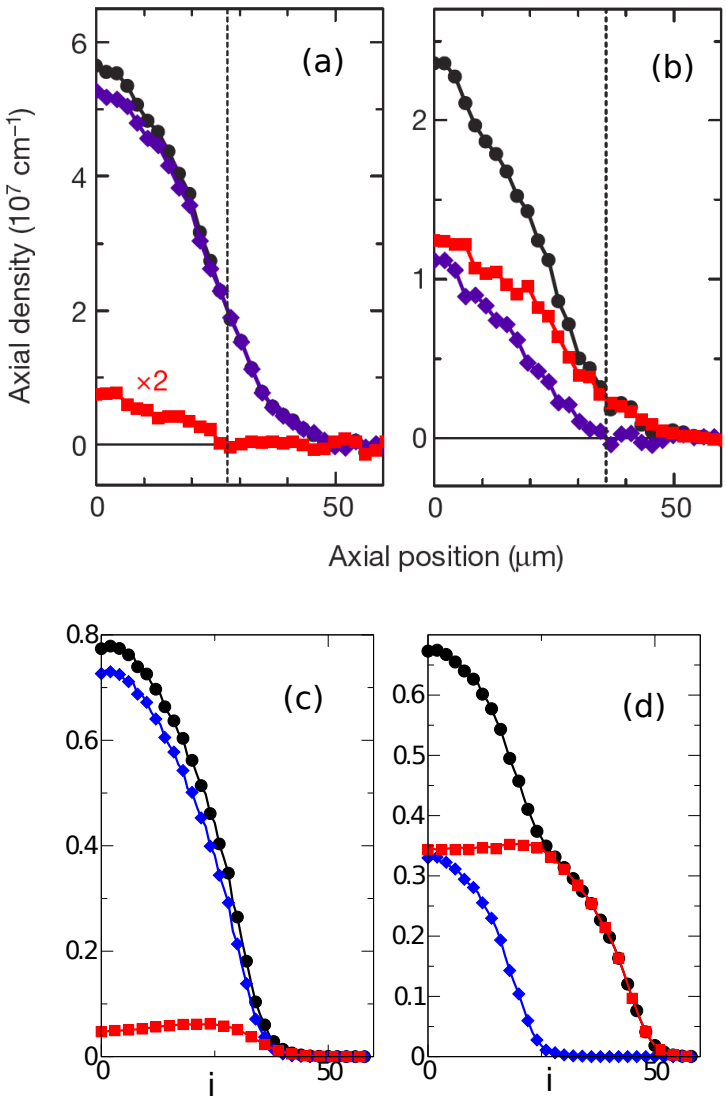

Figure 4.14: Qualitative comparison between experimental data and simulations. Black circles denote majority density, blue dimonds - minority density and red squares the density difference. Axial density from experiment at in (a) $P = 0.055$ in (b) $P = 0.33$, taken from Ref. [25]. Simulation results for $P = 0.05$ shown in (c) and $P = 0.56$ in (d). All data taken in a similar parameter range: temperature $\approx T/T_F = 0.1$ pair binding energy/ϵ_F=5.

As $|U|$ is increased, the peak at nonzero k forms and its height increases as shown in Fig. 4.15. However, we found that as $|U|$ continues to increase, the FFLO peak will reach a maximum height and then start to decrease. We also found that the peak is more sensitive to $|U|$ at higher T (compare Fig. 4.15 top and bottom panel). We believe the reason the peak starts to go down at high values of $|U|$ is that with increasing attraction, the pairing becomes increasingly localized in space and eventually the paired fermions form a very tightly bound bosonic molecule and the system resembles closely a usual Bose-Fermi mixture which does not exhibit FFLO peaks.

In the trapped case, the same question arises as to whether one can stabilize the FFLO phase at higher temperature simply by increasing the attractive interaction. The answer is the same as in the uniform case: As the attractive interaction is increased, the FFLO peak first increases in height but then saturates and starts to decrease as shown in Fig. 4.16 (top panel). In addition, as $|U|$ is increased, the partially polarized core region shrinks and the polarization in that zone increases (see Fig. 4.16 bottom panel). This has the effect of shifting the FFLO peak to larger values of k. For the fillings we considered here, the value of the interactions we took, $U = -10t$, appears to be near optimal.

4.5 Summary

In this chapter, we used three QMC algorithms (DQMC, canonical SGF and grand canonical SGF) to study the behaviour of one-dimensional imbalanced fermion systems with attractive interactions governed by the Hubbard Hamiltonian. We explored both the uniform and the confined cases.

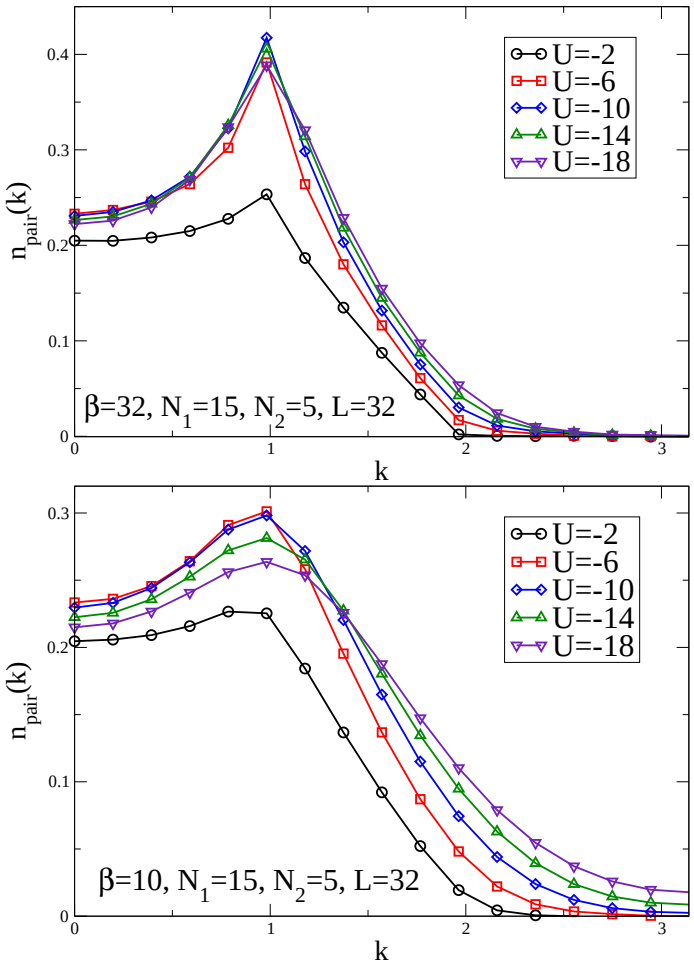

Figure 4.15: Pair momentum distribution with increasing interaction strength U at fixed $P = 0.25$ in an uniform system of the size $L = 32$. Top panel: low temperature $\beta = 25$, bottom panel: higher temperature $\beta = 10$.

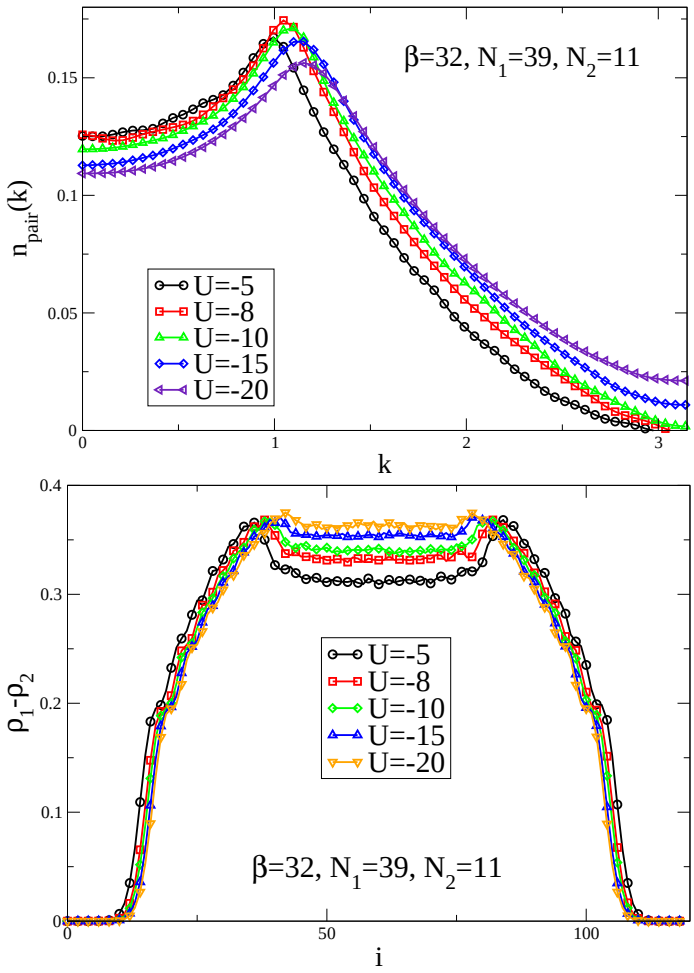

Figure 4.16: Pair momentum distribution (top panel) and density profile difference (bottom panel) with increasing interaction strength U at fixed $P = 0.56$ and a trapped system of $L = 120$ and $\beta = 32$.

In the uniform situation, we mapped the phase diagram in the polarization-temperature plane at two values of the total density (half filling and quarter filling) at the same interaction strength $U = -3.5t$. Both cases show the same general features: (1) The FFLO phase is very robust in the ground state and exists for a very wide range of polarizations; (2) at small polarization, the FFLO phase is very sensitive to temperature increase; (3) the FFLO phase persists to higher temperature when the polarization is larger and (4) the temperature at which the FFLO phase disappears is not high enough to break up the pairs leading to a spatially uniform polarized paired phase.

In the confined case, we performed our simulations for system parameters comparable to those in the experiment of Ref. [25]. We found the stability features of FFLO in the confined phase to be similar to those in the uniform case. At low polarization, the FFLO phase is destroyed even for a temperature as low as $T/T_F = 0.016$. However, and this is significant for experimental efforts to detect FFLO in the confined system, we found that at large polarization, the FFLO phase persists at $T/T_F > 0.11$ a temperature higher than that of the experiment, which has $T/T_F \approx 0.1$. Finally, the temperature at which the FFLO phase is destroyed is not high enough to break the pairs in disagreement with mean field results [86].

Chapter 5

Mass imbalanced system in 1D

5.1 Introduction

Up to now, the focus of our studies were mixtures of two species of fermions, where the masses of both types of particles are equal. In addition to such cases, which are of relevance in condensed matter and trapped ultra-cold atomic systems, there is great interest in the situation where the fermions of the two species have different masses. This arises naturally in trapped mixtures of different atomic species, *e.g.* K-Li, and also in cold dense quark matter where the c, b and t quarks are much heavier than the u, d and s quarks. It was argued theoretically that such mass and population imbalance leads to the BP phase [93, 94] with gapless excitations which can be stabilized by longer-range interactions [71]. In this chapter we examine this claim in one dimension using QMC simulations.

We study the effect of unequal masses on pair formation in fermionic systems with population imbalance loaded into optical lattices. The focus is on the one-dimensional system where the hopping parameters of the two species

are unequal and the extended Hubbard Hamiltonian is used to introduce longer-range interactions. We have considered three forms of the interactions and find in all cases that the system is unstable and collapses as the mass difference increases and that the ground state becomes an inhomogeneous collapsed state.

In order to study a mixture of particles with different masses we need to introduce species dependent hopping parameters. To look into beyond nearest-neighbor interaction effects, we use the extended Hubbard model as follows:

$$\hat{\mathcal{H}} = -\sum_{l\sigma} t_\sigma (c^\dagger_{l+1\,\sigma} c_{l\,\sigma} + c^\dagger_{l\,\sigma} c_{l+1\,\sigma}) + \sum_{i,j,\sigma,\sigma'} U_{ij,\sigma\sigma'} n_{i\,\sigma} n_{j\,\sigma'} \tag{5.1}$$

where $c^\dagger_{j\,\sigma}(c_{j\,\sigma})$ are fermion creation (annihilation) operators on spatial site j with the fermionic species labeled by $\sigma = 1, 2$ and $n_{j\,\sigma} = c^\dagger_{j\,\sigma} c_{j\,\sigma}$ is the corresponding number operator. The unequal masses are embodied in the unequal hopping parameters. We set the energy scale by taking $t_1 = 1$ and studying the system as t_2 gets smaller (the mass, m_2, of particles from species "2" increases). In general, the interaction term $U_{ij,\sigma\sigma'}$ can couple all fermions on all sites; in what follows we shall consider three different forms.

First: $U_{ij,\sigma\sigma'} = U\delta_{i,j}(1-\delta_{\sigma,\sigma'})$, *i.e.* only contact attraction ($U < 0$) between the two species.

Second: the interaction term of the Hamiltonian has the form $\mathcal{H}_I = \sum_i U n_{i1} n_{i2} + V \sum_{i,\sigma} n_{i\sigma} n_{i+1\sigma}$, *i.e.* contact attraction ($U < 0$) and nearest-neighbor repulsion between the same species $V > 0$.

Third: $\mathcal{H}_I = \sum_i (U n_{i1} n_{i2} + V_{12} n_{i1} n_{i+12})$, *i.e.* contact attraction ($U < 0$) and nearest-neighbor interaction between different species $V_{12} < 0$ and $V_{12} > 0$.

5.2 Heavy Majority: $t_1 > t_2$

We begin with the simplest form for the interaction term, $U_{ij,\sigma\sigma'} = U\delta_{i,j}(1 - \delta_{\sigma,\sigma'})$, *i.e.* only contact attraction ($U < 0$) between the two species. Figure 5.1 shows what happens to the minority (left panel) and majority (right panel) momentum distributions as the majority becomes heavier (t_2 is decreased). One can see that changing the hopping parameter of one species has influence on momentum distributions of both species.

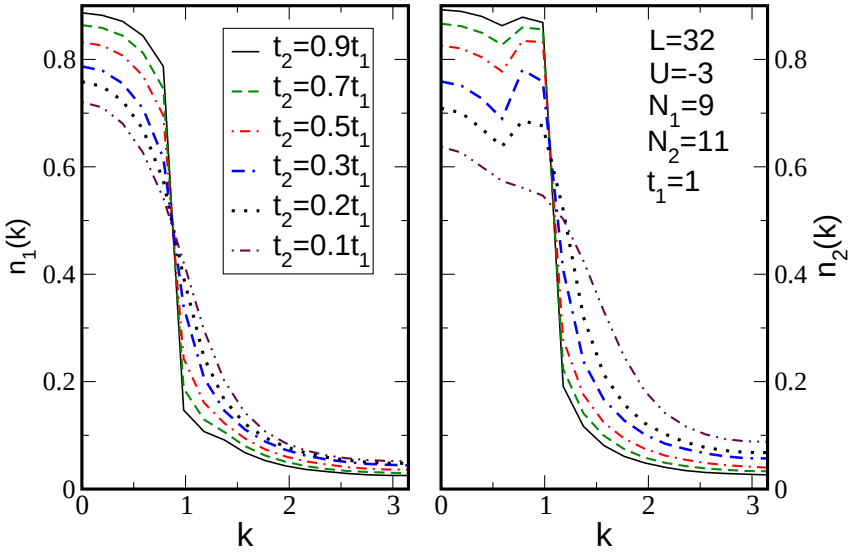

Figure 5.1: The momentum distribution for the minority $n_1(k)$ (left) and majority $n_2(k)$ (right) populations shown for different hopping parameters (mass of particle "2"). The simulation was done for $U = -3$ and $N_1 = 9$, $N_2 = 11$. U is given in units of t_1.

For $t_2 = 0.9t_1$, $n_\sigma(k)$ drops sharply at the respective Fermi momenta, (k_{F_1}, k_{F_2}) while at the same time, the pair momentum distribution, $n_{\text{pair}}(k)$, exhibits a maximum at $k = |k_{F_1} - k_{F_2}|$ (Fig. 5.2 left). This indicates pair formation at non-zero center-of-mass momentum and thus an FFLO phase. As the mass of the majority particles increases, t_2 decreases, the attractive interaction effectively increases because $|U|/t_2$ increases. The increased binding

is demonstrated by the average double occupation $\langle n_{i1}n_{i2}\rangle$ which takes values between N_1N_2/L^2 (no binding) and N_1/L (all minority particles have formed pairs). This quantity is shown in Fig. 5.2 (triangles, right panel) scaled by 4 for better visibility. Clearly, as t_2 decreases, $\langle n_{i1}n_{i2}\rangle$ increases toward its upper limit. As a consequence of this increased binding, the FFLO effect first intensifies, its peak at $k = |k_{F_1} - k_{F_2}|$ increases in height, reaches a maximum for $t_2 = 0.4t_1$, then decreases and disappears as shown in Fig. 5.2 (circles, right panel). Note, for example, that for $t_2 = 0.1t_1$ the peak of $n_{\rm pair}(k)$, Fig. 5.2 (left), is at $k = 0$.

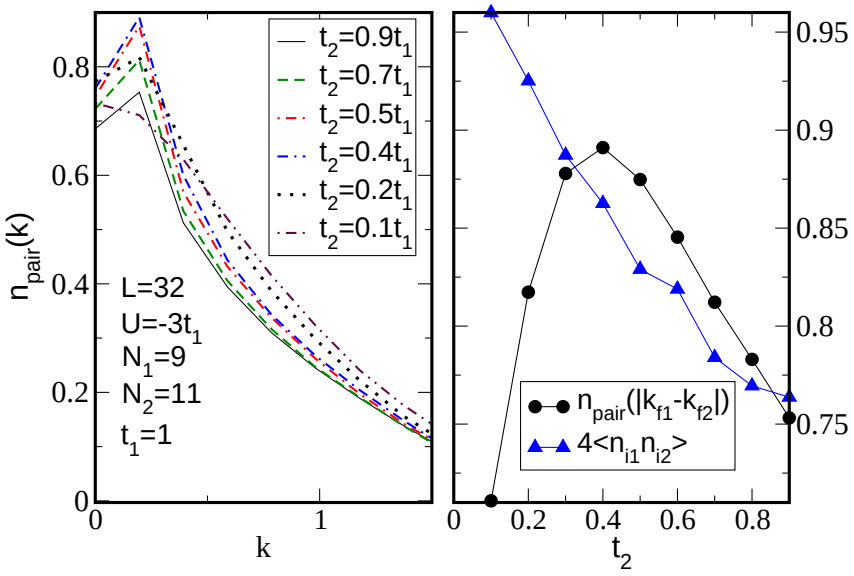

Figure 5.2: Left: The pair momentum distribution function $n_{\rm pair}(k)$. Right: The circles show the height of $n_{\rm pair}(|k_{F_1} - k_{F_2}|)$ vs t_2, the triangles show $\langle n_{i1}n_{i2}\rangle$ scaled by 4 for better visibility.

Also noteworthy is the appearance of a dip in $n_2(k)$, at $k \approx k_{F_1}$, whose depth increases with decreasing t_2, reaching a maximum for $t_2 = 0.4t_1$, corresponding to the maximum FFLO effect. Further decreasing t_2 washes this out. This feature can be understood as follows. As t_2 decreases, the interaction be-

tween the minority and majority effectively increases ($|U|/t_2$), thus increasing the depletion (drop of the filling much below $n_\sigma(k) = 1$) of $n_\sigma(k < k_{F_\sigma})$. Most of the depletion for both $n_1(k)$ and $n_2(k)$ happens for $k < k_{F_1}$ since this is where most of the minority resides. This depletion for $k < k_{F_1}$ leaves $n_2(k)$ with a bump for $k_{F_1} < k < k_{F_2}$.

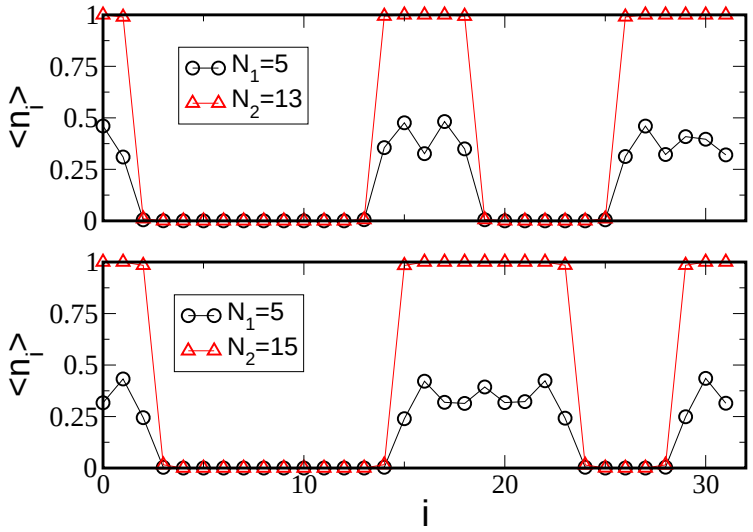

Figure 5.3: Average density profiles for collapsed systems. Here $U = -7t_1$ and $t_2 = 0.04t_1$. Note the Friedel-like oscillations in n_{i1}.

At first glance, it might seem that the disappearance of the FFLO peak, $n_{\text{pair}}(k = |k_{F_1} - k_{F_2}|)$, as t_2 decreases and the appearance of a peak $n_{\text{pair}}(k = 0)$ signals pair formation at $k = 0$ and thus a BP phase. However, a simple argument offers another option. The Fermi momentum of the majority is $k_{F_2} = \pi N_2/L$; consequently, as these particles get heavier, t_2 smaller, their kinetic energy becomes negligible and can be ignored. To minimize its free energy, the system will then optimize the potential and kinetic energies of the light particles. The optimal potential energy is obtained when the light particles are on the same sites as the heavy ones. On the other hand, the kinetic energy is optimized when the light particles are delocalized. Both these

energies can be optimized if the heavy particles coalesce, forming a contiguous region with one heavy particle per site, $n_{i2} = 1$. This region, then, acts as a platform on which the light particles can delocalize over its entire extent while always being in contact with the heavy particles thus minimizing their potential energy. This is indeed what happens as the density profiles, n_{i1} and n_{i2}, show in Fig. 5.3 for two polarizations. To summarize, as t_2 decreases, the system goes from an FFLO phase to a spatially collapsed one. In this case the spatial collapse corresponds to the system having regions void of particles and regions where all the particles reside. It is expected that at low temperature the system would eventually exhibit two domains (one with no particles and the other where the particles reside). The presence of four domains in Fig. 5.3 indicates that the simulation was not long enough to reach the configuration corresponding to the absolute minimum of energy when the two "droplets" would coalesce.

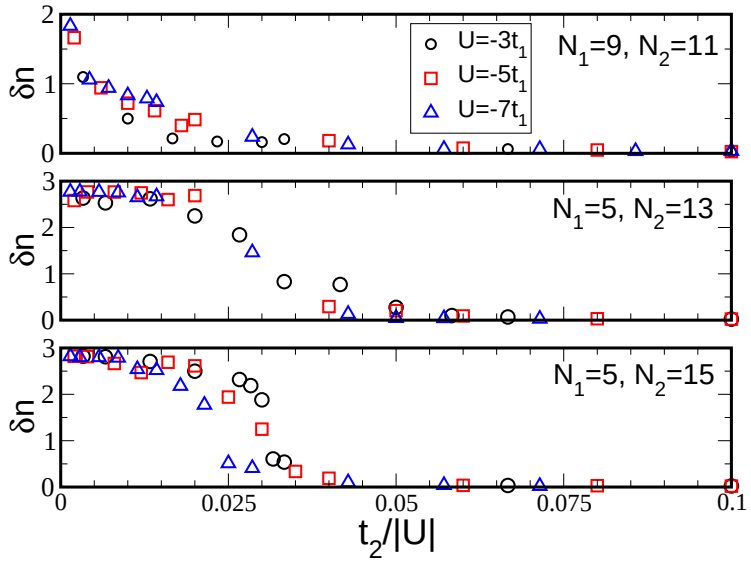

Figure 5.4: δn versus $t_2/|U|$ showing the collapse as t_2 gets small enough.

To quantify this collapse, we define the quantity $(\delta n)^2 \equiv \sum_i (\langle n_{i1} \rangle - N_1/L)^2$

which is essentially zero when the system is uniform ($\langle n_{i1} \rangle = N_1/L$) and grows as the collapse happens. One can also use $n_2(x)$ to define the δn, but the behavior is identical. We only show δn defined with $n_1(x)$. In Fig. 5.4 we show δn versus $t_2/|U|$ for three polarizations and three couplings in each case. We see that, indeed, the system collapses as t_2 decreases and that for a given polarization, this collapse appears to happen at approximately the same value of $t_2/|U|$. Also, the larger the polarization, the easier it is to trigger the collapse (larger t_2). This behavior holds for all the parameters we examined, specifically $-13 < U \leq -1$, and polarizations $0.1 \leq P \leq 0.55$

We, therefore, conclude that in the presence of only contact attraction, the BP phase is *not* realized as the majority population is made heavier; instead the system collapses.

To counter the tendency of the heavy particles to clump together as in Fig. 5.3, we introduce longer-range interaction. It is reasonable to suppose that nearest-neighbor (nn) repulsion between particles of the same species would tend to oppose such collapse. To this end we redid the above study but with the interaction term $H_I = \sum_i U n_{i1} n_{i2} + V \sum_{i,\sigma} n_{i\sigma} n_{i+1\sigma}$ with $U < 0$ and $V > 0$. We studied this for $0.1 \leq P \leq 0.44$ and with $-10t_1 \leq U \leq -4t_1$.

In the case of equal masses we look at the effect of turning on the repulsive nearest-neighbor interaction between fermions of the same species. The single particle momentum distribution is shown in Fig. 5.5. One observes rounding in the majority momentum distribution (top panel) and a bump appearing at high momenta in the minority (bottom panel). As the repulsion is increased in the case of the mixture of particles with equal masses the FFLO pairing is not destroyed, the height of the peak however is decreased as shown in Fig. 5.6 (top panel). Introducing the mass imbalance however destroys the FFLO pairing

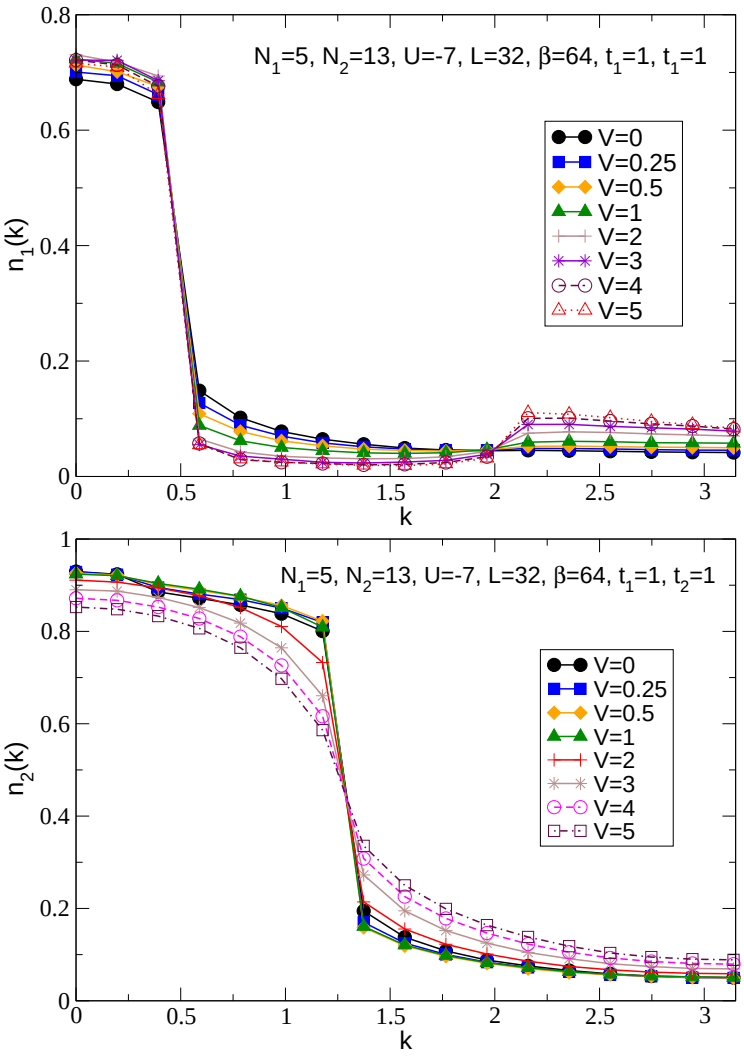

Figure 5.5: Momentum distributions $n_1(k)$ and $n_2(k)$ as the repulsive nearest-neighbor interaction between the same species V is increased. U and V are given in the units of t_1.

for $t_2/t_1 \leq 0.1$ as seen in Fig. 5.6 (bottom panel).

In order to clarify the state into which the system evolves when the FFLO peak disappears we look at the density distributions in the two parameter regimes: low mass imbalance (Fig. 5.7 top panel) and high mass imbalance (Fig. 5.7 bottom panel). In the case of low mass imbalance ($t_2/t_1 = 0.5$) where both species are delocalized over the whole system we observe the FFLO pairing as shown in Fig. 5.6 (bottom panel, black filled circles). In the case of high mass imbalance ($t_2/t_1 = 0.02$) where the particles form charge density wave over a large region of the lattice the particles get localized and the FFLO pairing disappears.

In the case when the masses are unequal we found that, indeed, the stability of the system against collapse is extended to smaller values of t_2 as shown in Fig. 5.8 but that eventually the system always collapses. Furthermore, before the collapse, the system always exhibits FFLO pairing while after collapse, the nn repulsion term, V, produces density oscillations as the presence of nearest neighbors is opposed as seen in Fig. 5.7 (bottom panel). Therefore, this second form of the interaction also fails to produce the BP phase.

We now turn to the third interaction form which was proposed in Ref. [71] and argued to yield the BP phase. This form extends beyond the contact term and acts only between particles from different species. The idea is based on the assumption of three competing homogeneous phases: a normal state of free fermions, a fully gapped BCS superfluid and a gapless BP phase. It was argued that by giving the interaction term structure in momentum space, one may be able to stabilize the BP phase; a Gaussian dependence on distance was used for the interaction potential in [71]. In our simulations we cut the range at the nn level and, therefore, have $H_I = \sum_i (U n_{i1} n_{i2} + V_{12} n_{i1} n_{i+12})$. Note that, unlike

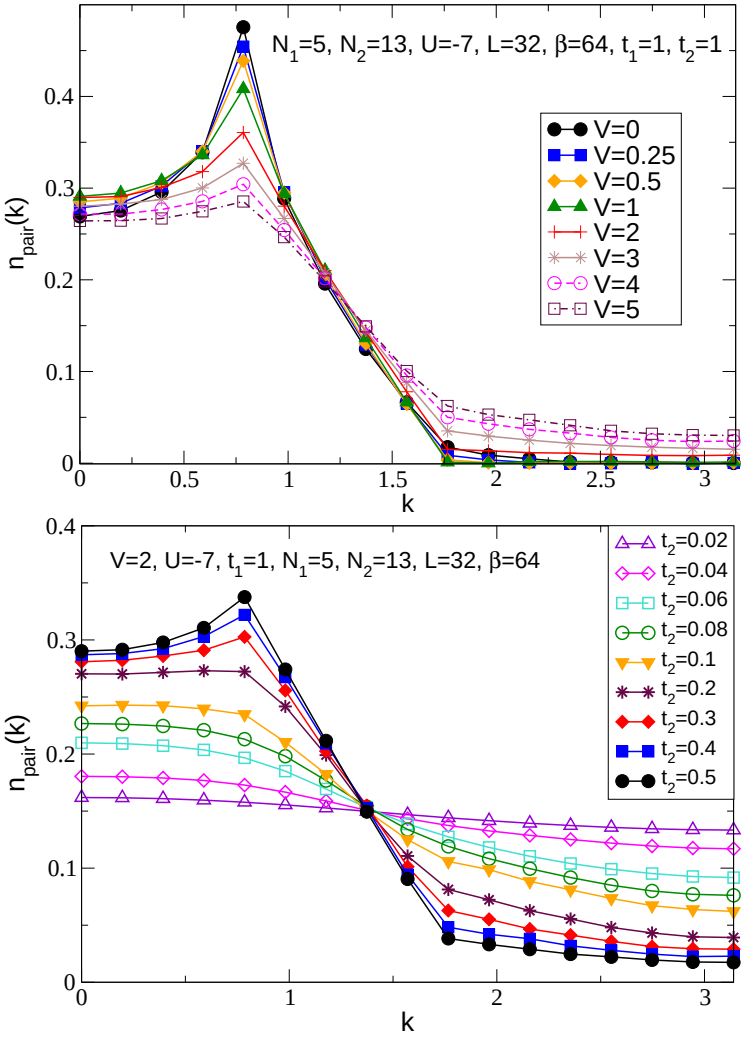

Figure 5.6: Top panel: In the case of $t_1 = t_2$ The FFLO peak in $n_{pair}(k)$ is present but decreasing in height as the repulsive nearest-neighbor interaction between the same species V is increased. Bottom panel: For $V = 2$ the pair momentum distribution for different mass imbalance ratios, shows that at a critical mass imbalance, here $t_2/t_1 = 0.1$ the FFLO peak disappears.

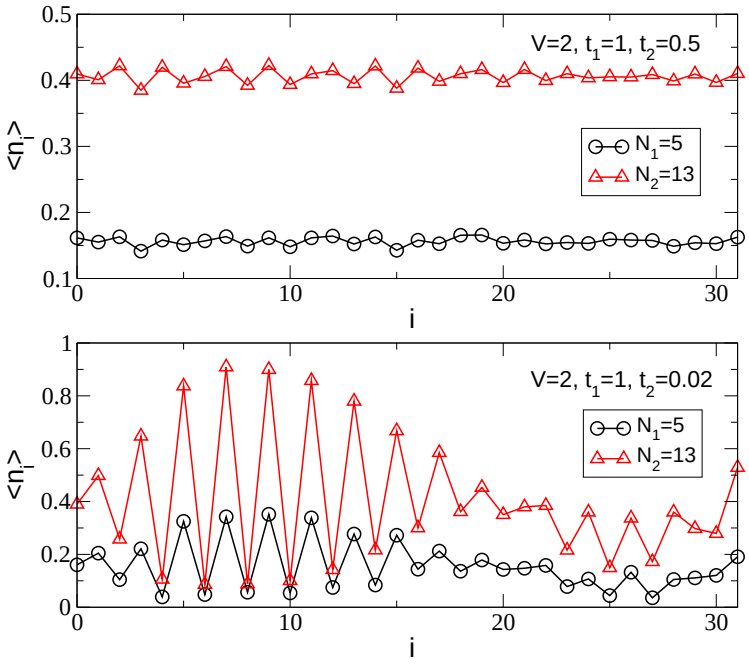

Figure 5.7: Density profiles of majority and minority particles with nearest-neighbor repulsion between the same species $V = 2$. The simulations are done at $U = -7$, $L = 32$ and $\beta = 64$.

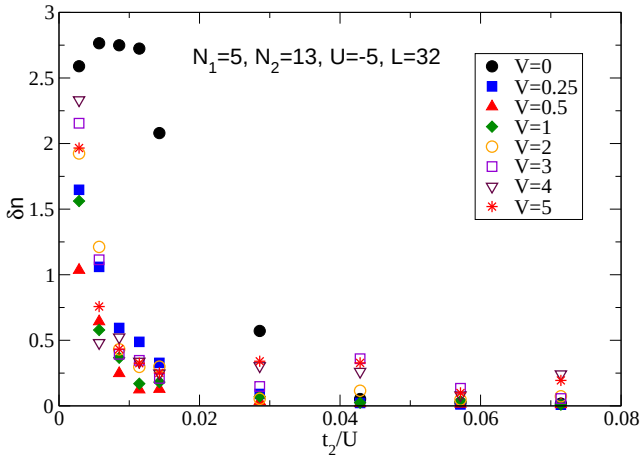

Figure 5.8: δn versus $t_2/|U|$ showing the collapse is pushed towards smaller t_2 when we turn on repulsive nearest-neighbor interaction V.

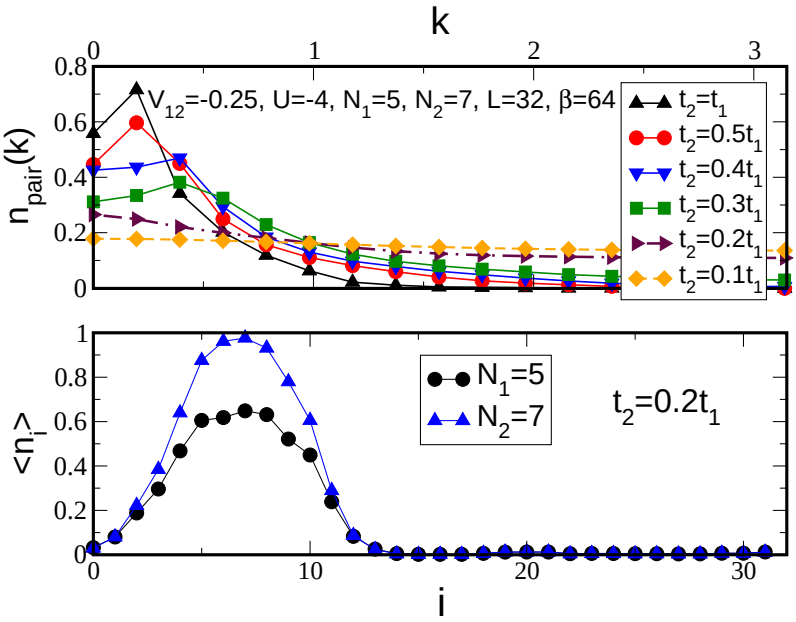

Figure 5.9: Top: Pair momentum distribution $n_{\text{pair}}(k)$ for several values of t_2 showing the disappearance of the FFLO peak. Bottom: Average density profiles for same parameters as top panel but $t_2 = 0.2t_1$ showing the system when it first collapses. The contact interaction is $U = -4$ and the nn interaction is $V_{12} = -0.25$ acting only between particles of opposite spin. U and V_{12} are given in units of t_1.

the previous form, V_{12} here acts only between n_1 and n_2. In momentum space, this has the form $U+2V_{12}\cos(q)$ at momentum q. With both $U < 0$ and $V_{12} < 0$ the interaction is more attractive at small q in contradistinction to the pure contact interaction which is independent of q. Our exact QMC results show, however, that the system is still unstable and collapses as t_2 decreases, just like in the contact interaction case. This is shown in Fig. 5.9 for the attractive nearest-neighbor interaction case: No BP phase has been found. In fact, with the longer-range attraction, the system is even *more* unstable as can be easily understood by the same argument concerning energy minimization presented before for the contact interaction case. The effect of the attractive nearest-neighbor inter-species interaction on single particle momentum distributions is shown in Fig. 5.10.

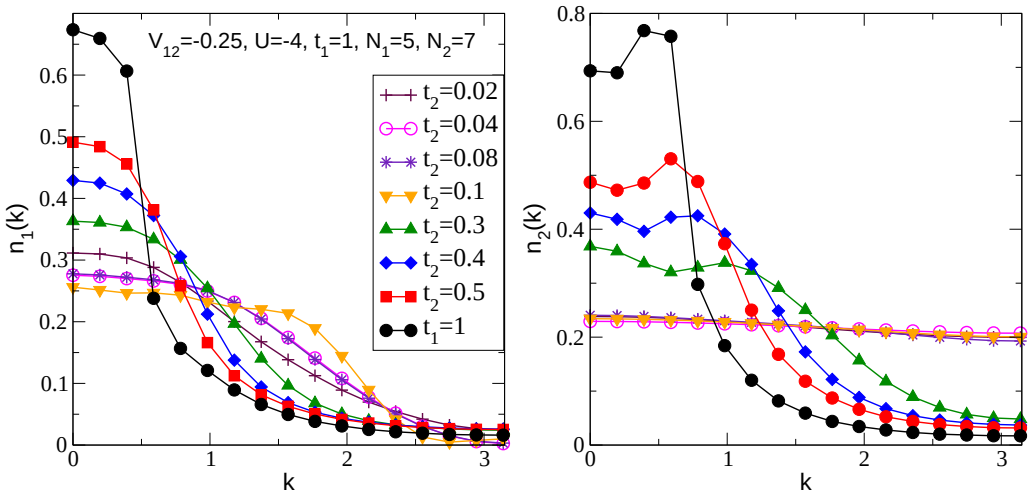

Figure 5.10: Momentum distributions $n_1(k)$ and $n_2(k)$ with attractive nearest-neighbor interaction between different species $V_{12} = -0.25$, $L = 32$ and $\beta = 64$.

We investigated also the case of repulsive nearest-neighbor interaction between different species ($V_{12} > 0$). First we look at the effect of this kind of interaction on the momentum distributions when the masses of the species are

equal. When the repulsion is high enough the momentum distribution of the minority loses the fermionic character and we do not observe a Fermi-step like distribution for $V_{12} \geq 3$ in Fig. 5.11 (left panel), while this effect is not present in the majority momentum distribution (right panel).

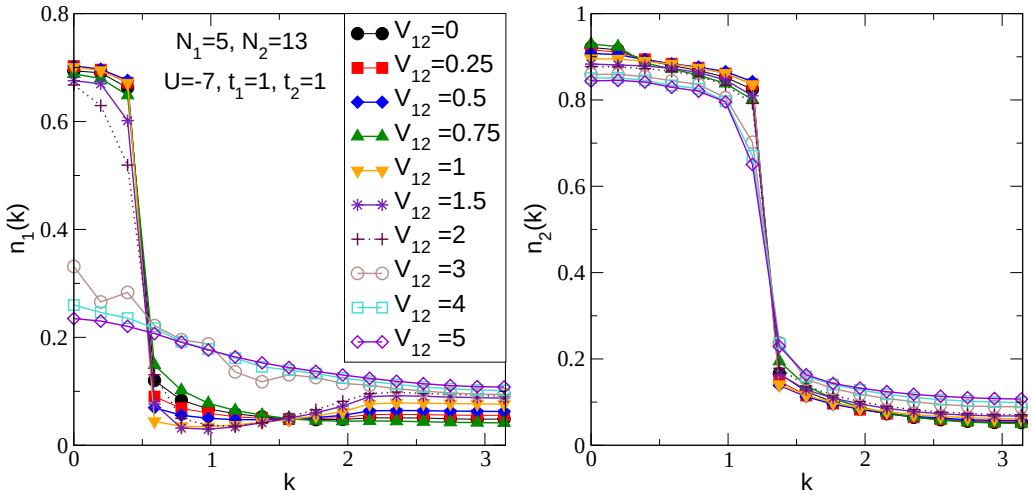

Figure 5.11: Momentum distributions $n_1(k)$ and $n_2(k)$ as the repulsive nearest-neighbor interaction between different species V_{12} is increased. At $V_{12} = 3$ the minority momentum distribution (left panel) is not a Fermi distribution anymore while the majority momentum distribution has a form of a Fermi step for all used values of interaction (right panel).$L = 32$ and $\beta = 64$.

For small values of the repulsion FFLO pairing is observed in the system as seen in Fig. 5.12. This pairing disappears at interactions $V_{12} \geq 3$ which is consistent with the change in the character of the momentum distribution of the majority species as shown above. The nearest-neighbor inter-species repulsion efficiently leads the system to collapse so that there is no FFLO pairing as seen for *e.g.* in the case of $V_{12} = 5$ in Fig. 5.12 (right panel).

To understand better the two regimes of weak and strong repulsive inter-species nearest-neighbor interaction it is interesting to look at the density profiles for equal masses $t_1 = t_2 = 1$ and unequal masses $t_2/t_1 = 0.02$. In the

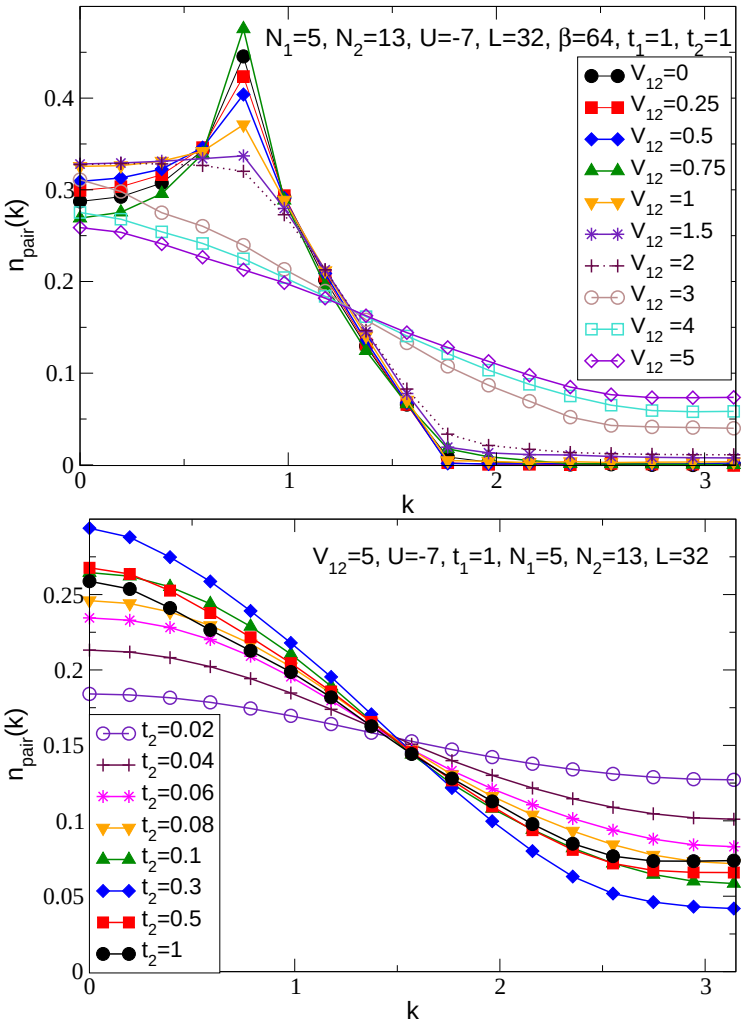

Figure 5.12: In the case of equal masses the FFLO peak in $n_{pair}(k)$ is present but decreasing in height as the repulsive nearest-neighbor interaction between different species V is increased (top panel). The momentum distribution of the pairs is shown for $V_{12} = 5$ and increasing mass imbalance (bottom panel).

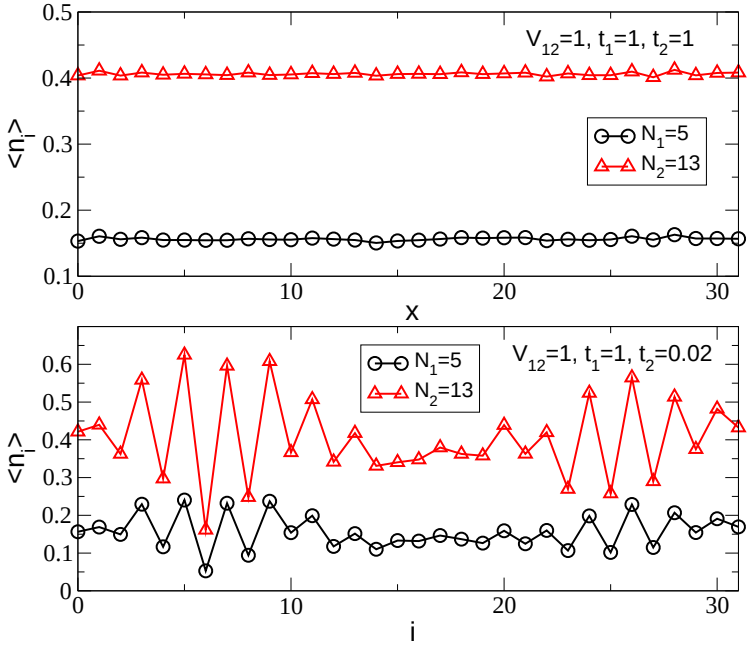

Figure 5.13: Density profiles of majority and minority particles with equal masses ($t_1 = t_2 = 1$ on the top panel) and unequal masses ($t_2/t_1 = 0.02$ on the bottom panel) for nearest-neighbor inter-species repulsion $V_{12} = 1$ and $U = -7$, $L = 32$ and $\beta = 64$.

case of weak interaction shown in Fig. 5.13 in the top panel we see homogenous densities of each species for equal masses which can be understood as delocalization of the particles with the goal of minimizing the kinetic energy. As can be seen in Fig. 5.12 (top panel) for $V_{12} = 1$ (orange triangles) the system exhibits FFLO pairing. For this value of nearest-neighbor interaction we observe that the FFLO peak disappears for $t_2/t_1 \leq 0.1$. It is interesting to look at the density profiles in the parameter regime where the peak disappears, shown in Fig. 5.13 (bottom panel). The particle densities are no longer homogenous, but the system collapses into regions with charged density wave where the potential energy is minimized as only every second site is doubly occupied and regions where both species are delocalized. Given the repulsive character of the nearest-neighbor interaction what is observed is a rather intuitive scenario. As mentioned before, when the majority is much heavier than the minority, the kinetic energy of the majority is not a significant contribution and the particles tend to get localized.

However for the strong interaction regime as seen in Fig. 5.12 (bottom panel) the system does not exibit the FFLO pairing even for equal masses. This can be understood when looking at the density profiles shown in Fig. 5.14. The nearest-neighbor inter-species repulsion is strong enough to induce collapse in the system with equal masses (top panel). The system minimizes the potential energy by forming a charge density wave where the minority species is localized in one region and the excess particles of the majority are free to move across the rest of the lattice thus minimizing their kinetic energy. When the majority particles are sufficiently heavier than the minority as shown Fig. 5.14 (bottom panel) the situation is identical to the one for weaker V_{12} and the system seems to minimize its potential energy by collapsing into a charge density wave spread

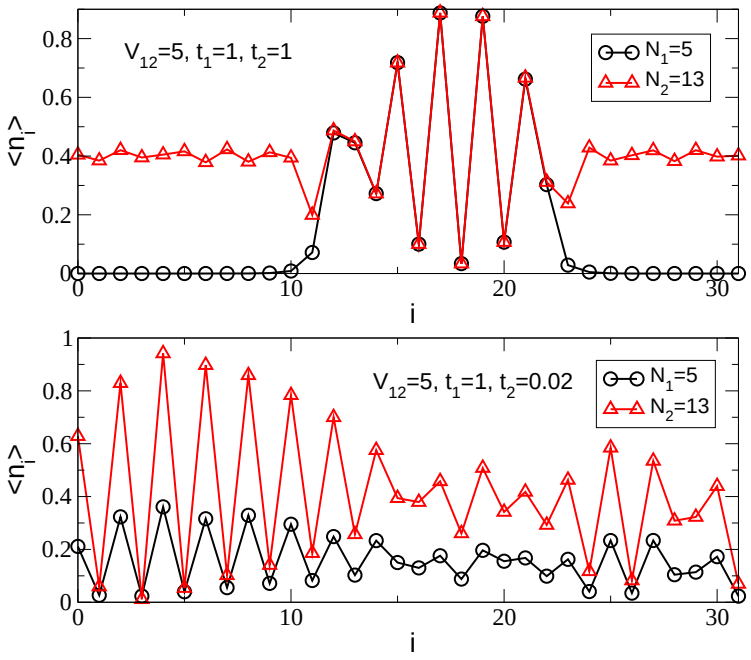

Figure 5.14: Density profiles of majority and minority particles with equal masses ($t_1 = t_2 = 1$ on the top panel) and unequal masses ($t_2/t_1 = 0.02$ on the bottom panel) for nearest-neighbor inter-species repulsion $V_{12} = 5$ and $U = -7$, $L = 32$ and $\beta = 64$.

over most of the system.

In Fig. 5.15 we can see that again the collapse is delayed to lower t_2 as compared to the case with $V_{12} = 0$, however it is not prevented.

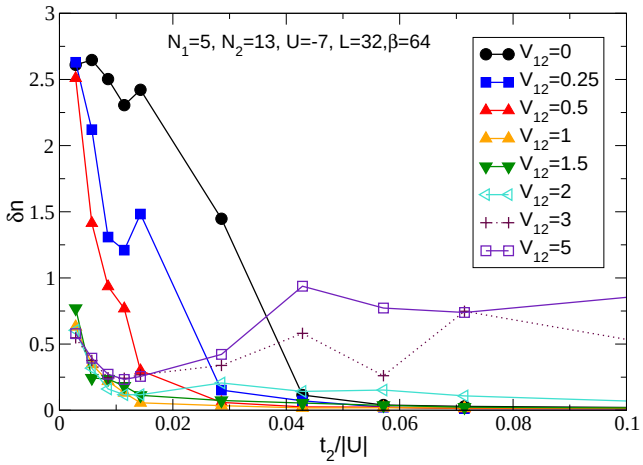

Figure 5.15: δn versus $t_2/|U|$ showing the collapse is pushed towards smaller t_2 when we turn on repulsive nearest-neighbor interaction between different speciesV_{12}.

5.3 Heavy Minority: $t_1 < t_2$

So far, we have considered the case where the heavy particles are the majority which, in case of only contact attraction, leads to collapsed configurations like those in Fig. 5.3. The question then is: Will the system still collapse when the heavy particles are the minority and what form will the collapsed configurations take? We now consider this case with a heavy minority population $N_1 = 9$, and a lighter majority, $N_2 = 13$, on a 32-site lattice with $\beta = 64$. As before, we fix the light population hopping $t_2 = 1$ to define the energy scale and we study the collapse as a function of the heavy minority hopping parameter, t_1/t_2, and the attractive interaction, $U/t_2 < 0$. In the top panel

of Fig. 5.16 we show, like in Fig. 5.4, δn as a function $t_1/|U|$ for five different values of the interaction, U.

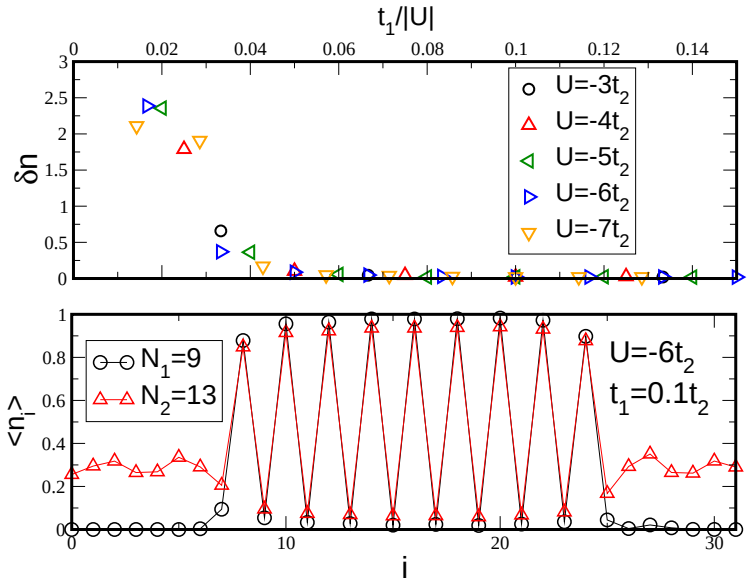

Figure 5.16: Top: δn rises sharply at $t_1/|U| \approx 0.03$ signalling a transition to an inhomogeneous density profile. Bottom: For $t_1/|U| < 0.03$, the system undergoes phase separation as shown in this typical density profile. Part of the system is in a charge density wave phase while the remainder is in a free fermion phase.

The behavior is similar to that in Fig. 5.4; we find that for these values of N_1 and N_2, δn increases sharply for $t_1/|U| \approx 0.03$ signalling spatial collapse in the system. One candidate for the collapsed configuration is that, as before, the heavy particles (the minority in this case) form a contiguous region thus providing a platform for the lighter particles. This would then result in a contiguous region with one heavy and one light particle per site and the excess light majority particles spread over the rest of the system. This, however, does not minimize the energy because the light particles residing on the heavy particle platform are blocked: They are in a Mott state and have zero kinetic energy. In the bottom panel of Fig. 5.16 we show a typical density profile of a

collapsed configuration. It is easy to understand energetically why this density wave structure is favored over the previous candidate: The light particles are never blocked in a Mott region and can always hop to neighboring sites to optimize the free energy.

We note that the configuration in Fig. 5.16 corresponds to phase separation: In one region the system is in a charge density wave phase, in the other region it has free fermions. These two phases co-exist.

5.4 Summary

In this chapter, we have studied, using exact QMC simulations, the effect of mass differences between two imbalanced Fermion populations. For the case where the majority population is the heavier, we performed our study with three possible interaction terms. In all three cases, we have found the system to be unstable and to collapse when the mass disparity is large enough: The BP phase is not realized by tuning the mass ratio between the two populations. For the case where the minority is heavier, we showed the system still collapses when the mass difference is large enough, but in this case it forms density wave structures.

We mention that the mass imbalanced mixture of Fermions in a harmonic trap, its equilibrium properties and dynamics were studied by Orso *et. al.* in [95]. A possible phase of trimers appearing in the uniform system at commensurate fillings was shown in [96].

Part II

Two dimensional system

Chapter 6

Introduction to population imbalanced systems in 2D

As was shown in the preceding part of this thesis and as is by now widely accepted, at $T = 0$ the FFLO phase is robust over a wide range of parameters in one-dimensional systems with imbalanced fermion populations. Also in the finite temperature study in Chapter 4, it was shown that the FFLO is stable over a wide range of parameters in the temperature-polarization phase diagram. The question of the stability of this phase in higher dimensions remains a subject of debate. It is believed that "nesting" of the Fermi surfaces stabilizes FFLO pairing. For example in one dimension one wave-vector connects all points on the Fermi surfaces of each species, which would enable all particles from the Fermi surfaces to participate in the formation of pairs with finite-momentum. The effect of "nesting" is considerably weaker in higher dimensions. In a two-dimensional lattice system, the shape of a Fermi surface depends on the filling as shown in Fig. 6.1

At half filling the Fermi surface becomes a square and touches the edge of

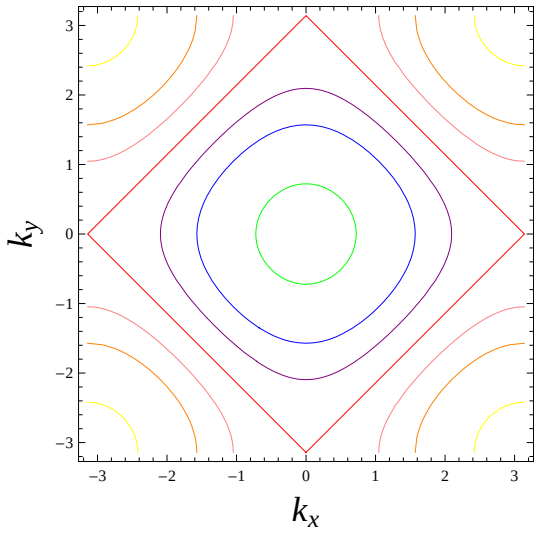

Figure 6.1: Fermi surface for fermions on a 2D square lattice with increasing filling from inside to outside. The half-filled Fermi surface is a square and exhibits nesting. The vectors (π, π) and $(-\pi, \pi)$ connect the regions of the Fermi surface.

the first Brillouin zone (Van Hove singularity). Around this filling, matching of the Fermi surfaces becomes more efficient, in other words the "nesting" is enhanced as compared to the situation when both Fermi surfaces are circular (low filling). This reasoning leads us to expect that FFLO pairing should be more prevalent around half filling than at lower fillings. This lattice enhanced stability of FFLO was studied using mean field (MF) methods in [11] and [91]. In the latter work, the authors point also to Hartree corrections and domain wall formation as additional reasons for enhancement.

Numerous theoretical studies of the system in higher dimensions do not offer a clear conclusion on the stability of the FFLO mechanism. In a variational MF study of a three dimensional system in the continuum with and without a trapping potential, it was observed that FFLO is a fragile state which can be realized only in a tiny sliver of the detuning-polarization phase diagram [97].

Furthermore, this study showed that in a trap, FFLO can exist only in a thin shell of the atomic cloud. Another study of a three dimensional Fermi gas at unitarity [98] shows that this phase is competitive over a large region in the phase diagram. However, the trap would need to be adjusted to allow FFLO to occupy a large enough spatial region to be observed. On the other hand, in a Bogoliubov-de Gennes study [33] of a trapped system, the calculated phase diagram indicates that the ground state of the system is always FFLO for any imbalance up to some critical value.

The unsettled status of this phase in higher dimensionality may be clarified with exact numerical simulations. However, simulations of the Hubbard model in three dimensions are not feasible for large systems at low enough temperatures due to the severity of the "fermion sign problem". On the other hand, exact QMC simulations in two dimensions are feasible but so far none have demonstrated the existence of the FFLO order in fermionic systems. In addition, two dimensional systems are intermediate between one dimension where MF is almost certain to fail and three dimensions where MF is more reliable. Consequently, there has been a concerted, yet inconclusive, effort to understand FFLO physics theoretically in two-dimensional systems. Homogeneous and trapped two-dimensional polarized Fermi gases have been studied with MF calculations which exclude the possibility of FFLO pairing (*e.g.* [99] and [100]). An interaction-polarization phase diagram is shown in [101] where FFLO pairing is seen to occupy a wide region. Koponen *et al.* [91] obtain MF phase diagrams in the polarization versus filling plane for one-, two- and three-dimensional systems. In the two-dimensional system, there is a very strong feature around the van Hove singularity of the majority component and the FFLO phase is present over a wide range of parameters around

this value. They also show temperature-polarization phase diagrams of one dimensional system which as our studies have shown do not agree with exact QMC results [73]. The temperature-polarization phase diagram in three dimensions is shown as well but not the two dimensional case. Studies of quasi two-dimensional systems have been done using MF and they predict a first-order transition to FFLO at finite temperature [102]. Another mean field study of two-dimensional two-orbital Hubbard model with p-orbitals and highly unidirectional hopping shows enhancement of the FFLO region in the phase diagram due to the one-dimensional character of the Fermi surface [103]. A DMRG study of population imbalanced Fermi gas on two-leg ladders has found FFLO pair correlations [104].

Additional motivation for studying the system in two dimensions is the hypothesis of a dimensionally driven crossover. As was mentioned before, it was observed that a fully paired (unpolarized) superfluid appears at the center for low polarizations [21, 22, 23] in the experiment in three dimensional cloud. On the other hand in the recent experiment by Liao *et. al.* [25] in the quasi-one-dimensional system, the fully paired superfluid was found at the edge of the cloud for $P < 0.15$. The question thus arises as to whether this is a dimensionally driven crossover and, if so, what is the mechanism behind it. Studying the intermediate situation of a two-dimensional system we could shed some light on this question. The relevance of these studies is proved also by the recent experimental study of the pairing of fermions in the crossover from three to two dimensions reported in [27] as well as a realization of the strongly interacting two-component Fermi gas confined to two dimensions in [28].

In this part of the thesis we present a study of the two dimensional Hubbard model with imbalanced populations of up and down spins that was done

using the Determinant Quantum Monte Carlo algorithm. It is important to emphasize that as far as we know these are the first exact Quantum Monte Carlo simulations for a two-dimensional lattice and imbalanced populations of fermions interacting attractively. Since the sign problem gets worse in higher dimensions the subject appeared at first to be too difficult to study using those methods, however, as it turned out, the simulations were feasible albeit very long.

The results for the uniform system are presented in Chapter 7. Our main result there is the demonstration of the robustness of the FFLO phase and the determination of the phase diagram in the temperature-polarization plane at low filling. We also compare the behavior of the system at low and half fillings. In Chapter 8, the system in a harmonic trap is examined. We present the density profiles and momentum distributions that are of experimental interest. In addition, a harmonic level basis is introduced which sheds new light on the character of the pairing in the trap.

6.1 2D Hubbard model

The system of interest is governed by the two-dimensional fermionic Hubbard Hamiltonian

$$\begin{aligned} \mathcal{H} &= -t \sum_{<i,j>\sigma} (c^{\dagger}_{i\sigma} c_{j\sigma} + c^{\dagger}_{j\sigma} c_{i\sigma}) - \sum_{i} (\mu_1 \hat{n}_{i1} + \mu_2 \hat{n}_{i2}) \\ &\quad + U \sum_{i} \left(\hat{n}_{i1} - \frac{1}{2} \right) \left(\hat{n}_{i2} - \frac{1}{2} \right) \\ &\quad + V_T \sum_{j} (j - j_c)^2 (\hat{n}_{j1} + \hat{n}_{j2}) \end{aligned} \tag{6.1}$$

Where $c^{\dagger}_{i\,\sigma}$ ($c_{i\,\sigma}$) create (annihilate) a fermion of spin $\sigma = 1, 2$ on lattice site i. The near neighbor, $< i, j >$, hopping parameter is t which we take equal to unity to set the energy scale. We consider only on-site interaction with an attractive coupling constant $U < 0$. The number of particles in each population is governed by its chemical potential (μ_σ). The harmonic trap is introduced via the V_T term in the Hamiltonian where j_c is the position of the center of the trap (chosen to be in the center of the lattice). All simulations are performed with periodic boundary conditions. In the confined case we ensured that the density vanishes at the edge of the lattice.

The main quantities of interest in this study are, as in the 1D case, the single particle Green functions G_σ and the pair Green function, G_{pair},

$$G_\sigma(l) = \langle c^{\dagger}_{i+l\,\sigma} c_{i\,\sigma} \rangle, \tag{6.2}$$

$$G_{\rm pair}(l) = \langle \Delta^{\dagger}_{i+l}\, \Delta_i \rangle, \tag{6.3}$$

$$\Delta_i = c_{i\,2}\, c_{i\,1}, \tag{6.4}$$

where Δ_i creates a pair on site i. The Fourier transform of G_σ gives the momentum distribution of the spins-σ species while the transform of $G_{\rm pair}$ yields the pair momentum distribution. In the trapped case, the density profiles of the two species are also studied by measuring the average density of each species at each site:

$$\langle n_{i\sigma} \rangle = \langle c^{\dagger}_{i\,\sigma} c_{i\,\sigma} \rangle \tag{6.5}$$

It is interesting to note that a well-known particle-hole transformation shows that this model is equivalent to a doped repulsive (positive U) Hubbard model. The transformation introduced by Emery in [105], and used by Moreo and Scalapino in [106], shows the correspondence between FFLO and striped

antiferromagnetic states appearing in the repulsive model. The Hamiltonian of interest is the one in Eq. 6.1 but with $V_T = 0$. Substituting $\bar{\mu} = \frac{\mu_1+\mu_2}{2}$ and $\delta\mu = \frac{\mu_1-\mu_2}{2}$, the equation becomes:

$$\begin{aligned}\mathcal{H} = & - t \sum_{<i,j>\sigma} (c^\dagger_{i\sigma} c_{j\sigma} + c^\dagger_{j\sigma} c_{i\sigma}) + U \sum_i \left(\hat{n}_{i1} - \frac{1}{2}\right)\left(\hat{n}_{i2} - \frac{1}{2}\right) \\ & - \sum_i \bar{\mu}\,(\hat{n}_{i1} + \hat{n}_{i2}) - \sum_i \delta\mu\,(\hat{n}_{i1} - \hat{n}_{i2})\,. \end{aligned} \tag{6.6}$$

The population imbalance now appears in the form of an external static magnetic field $\delta\mu$. We use the particle-hole transformation:

$$\begin{aligned} c_{i1} &\rightarrow (-1)^{i_x+i_y}\, d^\dagger_{i1} \\ c_{i2} &\rightarrow d_{i2}. \end{aligned} \tag{6.7}$$

The anticommutator becomes

$$\{c_{i1} c^\dagger_{j1}\} = -d^\dagger_{i1} d_{j1} - d_{j1} d^\dagger_{i1} = 0, \qquad i \neq j. \tag{6.8}$$

The hopping term is thus transformed and takes the same form as in the original Hamiltonian:

$$c^\dagger_{i\sigma} c_{j\sigma} = (-1)^{i_x+i_y}\, d_{i\sigma}\, (-1)^{j_x+j_y}\, d^\dagger_{j\sigma} = -d_{i\sigma} d^\dagger_{j\sigma} = d^\dagger_{j\sigma} d_{i\sigma}. \tag{6.9}$$

The kinetic term can be therefore written as:

$$\mathcal{H}_K = -t \sum_{<i,j>\sigma} (d^\dagger_{i\sigma} d_{j\sigma} + d^\dagger_{j\sigma} d_{i\sigma}) \tag{6.10}$$

The number operator of the first species transform into a number operator for

holes,

$$\hat{n}_{i\,1} = (-1)^{2(i_x+i_y)}\, d_{i\,1} d_{i\,1}^{\dagger} = 1 - d_{i\,1}^{\dagger} d_{i\,1} \tag{6.11}$$

where we used the anticommutation relation on the same site

$$\{c_{i\,1} c_{i\,1}^{\dagger}\} = d_{i\,1}^{\dagger} d_{i\,1} + d_{i\,1} d_{i\,1}^{\dagger} = 1. \tag{6.12}$$

The interaction term gains a minus sign and thus the model transforms to the positive U Hubbard model:

$$\begin{aligned} \mathcal{H}_U = \;& U \;\; \sum_i \left(1 - d_{i\,1}^{\dagger} d_{i\,1} - \frac{1}{2}\right)\left(d_{i\,2}^{\dagger} d_{i\,2} - \frac{1}{2}\right) \\ =\;& |U| \sum_i \left(d_{i\,1}^{\dagger} d_{i\,1} - \frac{1}{2}\right)\left(d_{i\,2}^{\dagger} d_{i\,2} - \frac{1}{2}\right) \end{aligned} \tag{6.13}$$

In the chemical potential term the transformation interchanges the roles of $\bar{\mu}$ and $\delta\mu$:

$$\mathcal{H}_{\mu} = -\sum_i \bar{\mu}\left(d_{i\,1}^{\dagger} d_{i\,1} - d_{i\,2}^{\dagger} d_{i\,2}\right) + \sum_i \delta\mu\left(d_{i\,1}^{\dagger} d_{i\,1} + d_{i\,2}^{\dagger} d_{i\,2}\right) - \mu_2 L \tag{6.14}$$

such that $\bar{\mu}$ is now the Zeeman field and $-\delta\mu$ the chemical potential that tunes the filling. L is the total number of sites. This transformation exhibits an equivalence between the attractive and repulsive Hubbard models. Using this particle-hole transformation Hirsch [56] showed that for the half filled band in the repulsive model the product of up and down determinants is always positive definite. The sign problem is, therefore, absent and the determinant product can be used as the Boltzmann weight in a quantum Monte Carlo simulations. This means there is no sign problem in the attractive Hubbard model at half filling when the populations are balanced. The case of no population imbalance

in the attractive model, $\delta\mu = 0$, corresponds to a repulsive Hubbard model in a Zeeman field (usually denoted as $h_z = \bar{\mu}$). The field is then responsible for breaking the XYZ rotational symmetry. The case of the polarized attractive system (also treated as Zeeman field) translates to a doped repulsive model.

We have studied the system described by the Hamiltonian Eq. 6.1 using the Determinant Quantum Monte Carlo algorithm described in section 2.3. As described there, tracing out the fermion operators leads to a partition function in the form of a product of two determinants, one for each spin. One of the advantages of this algorithm is that when the populations are balanced ($\mu_1 = \mu_2$) and $U < 0$ the determinants are identical up to a positive constant, so their product is always positive. However when the population are imbalanced ($\mu_1 \neq \mu_2$) the determinants are not the same any longer and the product can become negative resulting in the reappearance of the sign problem. Our simulations were done in a parameter regime (mostly low filling and not very low temperature $\beta = 10$) where the sign problem is sufficiently mild to get good statistics for the measurements of interest. In practice, this means that the average sign, $< sgn >$, does not go below 0.7. The sign problem gets much worse when the density is increased, thus our results for imbalanced populations around half filling are very limited.

6.2 Mean-field

Since QMC is limited by the sign problem in some parameter regimes, we also performed mean-field calculations to complement our numerical results. We also compare the QMC and MF results that we obtained in similar parameter regimes. The usual semi-classical local density approximation approach fails to

describe the physics of a trapped mixture of fermions on an optical lattice [107, 108]. Therefore, we take a different approach and treat the trapping potential as a spatially dependent chemical potential which we include directly in the mean-field approximation using a fully quantum mechanical Bogoliubov-de Gennes approach. In this method the mean-field parameter is site dependent and thus allows us to study the effects of inhomogeneity induced by the trap. The μ_σ, $\sigma = \pm 1$, controls the populations. Starting from the full Hamiltonian as in Eq. 6.1, one can derive the mean-field Hamiltonian with site dependent mean-field parameter:

$$\begin{aligned} H_{MF} &= \psi^\dagger M \psi + \frac{1}{U}\sum_i \Delta_i^* \Delta_i - \sum_i \mu_{i\,2} \\ M &= \begin{pmatrix} h_{ij\,1} & -\Delta_i \\ -\Delta_i^* & -h_{ji\,2} \end{pmatrix}, \end{aligned} \tag{6.15}$$

where $\Delta_i^* = U\langle c_{i\,1}^\dagger c_{i\,2}^\dagger \rangle$ are on-site pairing amplitudes. We use the notation where $\Psi^\dagger = \left(\cdots, c_{i1}^\dagger, \cdots, c_{i\,2}, \cdots\right)$ is the Nambu spinor and M is the Nambu matrix. The matrix h depicts the one particle Hamiltonian, namely hopping terms between nearest neighbors $< i, j > h_{ij\sigma} = -t$ and chemical potential terms which incorporate the trapping potential $h_{jj\sigma} = -\mu_{j\sigma} = -\mu_\sigma + V_T \left(j - j_c\right)^2 \hat{n}_{j\,\sigma}$. The matrix M is then diagonalized using Bogoliubov transformation,

$$\begin{pmatrix} c_{i\,1} \\ c_{i\,2}^\dagger \end{pmatrix} = \sum_n \begin{pmatrix} u_{n\,i\,1} & -v_{n\,i\,1}^* \\ v_{n\,i\,2} & u_{n\,i\,2}^* \end{pmatrix} \begin{pmatrix} \gamma_{n\,1} \\ \gamma_{n\,2}^\dagger \end{pmatrix}. \tag{6.16}$$

As mentioned earlier to account properly for spatial inhomogeneities, the BCS order parameter at each site, Δ_i, is an independent variable [107, 108, 109],

whose value is determined, for a given temperature, by a global minimization of the free energy, $F = -\frac{1}{\beta}\ln(\mathcal{Z})$, associated with the mean-field Hamiltonian

$$F = -\frac{1}{\beta}\sum_n \ln\left(1 + e^{-\beta\lambda_n}\right) + \frac{1}{U}\sum_i \Delta_i^*\Delta_i - \sum_i \mu_{i\,2}. \tag{6.17}$$

The λ_n are the $2L$ eigenvalues of the Nambu matrix M and L is the number of sites. We find the site-dependent values of the mean field parameter Δ_i by minimizing the free energy. The minimization is performed using a mixed quasi-Newton and conjugate gradient method and in order to ensure that the global minimum has been reached we performed additional checks.

Chapter 7

Translationally invariant system in 2D

We start the investigations into the physics of the two-dimensional system by studying the homogeneous two dimensional Hubbard model with balanced populations at low density. The dilute limit is the regime of interest to us as the influence of the lattice potential on the particles is weak and the results are relevant to the experiments and calculations done in the continuum limit. With balanced populations and the total density of $\rho = \rho_1 + \rho_2 = 0.3$, the pairs form with zero center of mass momentum and a sharp peak in the pair momentum distribution is expected at $\boldsymbol{k} = 0$. Figure 7.1 shows the momentum distributions for a system with $U = -3.5t$, $\rho_1 + \rho_2 = 0.3$ and $\beta = 30$ in a 16×16 optical lattice. The single particle momentum distribution, identical for the two spins, is shown in Fig. 7.1(a) while (b) shows the pair momentum distribution. As expected for weak to moderate values of $|U|$, the single particle distribution has the usual Fermi form and the pair momentum distribution exhibits a very sharp peak at $\boldsymbol{k} = 0$ indicating pairing with zero center of mass

momentum. This peak signals the presence of a condensate in the ground state of this system.

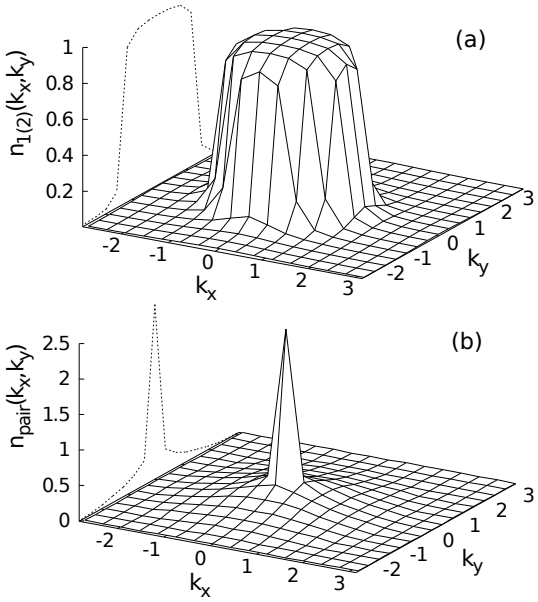

Figure 7.1: (a) Single particle momentum distribution, $n_1(k_x, k_y)$ (the same as $n_2(k_x, k_y)$). (b) Pair momentum distribution, $n_{pair}(k_x, k_y)$ exhibiting a sharp peak at zero momentum. The total density is $\rho_1 + \rho_2 = 0.3$ ($\rho_1 = \rho_2$), $\beta = 30$, $U = -3.5t$ and the system size is 16×16.

We now examine the polarized system. To this end, the chemical potentials μ_1 and μ_2 are made unequal so that $\rho_1 \neq \rho_2$ but $\rho = \rho_1 + \rho_2$ remains constant. When using a grand-canonical algorithm this requires tuning the chemical potentials appropriately as was described in the case of the one-dimensional system.

Figure 7.2 shows the momentum distributions for a system with $U = -3.5t$, $P = 0.6$, $\rho = 0.3$ and $\beta = 10$ in an optical lattice of size 16×16 for (a), (b) and (c) and 10×30 for (d). Panels (a) and (b) show the minority and majority single particle momentum distributions, $n_1(k_x, k_y)$ and $n_2(k_x, k_y)$, respectively. They exhibit the usual Fermi-like distributions. However, the pair momentum

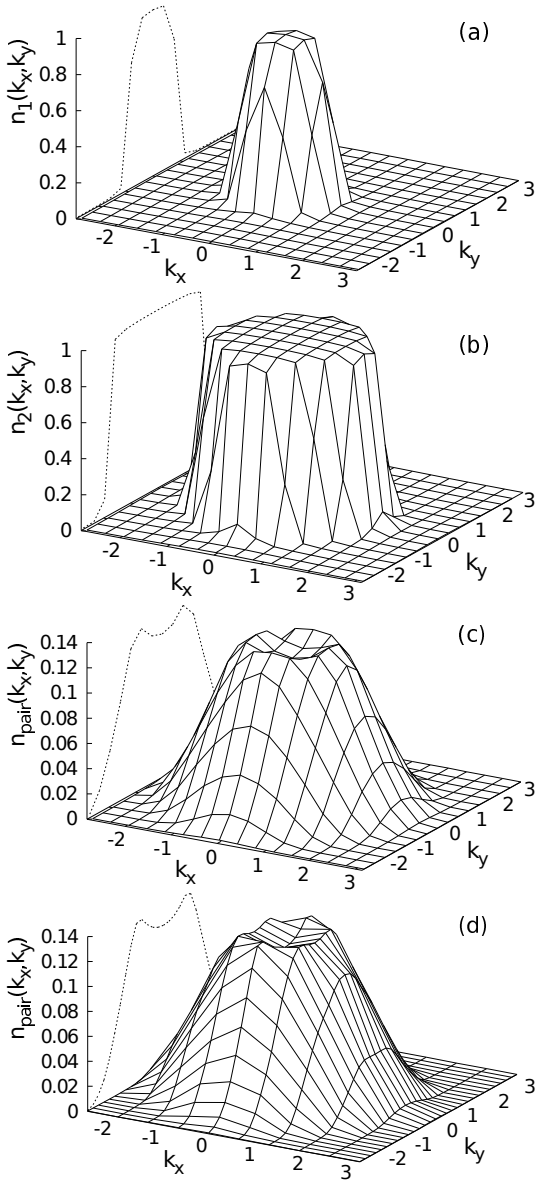

Figure 7.2: Momentum distributions of (a) minority and (b) majority populations. (c) shows the pair momentum distribution. The parameters are $\rho = \rho_1 + \rho_2 = 0.3$, $P = 0.6$, $\beta = 10$, $U = -3.5t$ in an optical lattice of size 16×16. (d) The pair momentum distribution for the same system but for a lattice of size 10×30.

distribution, $n_{\text{pair}}(k_x, k_y)$ (c), is strikingly different from the balanced case: It has a volcano-like shape with the maximum of the distribution at the rim of the crater of radius $|\boldsymbol{k}| = |\boldsymbol{k}_{F2} - \boldsymbol{k}_{F1}|$. $\boldsymbol{k}_{F1}$ and $\boldsymbol{k}_{F2}$ are the minority and

majority Fermi momenta respectively.

The behavior exhibited in Fig. 7.2 is for low filling, where the Fermi distributions of both species have cylindrical shape and the pairs are formed with equal probability in all radial directions. In this density regime, the signature for the FFLO phase is the presence of a circular ridge in the pair momentum distribution as seen in Fig. 7.2(c).

To study possible finite size effects, we performed our simulations for systems of various sizes. In particular, Fig. 7.2(d) shows the pair momentum distribution for the same parameters as (a,b,c) but with a system of size 10×30. It is seen that the peak in the pair momentum distribution is at the same values of $|\boldsymbol{k}| = |\boldsymbol{k}_{F1} - \boldsymbol{k}_{F2}|$ as the 16×16 system.

7.1 Phase Diagram

We now examine the effect of temperature on the FFLO phase. In particular, we map out the phase diagram in the temperature-polarization plane. Thermal effects are very important in experiments due to the difficulty in cooling fermionic atoms. The inset in Fig. 7.3 shows two-dimensional cuts in the three-dimensional pair momentum distribution for a 16×16 system with $U = -3.5t$, $\rho = 0.3$ and $P = 0.55$. We see that as the temperature is increased (β decreased) the FFLO peak at nonzero momentum decreases and, in fact, shifts towards zero momentum. Our criterion for the appearance of the FFLO phase is when the peak of the pair momentum distribution is no longer at zero momentum. As we saw in one dimension, the question is then: what replaces the FFLO phase? Have the pairs been broken by thermal fluctuations or has the system been homogenized, resulting in a uniform mixture of pairs and

excess unpaired particles of the majority population? The double occupancy, $D = \langle n_1(\boldsymbol{r}) n_2(\boldsymbol{r}) \rangle$, offers a measure of how tightly bound the pairs are: In the absence of pairing, $D = \rho_1 \rho_2$ while when the pairing is complete, $D = \rho_1$ where ρ_1 is the density of the minority population. These limits suggest the use of a normalized form, $(D - \rho_1\rho_2)/(\rho_1 - \rho_1\rho_2)$, which is now bounded by 0 and 1. Note that $\rho_1 = N_1/L^2$ while $\langle n_1(\boldsymbol{r}) \rangle$ is the average number of type 1 particles at $\boldsymbol{r}$. In the absence of pairing the two quantities coincide. We see in Fig. 7.3 that for $\beta > 3$ the normalized double occupancy is essentially constant signaling the continued presence of pairs. This means that when the FFLO peak first disappears at $3 < \beta < 4$, the pairs are still formed. We conclude, therefore, that the system leaves the FFLO phase to enter a polarized paired phase (PPP) phase.

When the thermal energy, $T = 1/\beta$, is of the order of the pair binding energy, $|U|$, the pairs are expected to break. We see in Fig. 7.3 that the double occupancy decreases precipitously only for $\beta < 1$ which is consistent with the value of $1/|U| = 1/3.5$ in our simulation. Similar behavior was found for the one-dimensional system [73].

We also note that, similarly to the one-dimensional case shown in Fig. 4.6, the double occupancy exhibits an enhancement just before the breaking of the pairs as seen in Fig. 7.3. The increase is explained by enhanced pairing due to depletion of the Fermi sea at high temperature.

The phase diagram is mapped by fixing the polarization, P, and increasing T until the peak in the pair momentum distribution shifts to zero momentum (inset Fig. 7.3). The phase diagram for $\rho = \rho_1 + \rho_2 = 0.3$ (red circles) and $\rho = 1$ (purple squares) is shown in Fig. 7.4. The solid circles show the boundary of the FFLO phase; the open circles indicate the largest P at which we were able

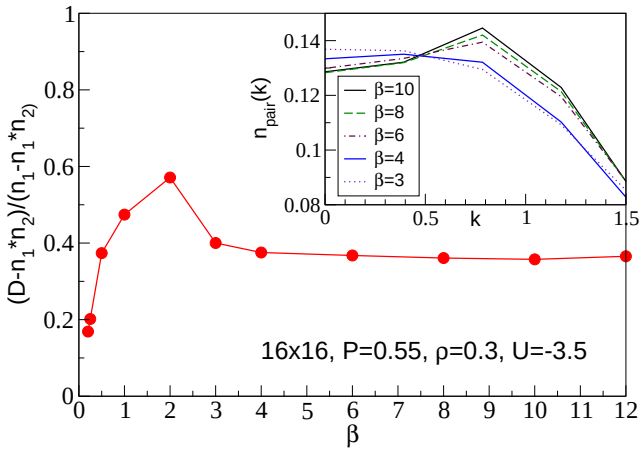

Figure 7.3: (The normalized double occupancy as a function of inverse temperature, β for $\rho = 0.3$, $P = 0.55$ and $U = -3.5t$. The lattice size is 16×16. Inset: Behavior of the pair momentum distribution as the temperature is increased (β is decreased).

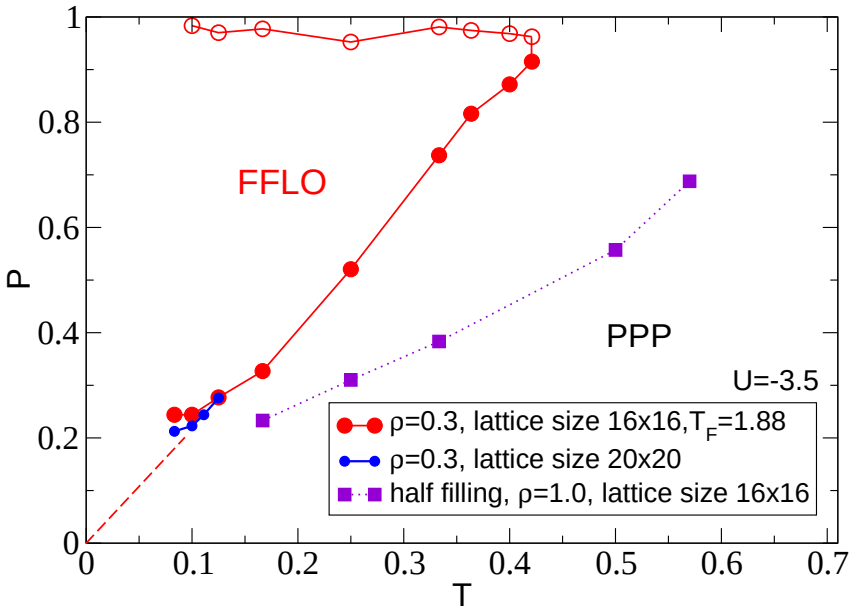

Figure 7.4: Finite temperature phase diagram of the system at $\rho = 0.3$

to study the system. Up to these high polarizations the system remained in the FFLO phase. The FFLO phase boundary at low P appears to extrapolate to $P \neq 0$ as $T \to 0$ for the 16×16 system. However, this is an effect of the

coarseness of the lattice grid. As P decreases, the peak in the pair momentum distribution falls between 0 and $2\pi/L$ and gives the impression of peaking at zero momentum. The smaller solid circles (blue) show the phase boundary for a 20×20 system; we see that the effect is corrected for a while, but then even larger systems are needed. This is not possible because as T decreases the sign problem becomes too severe. We believe that as soon as the system is polarized it goes into the FFLO phase if T is low enough. The long dashed line connecting this FFLO boundary to the origin schematizes this. Outside the FFLO phase the system is in the polarized paired phase (PPP) since the pairs are still formed and break only at higher T than shown in the figure. The squares in Fig. 7.4 show the phase boundary at these temperatures for the case of $\rho = 1$ (discussed below).

It is important to emphasize here that, in our discussion, the FFLO state is characterized by the behavior of the pair momentum distribution: If the peak is at non-zero momentum the system is in the FFLO phase. The question naturally arises as to whether the FFLO pairs have phase coherence and are, consequently, superfluid. In the balanced case, the phase diagram in the temperature versus filling plane was determined for $U = -4$ in Ref. [110]. By studying the pairing susceptibility which we define as $P_s = \sum_l G_{pair}(l)$ as a function of T as in Ref. [110], we find that in the balanced case of our system with $U = -3.5$ (black curve in Fig. 7.5), the critical temperature is $T_c \approx 0.1$ in good agreement with the $U = -4$ results [110].

However, studying the same pairing susceptibility in the polarized case showed no sign of s-wave superfluidity in the temperature range attainable by QMC as shown in Fig. 7.5. Our preliminary numerical results support approximate analytic results which indicate that polarization may suppress

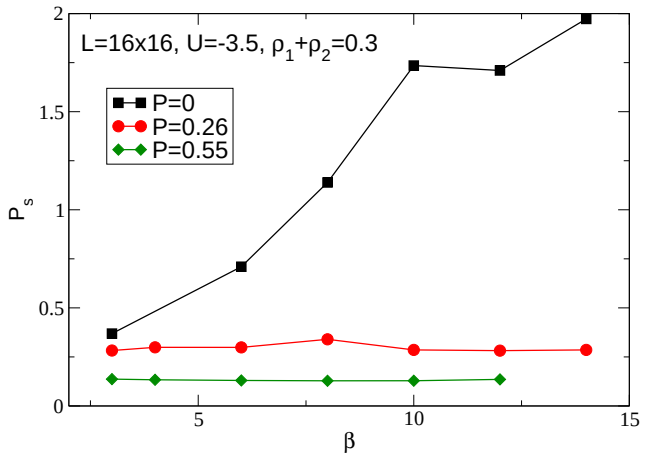

Figure 7.5: Pairing susceptibility for different polarizations (black line - balanced, $P = 0.26$ and $P = 0.55$) and with decreasing T.

superfluidity in the FFLO phase [111]. It is, therefore, currently not clear if when T is reduced even further, the FFLO phase will become superfluid. We note, however, that the current focus of most experimental measures of FFLO is the same non-zero momentum peak on which our simulations concentrate.

The phase diagram, Fig. 7.4, resembles the one found in one dimension [73] and shows that FFLO is very robust. The Fermi temperature is calculated as usual by considering a non-interacting system with balanced populations where We will sometimes use the non-interacting Fermi momentum value in the characterization of the system and its Fermi temperature which can be calculated in two dimensional system using the expression for Fermi momentum as $|k_F| = \sqrt{4\pi\frac{\rho}{2}}$ and gives for $\rho = 0.3$ a value $T_F = 1.88t$. The FFLO phase at high P survives up to $T = 0.2T_F$ while in one dimension [73] at $\rho = 0.25$, FFLO survives up to $T = 0.8T_F$ at high P. So, while FFLO is still robust in two dimensions, it is more easily destroyed by finite T. This is important to keep in mind in experiments.

7.2 System around half filling

In a two-dimensional lattice, the Fermi surface geometry evolves with the filling from closed, rotationally symmetric surfaces for low filling to a square at half filling to open surfaces for higher filling as shown in Fig. 6.1. Consequently, pairing at finite momentum occurs with different symmetries depending on the filling. The pairs form with equal probability in all radial directions in the case of low filling while they form in preferred directions when the Fermi surfaces are anisotropic.

As discussed in Chapter 6, there are claims that around the Van Hove singularity the FFLO pairing could be enhanced due to increased nesting. Indeed we observe that FFLO is stable over a wider range of temperatures and polarizations for $\rho = 1$. The squares in Fig. 7.4 show the FFLO-PPP boundary in the half filled case. It is seen that the FFLO phase persists to higher T than the low density case. However, when compared to $T_F = 6.28t$, FFLO is destroyed for $T \approx 0.08T_F$ as compared with $T \approx 0.2T_F$ for the half filled case in one dimension.

When the populations are imbalanced around half filling, one can readily see the effect of the interaction on the Fermi surfaces. Figure 7.6 shows the difference between the Fermi distributions of the species calculated using both mean field and QMC methods. The momentum distributions look approximately like nested squares parallel to each other in most of the momentum states, whereas the non-interacting distributions would look more rounded and not as parallel. Similar Fermi surface geometry in the context of LO states in 3D have been shown in [11].

The reason the system exhibits such Fermi surfaces can be understood as

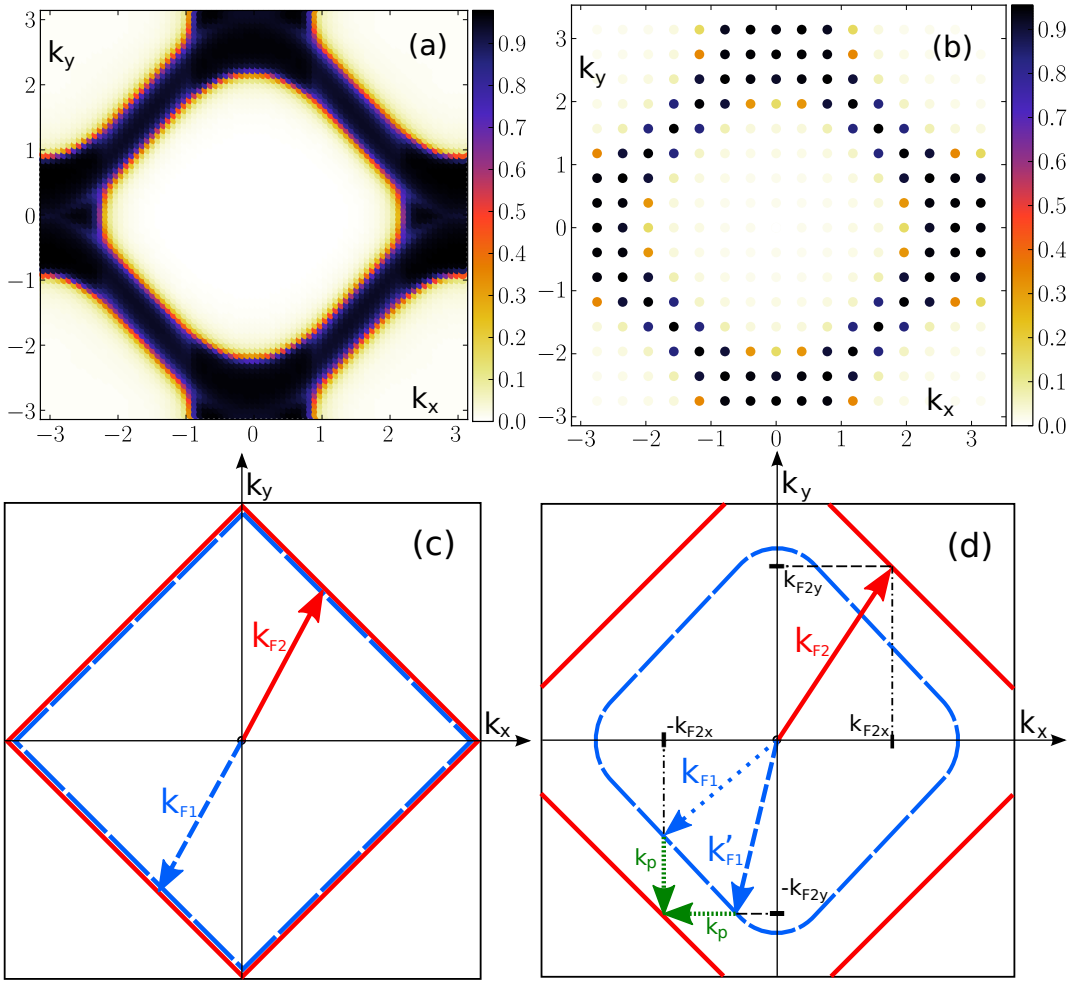

Figure 7.6: Top row: difference in the momentum distributions of majority and minority, showing parallel Fermi surfaces from the Mean-Field method (a) and from QMC (b). Bottom row: pairing schematic for balanced (c) and imbalanced (d) populations. In the situation where the populations of fermionic species are imbalanced (diagram on the right) a particle from the majority species forms a pair with a particle from the minority whose Fermi momentum either matches the k_x or k_y coordinate of the majority particle Fermi vector. The pair formed has a finite momentum equal to the distance of the two Fermi surfaces either along k_x or k_y.

follows. If we look at the region of $k_x > 0$ we can parametrize the linear part of the majority Fermi line as $k^+_{f,2}(k_x) = -k_x + \alpha_2$ for positive values and $k^-_{f,2}(k_x) = k_x - \alpha_2$ for negative values and doing the same for the minority we have $k^+_{f,1}(k_x) = -k_x + \alpha_1$ and $k^-_{f,1}(k_x) = k_x - \alpha_1$. (see Fig. 7.6). Pairing

happens here for a given k_x between the upper part of the majority branch and the lower part of the minority branch, $k^+_{f2}(k_x)$ pairs with $k^-_{f1}(-k_x)$. The momentum of the pair along y is the sum of these momenta and is equal to $q_y = k^+_{f2}(k_x) + k^-_{f1}(-k_x) = \alpha_2 - \alpha_1$. Therefore, thanks to the parallel Fermi lines, the pairing momentum is independent of k_x, leading to a strong enhancement of the pairing efficiency. The same construction can be done in the k_x direction, matching the y coordinate of the momentum vectors and the pairs will be moving along x with $\pm q_x$. In other words, for each k_x, we have, along k_y, the usual imbalanced 1D situation, *i.e.* two rectangular Fermi distributions, with different Fermi momenta. Again, the crucial point is both the majority and minority effective 1D Fermi momentum values change the same way with k_x: the two Fermi surfaces remain always at the same distance from each other. This pairing mechanism is illustrated in Fig. 7.6d. The excess fermions correspond to the part of the majority Fermi surface which can't be paired this way, *i.e.* the four regions around $(k_x = 0, ky = \pm\pi)$ and $(k_x = \pm\pi, ky = 0)$. Note that in the balanced case, this corresponds to the usual BCS pairing on a lattice: a particle of one species from the Fermi surface can form a pair with a particle from the other species with the Fermi vector of equal length but opposite direction (as shown in Fig. 7.6c). The resulting pair has, as expected, a zero center-of-mass momentum. The pairing along k_x and k_y might not seem the most intuitive scenario, since one can imagine the pairs forming with momentum along the diagonal with smaller $|\boldsymbol{k}_p|$. Since this pairing was not observed in any of our simulations, this probably means that, in a mean field approach, it only corresponds to a local minimum of the free energy.

However, since the shape of Fermi surfaces is affected by the nature of the

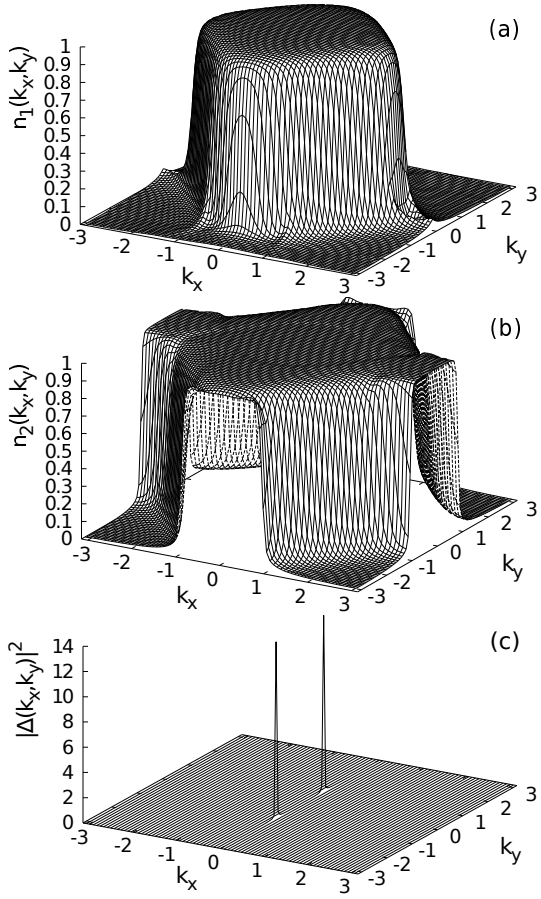

Figure 7.7: Momentum distributions of (a) minority, (b) majority and and (c) order parameter in k-space calculated using the Mean-Field method. $\rho = \rho_1 + \rho_2 = 1$. Here $P = 0.32$, $\beta = 25$, $U = -3.5t$ and the lattice size is 79×79. The pairing peaks are symmetric along k_x or k_y depending on the realization.

pairing, one cannot directly compare both situations from the present results and a more detailled study is needed, which was beyond the scope of our work. On the contrary, the mean-field calculations show sharp peaks either along k_x or k_y depending on the realization (see Fig. 7.7). In the Quantum-Monte Carlo simulations, since we average over all realizations, we see that the pair momentum distribution exhibits four peaks: two along k_x and two along k_y (see Fig. 7.8). It is important to notice a very good agreement between the results obtained by MF and QMC methods. Finally, we have also observed, as

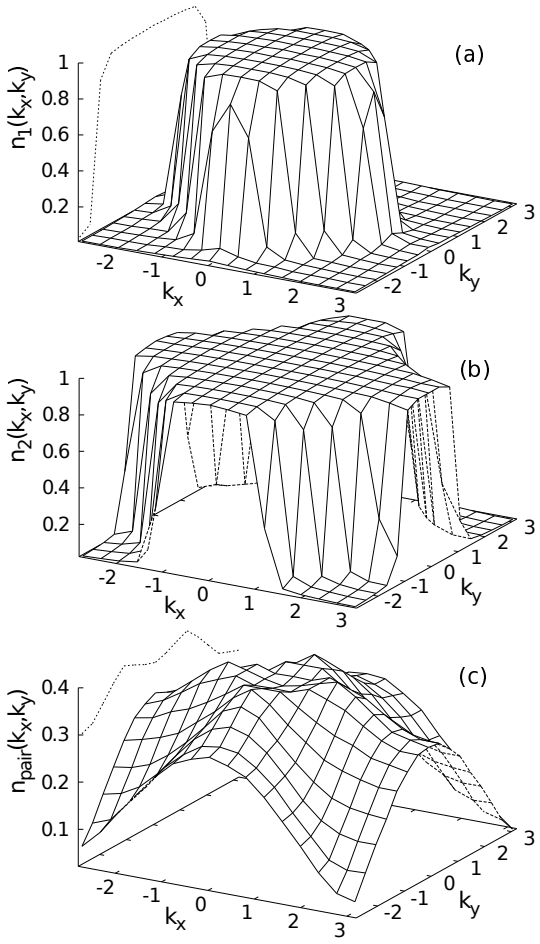

Figure 7.8: Momentum distributions of (a) minority, (b) majority and (c) pairs at $\rho = \rho_1 + \rho_2 = 1$, obtained from QMC. Here $P = 0.38$, $\beta = 10$, $U = -3.5t$ and the lattice size is 16×16. The pair momentum distribution depicts four peaks along the k_x and k_y axis.

expected, that the value of the position of the peaks, *i.e.* the center of mass of the pairs, increases with large population imbalance.

7.3 Summary

In this chapter our QMC calculations strongly emphasize that the FFLO state is the ground state of the fermionic Hubbard model on the two-dimensional

square lattice for a large range of parameters. At low filling, the FFLO state is similar to the bulk situation (*i.e.* particles having a quadratic dispersion relation), where the pairs have a vanishing total angular momentum, but a finite radial component for the center of mass momentum. An illustration of this is the volcano shaped pair momentum distribution. The phase diagram in the polarization and temperature plane exhibits similar behavior to the 1D system. Increasing polarization allows the FFLO state to survive higher temperatures. Stability is also increased near half-filling. Around half-filling, the underlying Fermi surface due to the lattice structure, leads to a FFLO state having only discrete value of the center of mass momentum, namely around $(kx = 0, ky = \pm q)$ and $(kx = \pm q, ky = 0)$. An explanation of this pairing is given in terms of matching fermionic momentum on the Fermi surfaces.

Chapter 8

Harmonically confined system in 2D

8.1 Harmonic level basis

One is used to describing free fermions on a lattice using intuition built on the free electron model. Each particle occupies a state with particular momentum $\boldsymbol{k}$ and at $T = 0$ the filled state with the highest $\boldsymbol{k}$ is called the Fermi level. BCS pairing mechanism is understood as pairing between fermions from the Fermi surface with opposite spins and opposite momenta. In this description the FFLO pairing model predicts forming a pair of fermions from different spin species with a finite momentum, where the momentum of the pair is the difference of the Fermi momenta of the two fermions. When we turn to study a harmonically confined system at low filling, for which only few harmonic levels are actually filled, the translationally invariant momentum space description is no longer the obvious one. An ideal gas confined in a harmonic trap is known to be fully characterized by the basis formed by harmonic oscillator

wave functions. In addition, for low fillings, only the bottom of the energy level structure will be filled. Then the kinetic part of the Hamiltonian is well described by the free particle one with an effective mass m^* given by $m^* = 1/2a^2t$, where a is the lattice spacing and t the tunneling amplitude. In the present case, setting the units $t = 1$ and $a = 1$, the effective mass is therefore $m^* = 1/2$.

In this chapter we explore the description of the interacting system in the harmonic basis. This transformation is the analog of the Fourier transformation used to go from real space to momentum space in the case of the free system. We will show that both BCS and FFLO models can be translated into the harmonic level basis as pairing of particles between harmonic levels and look into the limitations of this description. Since we are studying a two-dimensional system we use the eigenstates of the two-dimensional harmonic oscillator (see for example [112]). Due to rotational symmetry, the n^{th} harmonic level is $n+1$ times degenerate. We will label the states as follows: n is the principal quantum number and $m = -n, -n+2, ..., n$ is the orbital angular momentum quantum number. For simplicity we will sometimes use κ to label the set of quantum numbers, $\kappa = (n, m)$. The normalized Harmonic oscillator wave function in polar coordinates for a particular level is denoted by $\Phi_{n,m}(i)$ (where i is the lattice site).

$$\Phi_{n,m}(i) = \frac{e^{im\phi}}{\sqrt{2\pi}} \frac{(-1)^{n_r}}{l} \sqrt{2\frac{n_r!}{(n_r+|m|)!}} \left(\frac{s}{l}\right)^{|m|} \mathrm{L}_{n_r}^{|m|}\left(\left(\frac{s}{l}\right)^2\right) e^{-\frac{1}{2}\left(\frac{s}{l}\right)^2} \qquad (8.1)$$

where $L_n^{\alpha}(x) = \frac{1}{n!} x^{-\alpha} e^x \left(\frac{\mathrm{d}}{\mathrm{d}x}\right)^n x^{n+\alpha} e^{-x}$ is the Laguerre polynomial defined by Rodrigues formula. Here, instead of the principal quantum number n, a radial quantum number $n_r = \frac{(n-|m|)}{2}$ is used. The harmonic oscillator length is

$l = \sqrt{\frac{\hbar}{m*\omega}}$, m^* being the effective mass and $\omega = \sqrt{\frac{2V_T}{m^*}}$ the trapping frequency. In polar coordinates, s is taken to be the distance between the lattice site and the middle of the trap, the angle ϕ the angular coordinate.

In the description of the system we will use the Fermi momentum of the species which is calculated in the non-interacting limit. Since each n^{th} level is $n+1$ degenerate the total number of available states up to a given n is $n_{tot} = \frac{(n+1)(n+2)}{2}$. Distributing N particles between the states we find that the n_{max} up to which the states are occupied is given by $n_{max} = \frac{-1+\sqrt{1+8N}}{2} - 1$. Then the Fermi energy can be calculated as $E_F = \hbar\omega(n_{max} + \frac{1}{2}) = (n_{max} + \frac{1}{2})2\sqrt{V_T} = k_F^2$ and from there the Fermi momentum $k_F = \sqrt{(n_{max} + \frac{1}{2})2\sqrt{V_T}}$.

In the harmonic basis we define a creation operator of a particle in a level as:

$$\Psi^\dagger_{n,m} = \frac{1}{\sqrt{N}} \sum_i \Phi^*_{n,m}(i) c^\dagger_i, \tag{8.2}$$

which, in the continuum limit, leads to properly anti-commutating fermionic operators.

We calculate the single particle Green function between levels for each species as follows:

$$G_\sigma(\kappa, \kappa') = \langle \Psi^\dagger_{\kappa,\sigma} \Psi_{\kappa',\sigma} \rangle \tag{8.3}$$

As pairing is our main interest of investigation we also define a pair Green function using the creation and annihilation operators of a pair of fermions. Similarly to the homogenous case where the pairs are formed between particles having different momenta, the pairs here can have constituents occupying different harmonic levels:

$$G_{pair}(\kappa, \kappa') = \langle \Psi^\dagger_{\kappa',1} \Psi^\dagger_{\kappa,2} \Psi_{\kappa,2} \Psi_{\kappa',1} \rangle \tag{8.4}$$

Therefore, the usual BCS pairing with opposite momenta $\boldsymbol{k} \leftrightarrow -\boldsymbol{k}$ corrests-ponds to a pairing $(n, m) \leftrightarrow (n, -m)$, *i.e.*, to fermions (constituents of the pair) having the same principal quantum number and opposite orbital angular momentum quantum number. The FFLO pairing $\boldsymbol{k} \leftrightarrow -\boldsymbol{k}'$, for which the norms of the momenta are different, corresponds to a pairing $(n, m) \leftrightarrow (n', -m')$ between fermions having different principal quantum numbers, *i.e.* between fermions from different energy levels.

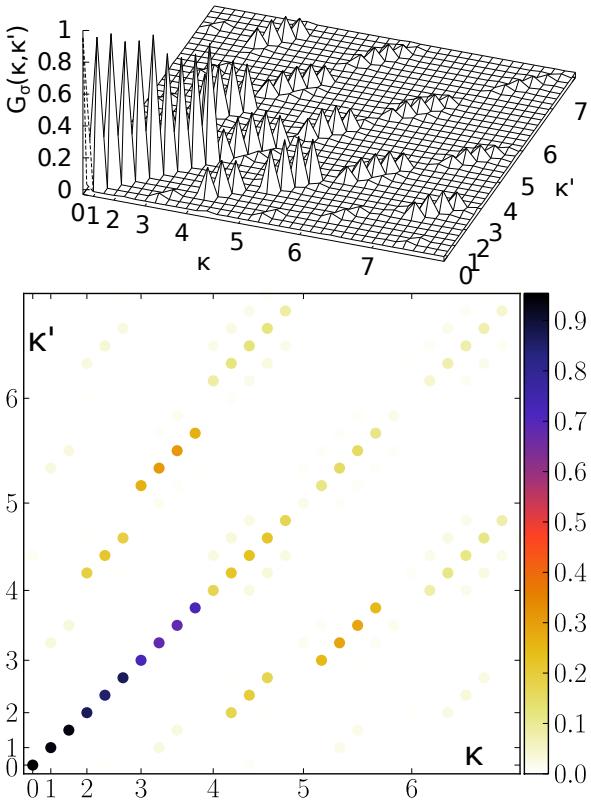

Figure 8.1: Single particle Green function $G_\sigma(\kappa, \kappa')$ in the harmonic level basis using QMC, in the balanced case. The total number of particles is 22.3, i.e ≈ 11 particles per spin. As one can see, the single particle Green function value on the diagonal sharply drops just before the 5^{th} level ($n = 4$) corresponding to 10 harmonic states, roughly the number of particles per spin. The off-diagonal elements are small compared to the diagonal ones, confirming the accuracy of the harmonic description of the system. States are labelled with $\kappa = (n, m)$ and only the principal quantum number n is displayed on the x and y axis.

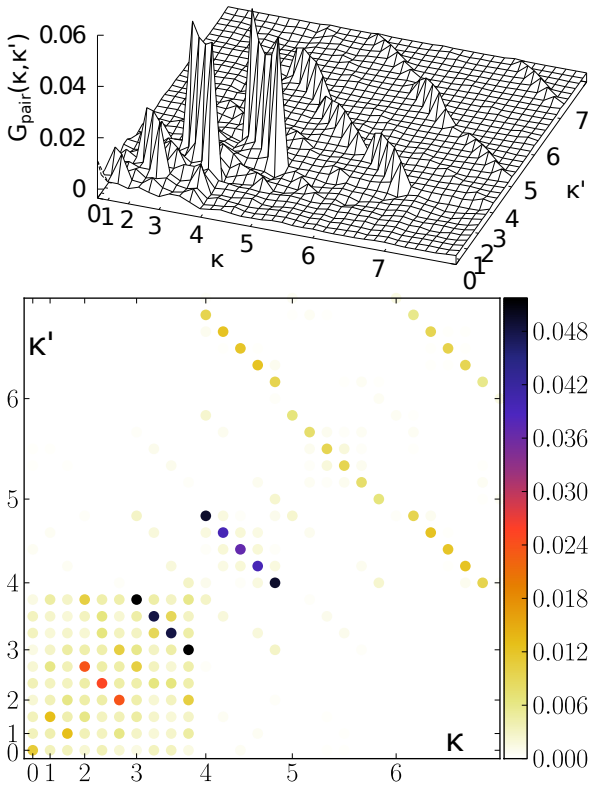

Figure 8.2: Pair Green function $G_{\text{pair}}(\kappa, \kappa')$ in the harmonic level basis using QMC. The total number of particles is 22.3 and the populations are balanced. One can clearly see that the pairing is maximum at the Fermi level $n = 4-5$, with opposite magnetic quantum numbers m. Off-diagonal pairing, *e.g.* between $\kappa = (6, m)$ and $\kappa' = (4, m')$, is almost negligible. By diagonal pairing we mean pairing between levels with equal principal quantum numbers.

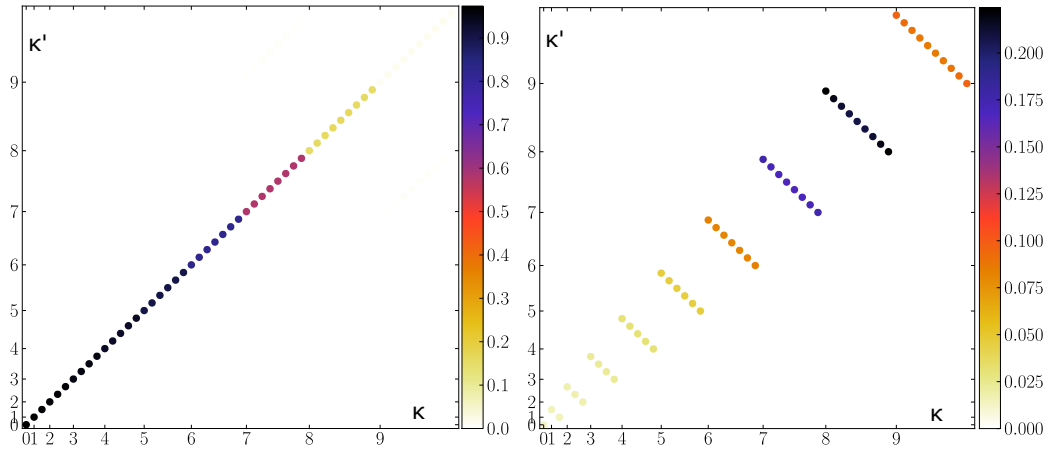

Figure 8.3: Single particle $G_\sigma(\kappa, \kappa')$ (left panel) and pair Green function $G_{\text{pair}}(\kappa, \kappa')$ (right panel) in the harmonic level basis using MF. Total number of particles is 80.4 and the populations are balanced. As in Fig. 8.1, the single particle Green's function is diagonal, with a value equal to 1 up to the Fermi level ($n \approx 8$) dropping to zero after. The pair Green's function emphasizes the diagonal pairing $(n, m) \leftrightarrow (n, -m)$.

In this section we present results for these correlation functions obtained using both QMC and MF method of balanced and polarized systems with low filling of the lattice. All QMC results were done on a 20×20 lattice at the inverse temperature $\beta = 10$ with interaction strength $U = -3.5$ and the trap potential $V_t = 0.065$ which translates to an effective harmonic frequency $\omega = 0.5$. The calculations using the Mean-Field method were performed on a bigger lattice of 41 by 41 sites, at the inverse temperature of $\beta = 25$ and taking the interaction strength to be $U = -3.0$. In the figures only values of n, the principal quantum number, are explicitly written, but correlations are calculated between all different n and m values. The m levels are arranged from $m = -n$ to n from left to right (or bottom to top). In the balanced case shown in Fig. 8.1 the single particle Green function is mainly diagonal which indicates that in this regime the harmonic level basis offers a good description

of the system. The diagonal part is the occupation of levels and where it drops to zero we define the Fermi level. We compare these results with those obtained using the Mean-Field method. Both single particle and pair Green functions shown in Fig. 8.3 agree qualitatively with the QMC results. The small off diagonal values in QMC, not present in the MF results, stems from the exact treatment of the interactions in QMC, and which are not taken into account in the MF calculations. In the regime of much higher fillings of the lattice (for example around half-filling), the effective mass approach is no longer valid and the MF results show that the harmonic basis is no longer relevant. We do not have any QMC results in that regime due to the sign problem.

When the populations are balanced, both Fig. 8.2 (QMC) and Fig. 8.3 (MF) emphasize that the pairing is maximum around the Fermi level and happens between particles from levels with the same n and for opposite m and m' values such that the total orbital angular momentum of the pair is 0. This situation is similar to the unconfined case, where the pairing occurs mostly between the $+\boldsymbol{k}_F$ and $-\boldsymbol{k}_F$ states.

At low imbalance, one observes that the pairing mostly occurs between levels with equal n, for instance in Fig. 8.4, where one observes diagonal pairing for $n = 3$ and for $n = 4$. However, one observes an off diagonal feature appearing that corresponds to pairing between the levels $n = 3$ and $n = 4$. When the system is imbalanced even more, the off-diagonal feature becomes the main pairing amplitude. For instance, as shown in Fig. 8.5, corresponding to a polarization $P = 0.22$, the diagonal pairing has almost completely disappeared and the pairing mostly occurs between the levels $n = 3$ and $n = 4$.

Since in this case pairing happens between an odd and an even level, it is impossible to match the m values and form pairs with total angular momentum

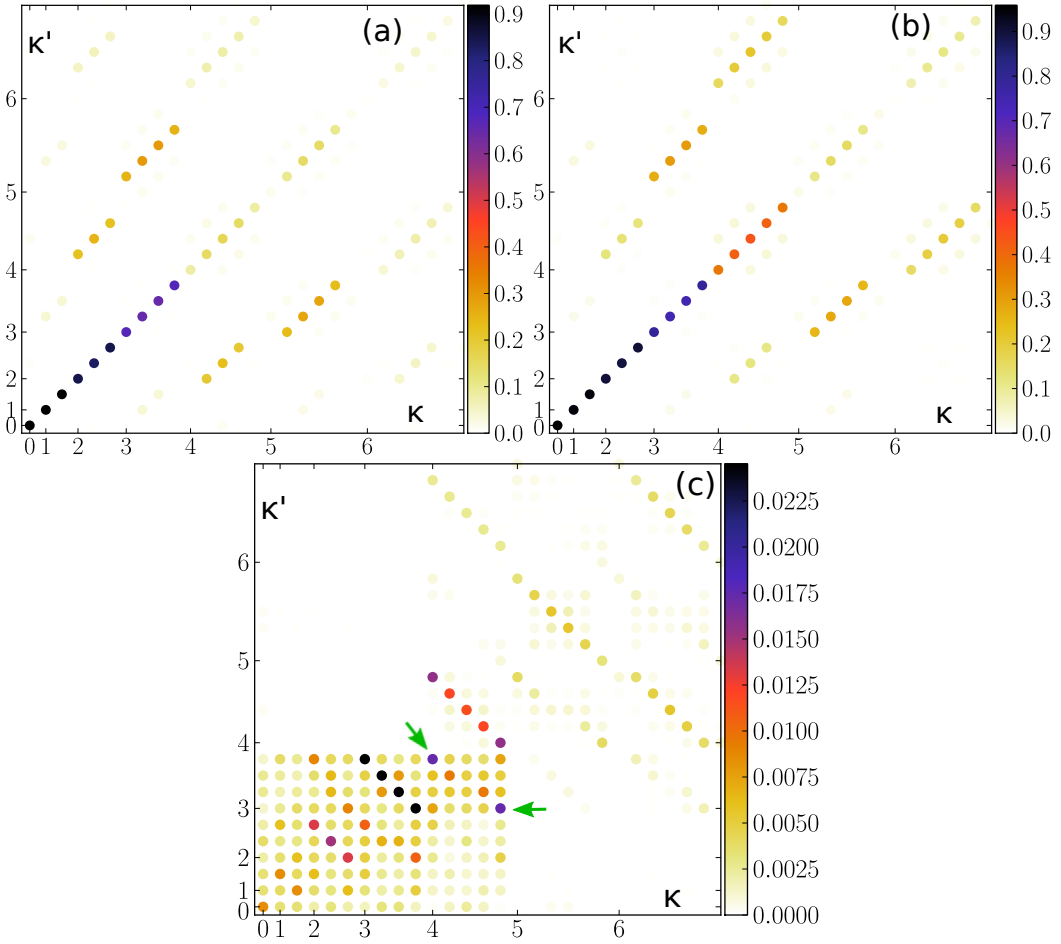

Figure 8.4: Single particle $G_\sigma(\kappa, \kappa')$ (a) and (b) and pair Green function $G_{\text{pair}}(\kappa, \kappa')$ (c) in the harmonic level basis (QMC results) for a low polarization situation ($P = 0.11$). The total number of particles is 25.5. Even though the Fermi-levels between the two species no longer match, the pairing is still diagonal for $n = 3$ and for $n = 4$ levels. However, one observes an off diagonal feature appearing that corresponds to pairing between the levels $\kappa = (4, -4)$ and $\kappa' = (3, 3)$ and respectively $\kappa = (4, 4)$ and $\kappa' = (3, -3)$ as indicated by arrows.

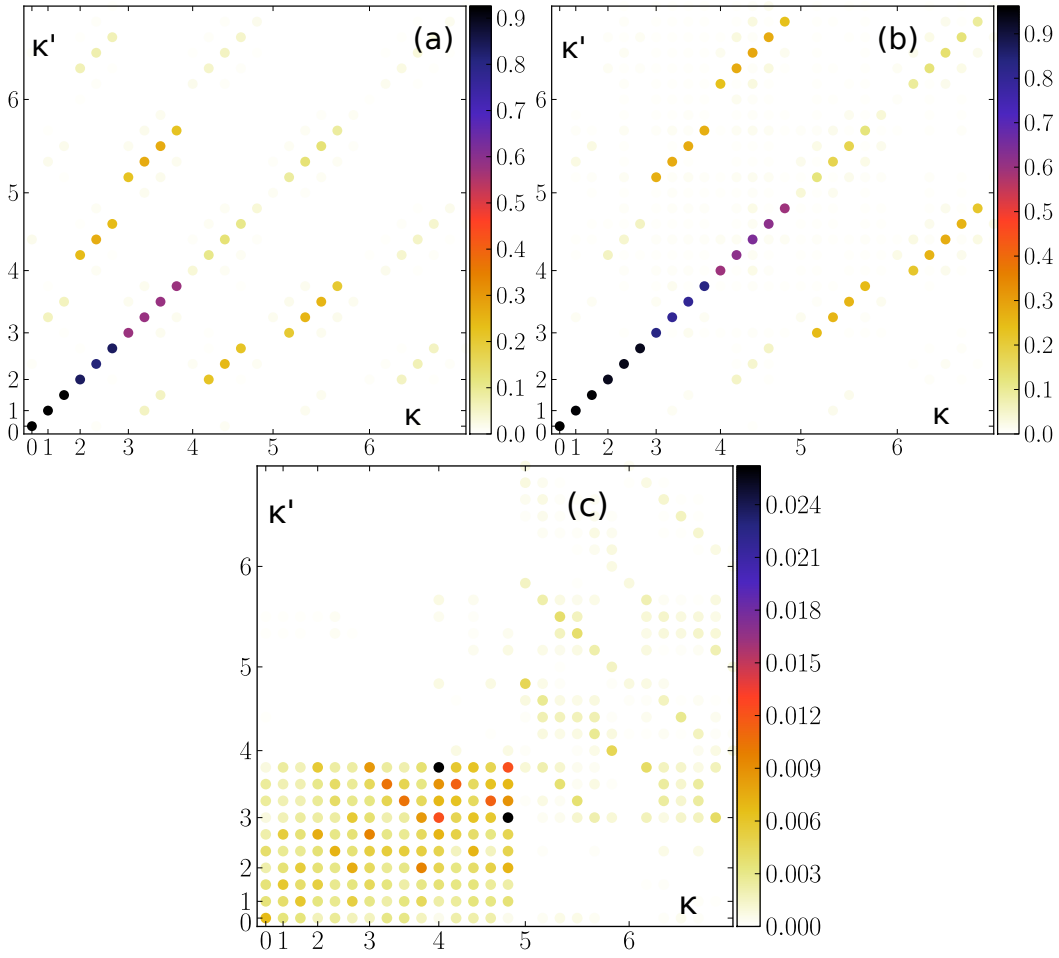

Figure 8.5: Single particle$G_\sigma(\kappa, \kappa')$ (a) and (b), and pair $G_{\text{pair}}(\kappa, \kappa')$ (c) Green function in the harmonic level basis (QMC results) for a medium polarization ($P = 0.22$). The total number of particles is 26.9. The diagonal pairing has almost completely disappeared and the pairing mostly occurs between the levels $n = 3$ and $n = 4$. More precisely, the strongest pairing occurs between $\kappa = (4, -4)$ and $\kappa' = (3, 3)$ and analogously between $\kappa = (4, 4)$ and $\kappa' = (3, -3)$. There is, in addition, a small contribution from the levels $\kappa = (4, -2)$ and $\kappa' = (3, 1)$ and $\kappa = (4, 2)$ and $\kappa' = (3, -1)$. Note that each pairing corresponds to a non-vanishing total angular momentum for the pair.

zero. We observed that the strongest pairing happens, for example, between $\kappa = (4, -4)$ and $\kappa' = (3, 3)$ and analogously between $\kappa = (4, 4)$ and $\kappa' = (3, -3)$. There is, in addition, a small contribution from the levels $\kappa = (4, -2)$ and $\kappa' = (3, 1)$ and $\kappa = (4, 2)$ and $\kappa' = (3, -1)$. In both cases the sum of the orbital angular momentum is non-zero. Imbalancing the system even more, we arrive at the situation where the difference between the Fermi levels of each species is $n_{F2} - n_{F1} = 2$. As illustrated in Fig. 8.6 for $P = 0.37$ the pairing occurs between the levels $n = 5$ and $n = 3$ and also $n = 4$ and $n = 2$ which means that the system can now achieve pairing with zero total orbital angular momentum. Still, there is small contribution of pairing between $\kappa = (5, -5)$ and $\kappa' = (3, 3)$ and $\kappa = (5, 5)$ and $\kappa' = (3, -3)$, for which $\Delta m = \pm 2$. For a comparison we show the results from the mean field simulations, depicting a similar behavior. In the realization shown in Fig. 8.7 the Fermi levels of the species are $n = 7$ and $n = 9$ and we see that pairing occurs between those levels as well as between the two levels below $n = 6$ and $n = 8$. The largest m values are almost unpaired for they would have led to non-zero total angular momentum. We conclude that in the low filling regime and at intermediate interaction strength, we can understand the FFLO pairing mechanism in a trapped system as pairing between fermions from different harmonic levels. We observe that the pairs are formed in such a way that the total orbital angular momentum of all pairs is always zero, and the orbital angular momentum is minimized for each pair. Finally, similarly to the untrapped case where the pairs are produced with a finite center of mass momentum (vanishing for the balanced case), the FFLO state in the harmonic trap corresponds, in a classical picture, to pairs whose center of mass is oscillating around the minimum of the trap with an amplitude increasing with population imbalance.

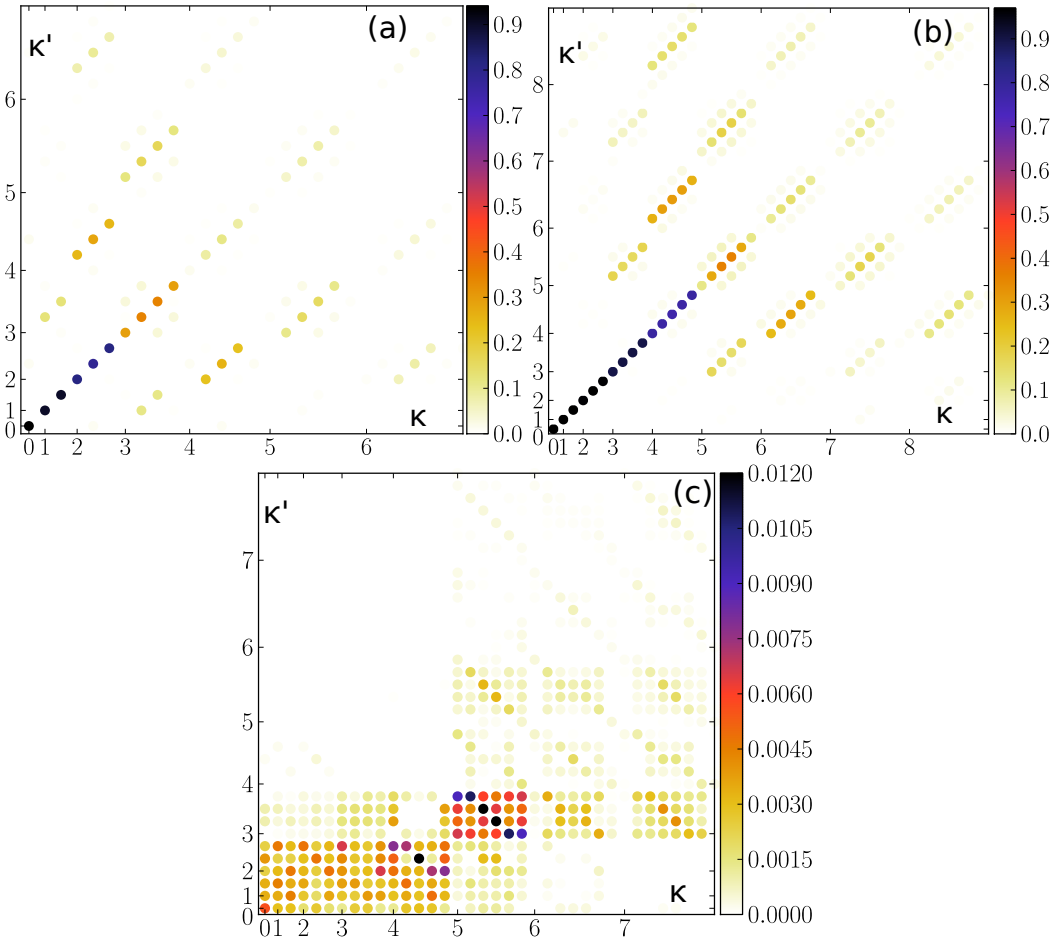

Figure 8.6: Single particle $G_\sigma(\kappa, \kappa')$ (a) and (b) and pair Green function $G_{\text{pair}}(\kappa, \kappa')$ (c) in the harmonic level basis (QMC results) for a strong polarization ($P = 0.37$). The total number of particles is 27.4. The pairing occurs between the levels $n = 5$ and $n = 3$ and also $n = 4$ and $n = 2$, *i.e.* with total zero orbital angular momentum. Still, there is small contribution to pairing between $\kappa = (5, -5)$ and $\kappa' = (3, 3)$ and $\kappa = (5, 5)$ and $\kappa' = (3, -3)$.

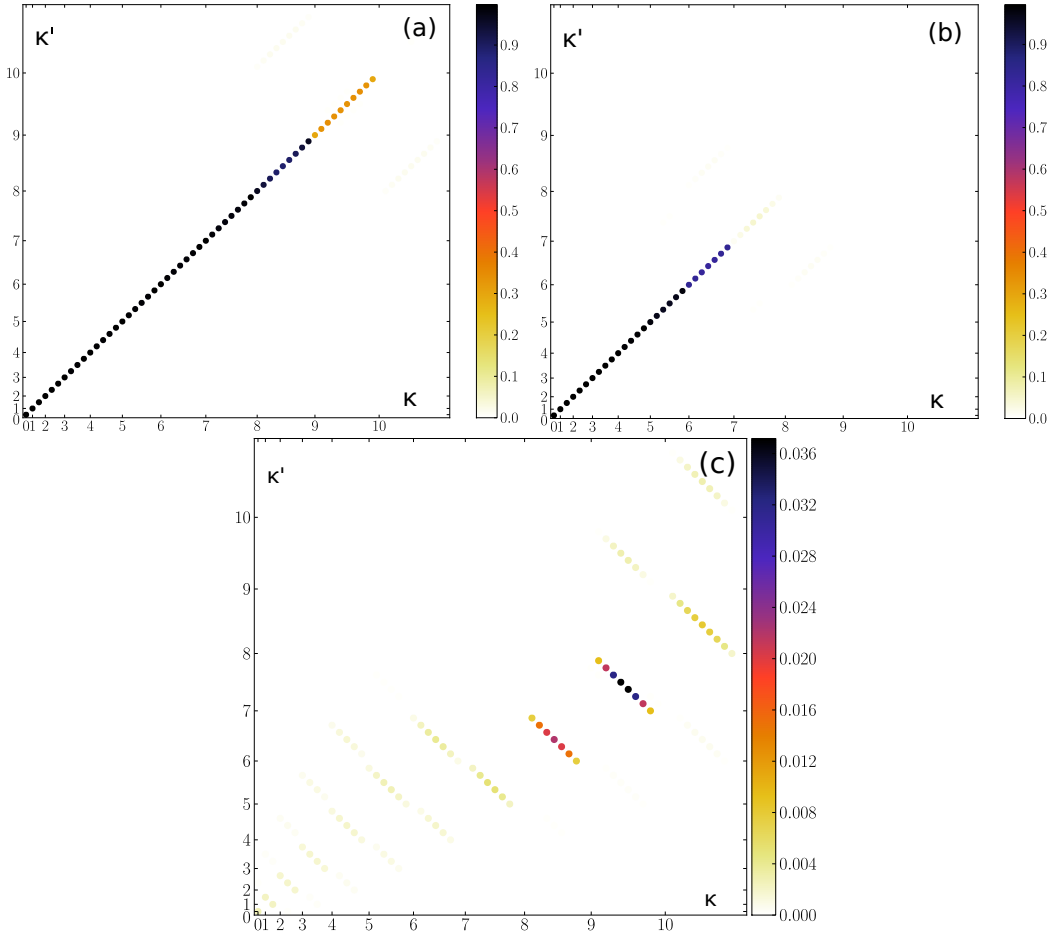

Figure 8.7: Single particle $G_\sigma(\kappa, \kappa')$ (a) and (b) and pair Green function $G_{\text{pair}}(\kappa, \kappa')$ (c) in the harmonic level basis (MF results) for a polarization $P = 0.27$. The results are similar to the QMC results: pairing is maximum among the Fermi-levels $n = 7$ and $n = 9$ and also among the two levels below $n = 6$ and $n = 8$. The largest m values are almost unpaired, for they would have led to non-zero total angular momentum.

8.2 System at low filling

Fermion systems with imbalanced populations have been realized experimentally in one- and elongated three-dimensional harmonic traps. The density profiles of the populations were found to be qualitatively different in the two cases. In three dimensions, one observes the formation of concentric shells where, for very low polarization, the core is fully paired, *i.e.* zero local magnetization, and the wings are partially polarized [22, 23]. On the other hand, it was observed in one-dimensional systems that, for low polarization, the unpolarized fully paired populations are located at the edges of the cloud while the core is partially polarized [25]. The role of dimensionality in this qualitatively different behavior has been a focus of studies on this system. Consequently, the behavior of the system in two dimensions is of considerable interest.

We present here results of our DQMC study of the trapped two dimensional system. The presence of the trap imposes constraints which make the simulations much harder than the uniform case. The number of particles should not be too large to make sure that the local density in the core regions is not close to half filling but should be large enough so that at large P, the minority population will still be appreciable. Another constraint is that the size of the lattice be large enough to ensure that particles do not leak out. These constraints limit our ability to do simulations for system sizes beyond 20×20.

As for the uniform system, the most important indicator of the presence of the FFLO state is the pair momentum distribution. Although the plane wave basis is not the natural one in the harmonically confined case, we study the momentum distributions because they are of experimental interest. We will show that despite the shortcomings of this language one can still detect the

FFLO pairing signal this way. In addition, since the trap destroys translational invariance it is very useful to study the density profiles and local magnetization, $m(x,y) = \rho_2(x,y) - \rho_1(x,y)$ where ρ_2 (ρ_1) is local density of the majority (minority). We start with the unpolarized system. Figure 8.8(a) shows the

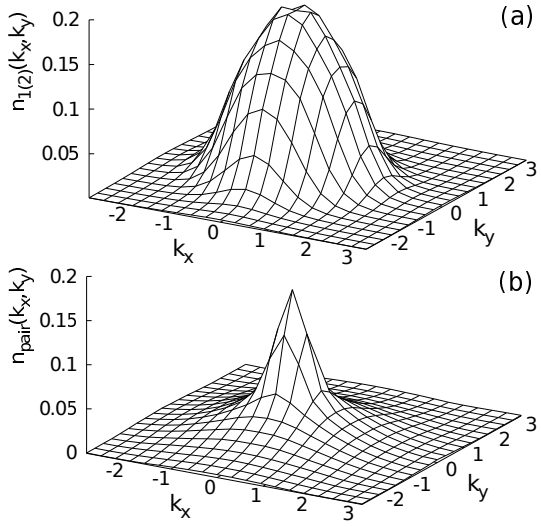

Figure 8.8: Momentum distributions of (a) the single particles, $n_1(k_x,k_y) = n_2(k_x,k_y)$ and (b) the pairs $n_{pair}(k_x,k_y)$. The total number of particles is 22.3, $P = 0$, $\beta = 10$, $U = -3.5t$, the trap potential is $V_t = 0.065$ and the lattice size 20×20.

momentum distribution of the particles (the two populations are identical) for a system with a total of 22.3 particles, $P = 0$, $\beta = 10$, $U = -3.5t$ and a lattice size of 20×20. The trap potential is given by $V_t = 0.065$. Figure 8.8(b) shows the pair momentum distribution which exhibits a sharp peak at zero momentum. Now we polarize the system keeping the total number of particles constant which corresponds to the experimental situation. Figure 8.9 shows the momentum distributions of the (a) minority and (b) majority populations and (c) the pairs. The system has a total of 21.4 particles, $P = 0.55$, $\beta = 10$, $U = -3.5t$ and a trap potential $V_t = 0.065$ on a 20×20 lattice. The Fermi temperature of the system is $T_F = 1.86$. Figure 8.9(c) is qualitatively different

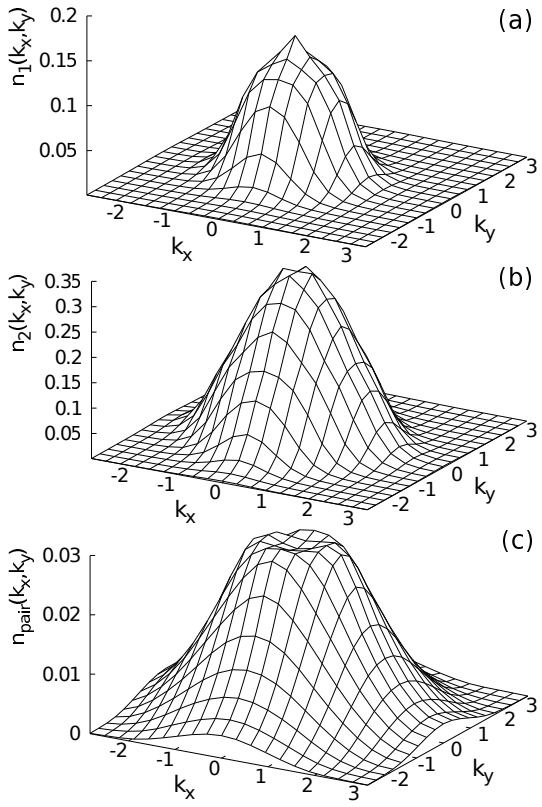

Figure 8.9: The momentum distributions of (a) the minority and (b) majority populations and (c) the pairs. The total number of particles is 21.4, $P = 0.55$, $\beta = 10$, $U = -3.5t$ on a 20×20 lattice. The trap potential is $V_t = 0.065$ and the Fermi temperature is $T_F = 1.86$.

from Fig. 8.8(b) and shows clearly that when the confined system is polarized it exhibits FFLO states with pairs forming with nonzero center of mass momentum. This behavior was observed for a wide range of polarizations and interaction strengths. The vertical scale in Fig. 8.9(c) shows that the number of pairs is very small. This is due to the small total number of particles in the system. A simulation for a larger system but with the same characteristic density [113] should give a stronger signal in the form of higher peaks at nonzero momentum. This effect of the total number of particles was shown in the one dimensional uniform case in Ref. [76].

Density profiles are the basic quantities that characterize the trapped system. The first experimental results in a three-dimensional system show the formation of concentric shells where, for very low polarization, the core is fully paired (no local magnetization) and the wings are partially polarized (see [22] and [23]). On the other hand, in the one-dimensional system, it has been observed that there exists a low polarization regime where the unpolarized superfluid is located at the edge of the cloud, and the core is partially polarized [25]. The issue of this dimensionally driven transition caused considerable interest. It is interesting to look at the intermediate two dimensions and study the behavior of the density profiles to see whether it follows more closely any of the two limiting scenarios. In our simulations, we measure the density profiles of each species and we calculate the local magnetization $m(x, y) = \rho_1(x, y) - \rho_2(x, y)$. The profiles shown in Fig. 8.10 correspond to the situation when FFLO-type pairing is observed in the system as in Fig. 8.9. One sees that the system is partially polarized at the core and fully polarized in the wings (where we see no minority particles). There is no fully paired phase where $m(x, y)$ would disappear within the size of the cloud.

In the very low polarization regime we observe oscillations appearing in the profile of the local magnetization as shown in Fig. 8.11. We looked in detail into these results in order to establish whether the oscillations are linked to the FFLO type pair density wave behavior. We found, however, that the oscillations are present in the system even when there is no interaction between particles as seen in Fig. 8.11 (dashed line). From both the MF and QMC, one can see that the interaction might change the profile, but does not crucially change the oscillation pattern. Therefore, we attribute the oscillations to the underlying harmonic levels rather than to the FFLO order. In the balanced

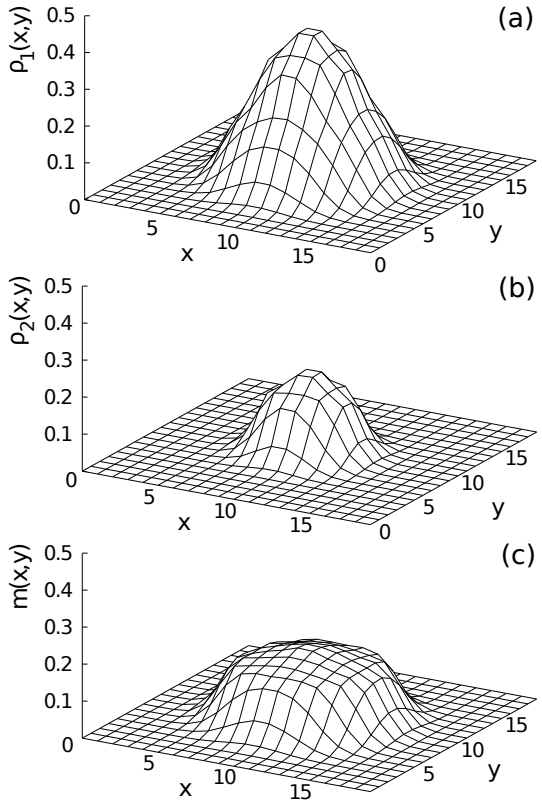

Figure 8.10: Density distributions of majority $n_1(x, y)$, minority $n_2(x, y)$ and the local magnetization $m(x, y)$. Total number of particles is 21.4, $P = 0.55$, $\beta = 10$, Lattice size 20x20, Trap potential $V_t = 0.065$.

case, it has already been shown that the density of a fermionic cloud in a trap can exhibit oscillations with minima or maxima in the center of the trap depending on whether the last filled state corresponds to an odd or even harmonic level [114]. One can also see that according to the MF calculations, the excess particles seem to accumulate at the edges of the trap, which has already been observed for example in Ref. [107]. However, we do not observe this pushing out of the excess particles to the outer shell of the cloud in the QMC results.

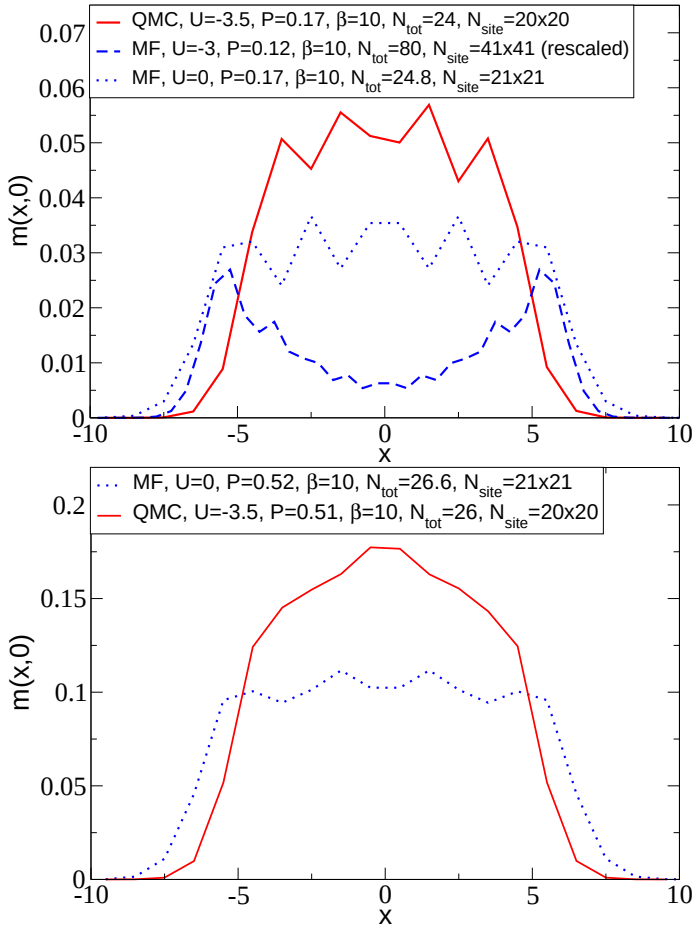

Figure 8.11: Cut through the center of the trap showing the local magnetization $m(x, y)$ for low polarization (top panel) and high polarization (bottom panel). Comparison of interacting and non interacting profiles using MF and QMC.

8.3 System around half filling: Mean-Field study

As mentioned earlier, the Quantum Monte-Carlo method suffers from a stronger sign problem for higher fillings. However, we successfully studied the system imbalance around half-filling of the lattice in the trap using the Mean-Field method. In figures 8.12, 8.13, 8.14, 8.15 the order parameter is shown in real space as well as in Fourier space for increasing value of the polarization. The numerical results were obtained for a lattice size 41×41, an interaction strength

$U = -5$ and chemical potential at the center of the trap corresponding to half filling. At low polarization ($P = 0.13$), Fig. 8.12, the structure is similar

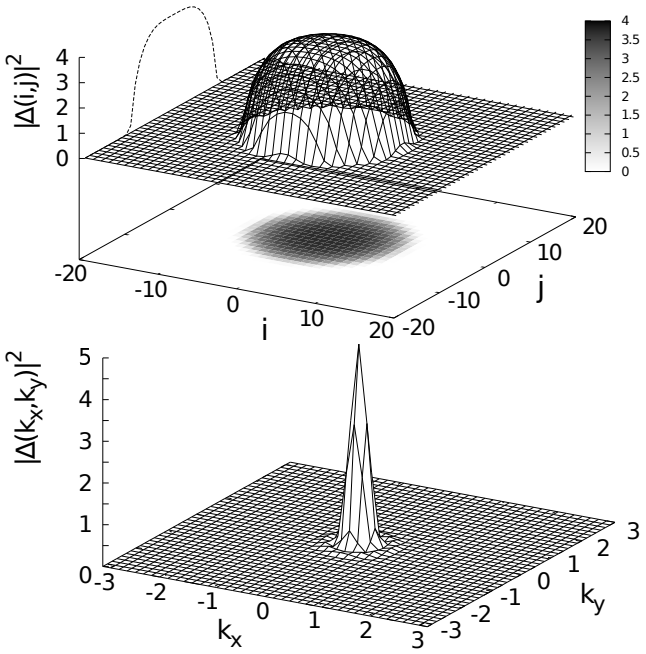

Figure 8.12: Mean field parameter $\Delta(\boldsymbol{r})$ in real space (top) and in Fourier space $\Delta(\boldsymbol{k})$ (bottom) for the low polarization value ($P = 0.13$), around the half-filling situation, in the presence of an harmonic trap. The structure is similar to the balanced case, *i.e.* a maximum number of pairs at the center of the trap, decreasing on the border. The Fourier transform simply depicts a peak at $\boldsymbol{k} = 0$, emphasizing a BCS-like pairing.

to the balanced case, *i.e.* a maximum number of pairs at the center of the trap, decreasing on the border. The Fourier transform simply depicts a peak at $\boldsymbol{k} = 0$, emphasizing BCS-like pairing. At higher polarization $P = 0.43$, Fig. 8.13, a structure in the pairing order Δ appears at the center of the trap, leading to clear oscillations in Fourier space. This pattern appears first at the center of the trap simply because it corresponds to half filling which, as explained in a previous section, is strongly unstable towards the FFLO state.

Indeed, this is emphasized by the two figures 8.14 and 8.15, corresponding

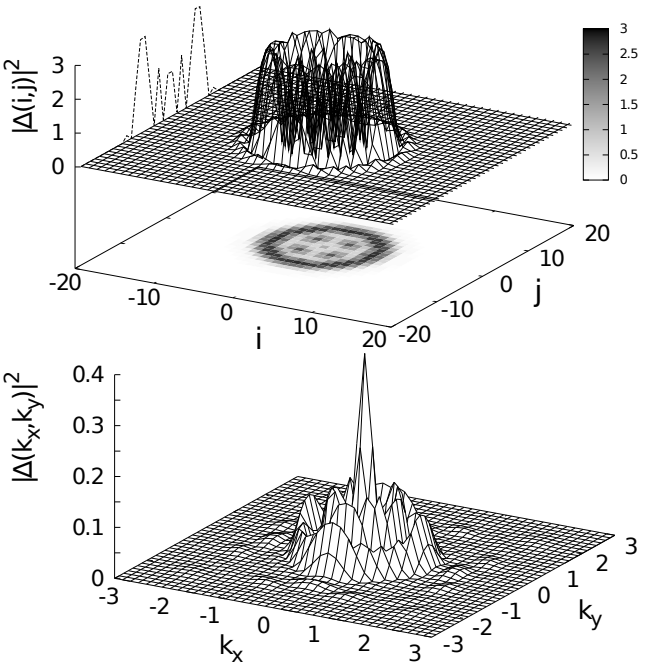

Figure 8.13: Mean field parameter $\Delta(\boldsymbol{r})$ in real space (top) and in Fourier space $\Delta(\boldsymbol{k})$ (bottom) for the polarization value $P = 0.43$. A structure in the center of the trap is clearly visible, leading to oscillations in the Fourier transform.

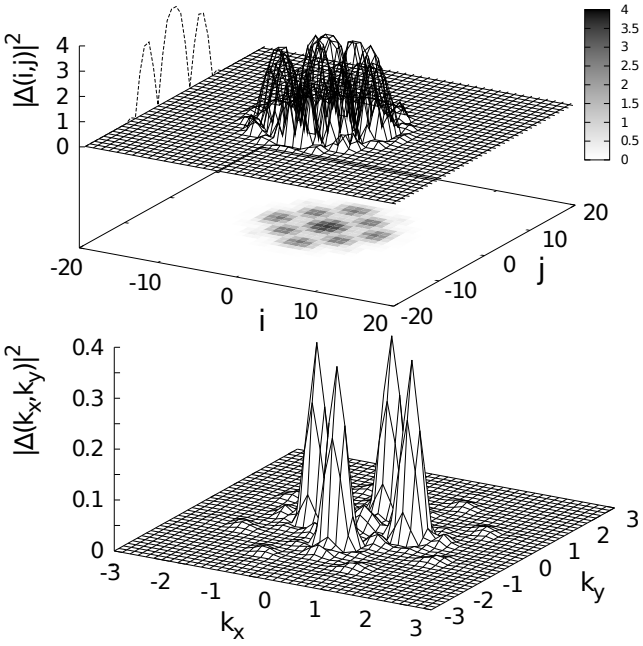

Figure 8.14: Mean field parameter $\Delta(\boldsymbol{r})$ in real space (top) and in Fourier space $\Delta(\boldsymbol{k})$ (bottom) for the polarization value $P = 0.48$. The checkerboard pattern is a clear signature of the FFLO state. The Fourier transform depicts four peaks at the positions $(k_x = 0, k_y = \pm q)$ and $(k_x = \pm q, k_y = 0)$, precisely like in the homogeneous situation at half-filling.

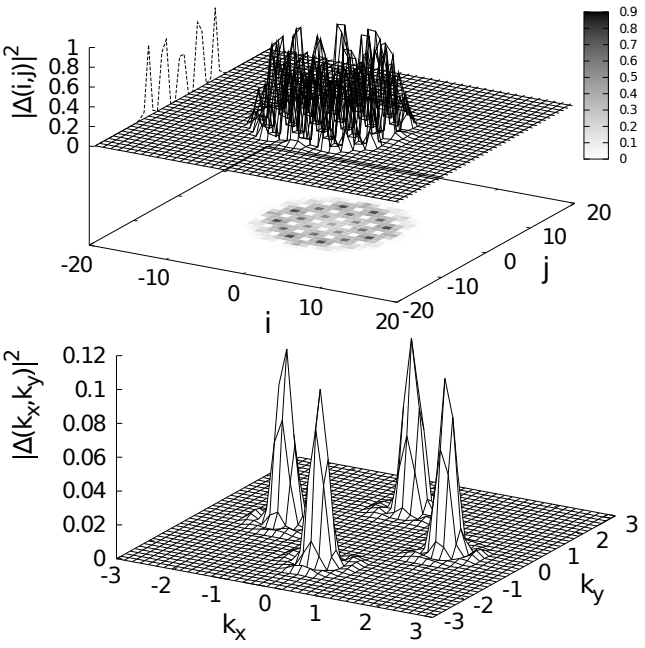

Figure 8.15: Mean field parameter $\Delta(\boldsymbol{r})$ in real space (top) and in Fourier space $\Delta(\boldsymbol{k})$ (bottom) for the polarization value $P = 0.66$. The checkerboard pattern depicts now a shorter period in real space, translating into a larger spreading of the four peaks in the Fourier space and corresponding to pairs having a larger center of mass momentum compared to Fig. 8.14.

respectively to polarization $P = 0.48$ and $P = 0.66$. The checkerboard pattern of $|\Delta|^2$ in real space becomes more and more visible. Note that similar results have been previously shown in [116]. However we would like to emphasize the link between this pattern and the nature of the pairing in the homogenous situation. Indeed, in Fourier space four peaks are clearly observed. Their positions, $(k_x = 0, k_y = \pm q)$ and $(k_x = \pm q, k_y = 0)$, precisely match the ones observed in the homogeneous situation, both in the QMC and the MF results around half filling. In addition, one can see that the oscillation period of the order parameter becomes shorter with higher polarization, *i.e.* corresponding to a larger center of mass momentum q of the pair, which is depicted by the spreading of the four peaks further away from $\boldsymbol{k} = 0$. This also shows that the oscillations in real space are not related to the underlying harmonic levels, but really to the FFLO order. From the experimental point of view, this signature of the FFLO order could be measured either directly in the density of pairs or in their velocity distribution. Of course, the present mean field calculation does not include the thermal fluctuations which are crucial to properly describe the condensation of the pairs which, at large interaction, arises at a temperature $k_B T \approx t^2/U$ lower than the pair formation temperature $k_B T \approx U$ [109, 115, 117, 118].

8.4 Summary

In this chapter we show that the FFLO pairing is also observed in the 2D system in the presence harmonic confinement and the pair momentum distribution exhibits the characteristic volcano shape. At low fillings, we introduce the harmonic level basis which gives rise to a simple understanding of the

pairing mechanism. We show that FFLO-type pairing in a trap corresponds to forming pairs between fermions occupying different harmonic levels. In addition, we have shown that the harmonic levels are at the origin of the oscillations that we have seen in the local magnetization, which, therefore, are not a signature of the FFLO state. Finally, still in the presence of an harmonic confinement, but around half filling, we have shown that the pairing mechanism is essentially identical to the homogeneous situation, leading to clear signatures in the pair density, both in real space (checkerboard pattern) and in Fourier space (four peaks), which allows for a possible experimental observation with cold atoms.

Chapter 9

Conclusions and outlook

Motivated by the interest in pairing of fermions in systems where the populations are imbalanced, we have studied the subject by means of large scale Quantum Monte Carlo simulations. Specifically, we have simulated the physics of the one- and two-dimensional Hubbard model with two species of fermions interacting attractively and investigated the possible phases appearing in the system.

We have looked first into the pairing mechanisms observed in a one dimensional system both in the absence as well as presence of the confining potential which breaks translational invariance. We have shown that pairing with nonzero center-of-mass momentum - FFLO pairing - is the dominant phase in the ground state of the system for a wide range of polarizations. We have addressed the experimentally relevant issue of the stability of the FFLO phase at finite temperatures. We showed how the peak in the pair momentum distribution at nonzero momentum is influenced by changing temperature and polarization. The FFLO phase was found to persist to higher temperature when the polarization is larger. In disagreement with Mean-Field results [86],

the pairs persist to much higher temperature than the temperature at which the FFLO peak disappears. Most interestingly, we have shown that in the confined case and with parameters close to those of the cold atom experiment of Ref. [25], the FFLO pairing can persist up to $T/T_F = 0.1$ which is currently achievable experimentally. These results are contrary to the expectations that the FFLO phase is a fragile state with respect to increased temperature. It gives a positive outlook on the ongoing experimental effort and the feasibility of observation of the FFLO phase in cold fermionic gases. We have also addressed the question of equivalence of the canonical and grand-canonical ensembles and shown that in this context they are equivalent. Thus the stabilization of sought-after phases is not favored by one ensemble or another.

In the one-dimensional geometry we have also investigated the effect of mass differences between two imbalanced fermion populations. Contrary to theoretical claims [93, 94] the Breached Pairing (Sarma) phase was not realized by tuning the mass ratio between the two populations. We have studied the system with three different interaction terms and found it to be unstable and to undergo a collapse when the mass disparity was large enough.

In two dimensions we took up the challenge of studying the system with Quantum Monte Carlo. Our results fill the lack of exact numerical studies of an imbalanced population Fermi mixture in 2D. It is believed that the FFLO pairing is unstable with respect to increased dimensionality and that it would appear only in a small parameter regime in dimensions higher than one. Contrary to this belief, our results, based on QMC and MF calculations, strongly emphasize that the FFLO state is the ground state of the fermionic Hubbard model on the square lattice, both with or without harmonic confinement. The phase is also robust with respect to finite temperature as shown in the

temperature-polarization phase diagram. As expected, the phase has enhanced stability around the density region of half-filling of the lattice where there is nesting of Fermi surfaces. Unexpectedly, we find that around half-filling, due to the geometry of the Fermi surfaces, the FFLO state is realized with discrete values of the center-of mass momentum, along k_x or k_y (and not along the diagonal). In the harmonically confined system we provide a simple picture of the pairing mechanism with the use of harmonic level basis. In the low filling regime and at intermediate interaction strength we can view the FFLO pairing in a trapped system as pairing between fermions occupying different harmonic levels. Since the density profiles are an important tool in experimental characterization of the system, we also study the local densities of the species in harmonic confinement. Our measurements of the density profiles of the confined system in a two-dimensional lattice do not reveal any region in which the system is fully paired. In the parameter regime studied, the core of the cloud is always partially polarized and the excess majority particles form a fully polarized outer shell. This result is relevant in the context of possible dimensionally driven transition between systems in one and three dimensions. In the former, and at low polarization a fully paired region is observed in the wings of the cloud while the core is partially polarized. In the 3D system, on the contrary, the core was observed to be fully paired and the wings partially polarized. It could be a potentially interesting extension of our work to study the transition from a one-dimensional to two-dimensional system by tuning the perpendicular hopping.

At this point we point out other possible extensions of the work presented in this thesis.

The subject of superfluidity in two-dimensional system with population

imbalance is of considerable interest. We have shown preliminary results that hint to the suppression of the superfluidity due to imbalance. Further studies would be necessary to explore the subject more deeply and to be able to make definite statements.

With our methods calculation of imaginary time displaced Green functions $G(\tau)$ is feasible. Performing numerical inverse Laplace transform, for example using the Maximum Entropy method, one can extract information about dynamical quantities such as spectral functions $A(\omega)$ and dispersion relations. Dynamical quantities can provide a body of additional information helpful to characterize the phases realized in the system. The measurements of the time displaced Green functions are very costly in computation time in the case of QMC approach. For the system of imbalanced populations of fermions, dynamic quantities have been calculated using the Density Matrix Renormalization Group in Ref. [119] where they reported a spin gap, as expected. However the applicability of this method is limited to one dimension. In principle the calculation of the time displaced Green functions and excitation spectra for a two-dimensional model is feasible with the QMC methods available to us.

Another possibility to realize exotic pairing states, such as FFLO or BP, is in a system with balanced populations of Fermions in 2D but with anisotropic hopping parameters as proposed in [120]. The possible experimental realization of this model is based on the idea of using spin-dependent optical lattices. In this setup the populations are balanced but there is a mismatch between Fermi surfaces which results from tuning the hopping of each species such that, for example, one of them preferentially hops along the x direction and the other along y. The system exhibits a rich phase diagram in the Mean-Field approximation with potential to realize different pairing scenarios. We have

performed preliminary simulations of this model using QMC, but found that the sign problem was severe. More systematic attempt to study the system in a wide parameter range could possibly bring further insight into the physics of this model.

Bibliography

[1] J. Bardeen, L. N. Cooper and J. R. Schrieffer, *Theory of Superconductivity*, Phys. Rev. **108**, 1175 (1957).

[2] L. N. Cooper, *Bound Electron Pairs in a Degenerate Fermi Gas*, Phys. Rev. **104**, 1189 (1956).

[3] V. L. Ginzburg and D. A. Kirzhnits, *On superfluidity of neutron stars*, Soviet Phys. JETP **20**, 1346 (1965); *Superconductivity in White Dwarfs and Pulsars*, Nature **220**, 148 (1968).

[4] J. E. Golub, K. Kash, J. P. Harbison, and L. T. Florez, *Long-lived spatially indirect excitons in coupled GaAs/AlxGa1-xAs quantum wells*, Phys. Rev. **B41**, 8564 (1990).

[5] M. Tinkham, *Introduction to Superconductivity*, McGraw-Hill (1996).

[6] R. Casalbuoni and G. Nardulli, *Inhomogeneous superconductivity in condensed matter and QCD*, Rev. Mod. Phys. **76**, 263 (2004).

[7] P. Fulde and A. Ferrell, *Superconductivity in a Strong Spin-Exchange Field*, Phys. Rev. **135**, A550 (1964).

[8] A. Larkin and Y. N. Ovchinnikov, *Inhomogeneous state of superconductors*, Zh. Eksp. Teor. Fiz. **47**, 1136 (1964) [Sov. Phys. JETP **20**, 762 (1965)].

[9] R. Combescot, *Introduction to FFLO phases and collective mode in the BEC-BCS crossover*, Proceedings of the International School of Physics "Enrico Fermi", Ultra-cold Fermi Gases Edited by M. Inguscio, W. Ketterle, C. Salomon, Volume 164, 2007, IOS Press.

[10] G. Sarma, Phys. Chem. Solids **24**, 1029 (1963); S. Takada and T. Izuyama, Prog. Theor. Phys. **41**, 635 (1969).

[11] Y. L. Loh and N. Trivedi, *Detecting the Elusive Larkin-Ovchinnikov Modulated Superfluid Phases for Imbalanced Fermi Gases in Optical Lattices*, Phys. Rev. Lett. **104**, 165302 (2010).

[12] M. Taglieber, A.-C. Voigt, T. Aoki, T. W. Hänsch, and K. Dieckmann, *Quantum Degenerate Two-Species Fermi-Fermi Mixture Coexisting with a Bose-Einstein Condensate*, Phys. Rev. Lett. **100**, 010401 (2008).

[13] M. Dalmonte, K. Dieckmann, T. Roscilde, C. Hartl, A. E. Feiguin, U. Schollwck, F. Heidrich-Meisner, *Dimer, trimer and FFLO liquids in mass- and spin-imbalanced trapped binary mixtures in one dimension*, Phys. Rev. **A85**, 063608 (2012)

[14] H. A. Radovan, N. A. Fortune, T. P. Murphy, S. T. Hannahs, E. C. Palm, S. W. Tozer and D. Hall, *Magnetic enhancement of superconductivity from electron spin domains*, Nature **425**, 51 (2003).

[15] C. A. R. Sa de Melo, *When fermions become bosons: Pairing in ultracold gases*, Physics Today, vol. 61, issue 10, p. 45 (2008).

[16] S. Jochim, M. Bartenstein, A. Altmeyer, G. Hendl, S. Riedl, C. Chin, J. Hecker Denschlag and R. Grimm, *Bose-Einstein Condensation of Molecules*, Science **302**, 2101 (2003).

[17] M. W. Zwierlein, C. A. Stan, C. H. Schunck, S. M. F. Raupach, S. Gupta, Z. Hadzibabic and W. Ketterle, *Observation of Bose-Einstein Condensation of Molecules*, Phys. Rev. Lett. **91**, 250401 (2003).

[18] M. Greiner, C. A. Regal and D. S. Jin, *Emergence of a molecular BoseEinstein condensate from a Fermi gas*, Nature **426** 537 (2003).

[19] C. A. Regal, M. Greiner and D. S. Jin, *Observation of Resonance Condensation of Fermionic Atom Pairs*, Phys. Rev. Lett. **92**, 040403 (2004).

[20] M. W. Zwierlein, C. A. Stan, C. H. Schunck, S. M. F. Raupach, S. Kerman and W. Ketterle, *Condensation of Pairs of Fermionic Atoms near a Feshbach Resonance*, Phys. Rev. Lett. **92**, 120403 (2004).

[21] M. W. Zwierlein, A. Schirotzek, C. H. Schunck and W. Ketterle, *Fermionic Superfluidity with Imbalanced Spin Populations*, Science **311**, 492 (2006)

[22] M. W. Zwierlein, C. H. Schunck, A. Schirotzek and W. Ketterle, *Direct observation of the superfluid phase transition in ultracold Fermi gases*, Nature **442**, 54 (2006); Y. Shin, M. W. Zwierlein, C. H. Schunck, A. Schirotzek and W. Ketterle, *Observation of Phase Separation in a Strongly Interacting Imbalanced Fermi Gas*, Phys. Rev. Lett. **97**, 030401 (2006); Y. Shin, C. H. Schunck, A. Schirotzek and W. Ketterle, *Phase diagram of a two-component Fermi gas with resonant interactions*, Nature **451**, 689 (2008).

[23] G. B. Partridge, W. Li, R. I. Kamar, Y. Liao and R. G. Hulet, *Pairing and Phase Separation in a Polarized Fermi Gas*, Science **311**, 503 (2006); G. B. Partridge, W. Li, Y. A. Liao, R. G. Hulet, M. Haque and H. T. C. Stoof, *Deformation of a Trapped Fermi Gas with Unequal Spin Populations*, Phys. Rev. Lett. **97**, 190407 (2006).

[24] F. Chevy, *Unitary polarized Fermi gases*, , Proceedings of the International School of Physics Enrico Fermi, Ultracold Fermi gases, Course CLXIV, edited by M. Inguscio, W. Ketterle and C. Salomon (IOS Press, Amsterdam) (2008).

[25] Y. Liao, A. S. C. Rittner, T. Paprotta, W. Li, G. B. Partridge, R. G. Hulet, S. K. Baur and E. J. Mueller, *Spin-imbalance in a one-dimensional Fermi gas*, Nature **467**, 567 (2010).

[26] A. Lüscher, R. M. Noack, and A. M. Läuchli, *The FFLO state in the one-dimensional attractive Hubbard model and its ngerprint in the spatial noise correlations*, Phys. Rev. **A78**, 013637 (2008).

[27] A. T. Sommer, L. W. Cheuk, M. J. H. Ku, W. S. Bakr and M. W. Zwierlein, *Evolution of Fermion Pairing from Three to Two Dimensions*, Phys. Rev. Lett. **108**, 045302 (2012).

[28] B. Fröhlich, M. Feld, E. Vogt, M. Koschorreck, W. Zwerger and M. Köhl, *Radio-Frequency Spectroscopy of a Strongly Interacting Two-Dimensional Fermi Gas*, Phys. Rev. Lett. **106**, 105301 (2011).

[29] E. Wille, F. M. Spiegelhalder, G. Kerner, D. Naik, A. Trenkwalder, G. Hendl, F. Schreck, R. Grimm, T. G. Tiecke, J. T. M. Walraven, S. J. J. M. F. Kokkelmans, E. Tiesinga, and P. S. Julienne, *Exploring*

an Ultracold Fermi-Fermi Mixture: Interspecies Feshbach Resonances and Scattering Properties of ^{6}Li *and* ^{40}K, Phys. Rev. Lett. **100**, 053201 (2008).

[30] P. Castorina, M. Grasso, M. Oertel, M. Urban and D. Zappalà, *Non-standard pairing in asymmetric trapped Fermi gases*, Phys. Rev. **A72**, 025601 (2005).

[31] D. E. Sheehy and L. Radzihovsky, *BEC-BCS Crossover in Magnetized Feshbach-Resonantly Paired Superfluids*, Phys. Rev. Lett. **96**, 060401 (2006).

[32] J. Kinnunen, L. M. Jensen and P. Törmä, *Strongly Interacting Fermi Gases with Density Imbalance*, Phys. Rev. Lett. **96**, 110403 (2006).

[33] K. Machida, T. Mizushima and M. Ichioka, *Generic Phase Diagram of Fermion Superfluids with Population Imbalance*, Phys. Rev. Lett. **97**, 120407 (2006).

[34] K. B. Gubbels, M. W. J. Romans and H. T. C. Stoof, *Sarma Phase in Trapped Unbalanced Fermi Gases*, Phys. Rev. Lett. **97**, 210402 (2006).

[35] P. Pieri and G. C. Strinati, *Trapped Fermions with Density Imbalance in the Bose-Einstein Condensate Limit*, Phys. Rev. Lett. **96**, 150404 (2006).

[36] M. M. Parish, F. M. Marchetti, A. Lamacraft and B. D. Simons, *Finite-temperature phase diagram of a polarized Fermi condensate*, Nature Phys. **3**, 124 (2007).

[37] H. Hu, X.-J. Liu and P. D. Drummond, *Phase Diagram of a Strongly Interacting Polarized Fermi Gas in One Dimension*, Phys. Rev. Lett. **98**, 070403 (2007).

[38] Y. He, C.-C. Chien, Q. Chen and K. Levin, *Single-plane-wave Larkin-Ovchinnikov-Fulde-Ferrell state in BCS-BEC crossover*, Phys. Rev. **A75**, 021602(R) (2007).

[39] E. Gubankova, E. G. Mishchenko, and F. Wilczek, *Breached Superfluidity via p-Wave Coupling*, Phys. Rev. Lett. **94**, 110402 (2005).

[40] T. Koponen, J.-P. Martikainen, J. Kinnunen and P. Törmä, *Fermion pairing with spin-density imbalance in an optical lattice*, New J. Phys. **8**, 179 (2006).

[41] X.-J. Liu, H. Hu, P. D. Drummond, *Fulde-Ferrell-Larkin-Ovchinnikov states in one-dimensional spin-polarized ultracold atomic Fermi gases*, Phys. Rev. **A76**, 043605 (2007).

[42] D. T. Son and M. A. Stephanov, *Phase diagram of a cold polarized Fermi gas*, Phys. Rev. **A74**, 013614 (2006).

[43] G. Orso, *Attractive Fermi Gases with Unequal Spin Population in Highly Elongated Traps*, Phys. Rev. Lett. **98**, 070402 (2007).

[44] X. W. Guan, M. T. Batchelor, C. Lee and M. Bortz, *Phase transitions and pairing signature in strongly attractive Fermi atomic gases*, Phys. Rev. **B76**, 085120 (2007).

[45] F. Chevy, C. Mora, *Ultra-cold polarized Fermi gases*, Report in Rep. Prog. Phys. **73**, 112401 (2010).

[46] D. Jaksch, C. Bruder, J. I. Cirac, C. W. Gardiner, P. Zoller, *Cold Bosonic Atoms in Optical Lattices*, Phys. Rev. Lett. **81**, 2876 (1999).

[47] J. Hubbard, *Electron Correlations in Narrow Energy Bands*, Proc. R. Soc. London, Ser. A **276**, 238-257 (1963).

[48] R. T. Scalettar, *Notes on Hubbard model*, available at http://leopard.physics.ucdavis.edu/rts/michigan/hubbard7.pdf

[49] Z. Bai, W. Chen, R. T. Scalettar, I. Yamazaki, *Lecture Notes on Advances of Numerical Methods for Hubbard Quantum Monte Carlo Simulation*, available at http://www.cs.ucdavis.edu/research/tech-reports/2007/CSE-2007-36.pdf

[50] M. Suzuki, *Relationship between d-Dimensional Quantal Spin Systems and* $(d+1)$*-Dimensional Ising Systems —Equivalence, Critical Exponents and Systematic Approximants of the Partition Function and Spin Correlations*, Prog. Theor. Phys. **56**, 1454-1469 (1976).

[51] S. Sachdev, *Quantum Phase Transitions* (p. 28), Cambridge University Press (1999).

[52] R. T. Scalettar, *How to write a DQMC code*, available at http://leopard.physics.ucdavis.edu/rts/michigan/howto1.pdf

[53] J. E. Hirsch, *Discrete Hubbard-Stratonovich transformation for fermion lattice models*, Phys. Rev. **B28**, 4059-4061 (1983).

[54] J. E. Hirsch, *Erratum: Discrete Hubbard-Stratonovich transformation for fermion lattice models*, Phys. Rev. **B29**, 4159 (1984).

[55] R. Blankenbecker, D. J. Scalapino, and R. L. Sugar, *Monte Carlo calculaitons of coupled Boson-fermion systems I*, Phys. Rev. **D24**, 2278-2286 (1981).

[56] J. E. Hirsch, *Two-dimensional Hubbard model: numerical simulation study*, Phys. Rev. **B31**, 4403-4419 (1985).

[57] S. R. White, D. J. Scalapino, R. L. Sugar, E. Y. Loh, J. E. Gubernatis, and R. T. Scalettar, *Numerical study of the two-dimensional Hubbard model*, Phys. Rev. **B40**, 506 (1989).

[58] H. Gould, J. Tobochnik and W. Christian, *Introduction to Computer Simulation Methods*, Addison-Wesley (2006).

[59] R.T. Scalettar, *Error Analysis in Monte Carlo*, available at http://leopard.physics.ucdavis.edu/rts/michigan/erroranal.pdf

[60] J. E. Hirsch, R. L. Sugar, D. J. Scalapino and R. Blackenbecler, *Monte Carlo simulations of one dimensional fermion systems*, Phys. Rev. **B26**, 5033 (1982).

[61] R.T. Scalettar, *World-Line Quantum Monte Carlo*, published in Quantum Monte Carlo Methods in Physics and Chemistry, M.P. Nightingale and C.J. Umrigar (eds), Kluwer (1999).

[62] A. A. Abrikosov, L. P. Gorkov and I. E. Dzyaloshinski, *Methods of Quantum Field Theory in Statistical Physics* (p.48), Dover Publications (1963).

[63] N. V. Prokof'ev, B. V. Svistunov, I. S. Tsupitsyn, *"Worm" algorithm in quantum Monte Carlo simulations*, Phys. Lett. **A238**, 253-257 (1998).

[64] N. V. Prokof'ev, B. V. Svistunov, I. S. Tsupitsyn, Exact Quantum Monte Carlo Process for the Statistics of Discrete Systems, Sov. Phys. JETP Letters **64**, 911 (1996).

[65] S. M. A. Rombouts, K. Van Houcke, and L. Pollet, *Loop Updates for Quantum Monte Carlo Simulations in the Canonical Ensemble*, Phys. Rev. Lett. **96**, 180603 (2006); K. Van Houcke, S. M. A. Rombouts, and L. Pollet, *Quantum Monte Carlo simulation in the canonical ensemble at finite temperature*, Phys. Rev. **E73**, 056703 (2006).

[66] V. G. Rousseau, *Stochastic Green function algorithm*, Phys. Rev. E **77**, 056705 (2008).

[67] V.G. Rousseau, *Directed update for the stochastic Green function algorithm*, Phys. Rev. E **78**, 056707(2008).

[68] N. Metropolis, A. W. Rosenbluth, M. N. Metropolis, A. H. Teller and E. Teller, *Equation of State Calculations by Fast Computing Machines* , J. Chem. Phys. **21**, 1087 (1953).

[69] T. Giamarchi, *Quantum Physics in One Dimension* (p.160), Oxford University Press (2004).

[70] L. Pollet, PhD Thesis: *Ultracold atoms in an optical lattice: a numerical approach*, available at: http://www.nustruc.ugent.be/doc/thesislode.pdf

[71] M. M. Forbes, E. Gubankova, W. V. Liu and F. Wilczek, *Stability Criteria for Breached-Pair Superfluidity*, Phys. Rev. Lett. **94**, 017001 (2005).

[72] G. G. Batrouni, M. J. Wolak, F. Hébert, V. G. Rousseau, *Pair formation and collapse in imbalanced Fermion populations with unequal masses*, Europhysics Letters **86**, 47006 (2009).

[73] M. J. Wolak, V. G. Rousseau, C. Miniatura, B. Grémaud, R. T. Scalettar and G. G. Batrouni, *Finite temperature QMC study of the one-dimensional polarized Fermi gas*, Phys. Rev. **A82**, 013614 (2010).

[74] M. J. Wolak, B. Grémaud, R. T. Scalettar, and G. G. Batrouni *Pairing in a two-dimensional Fermi gas with population imbalance*, accepted for publication in PRA and available at http://arxiv.org/abs/1206.5050

[75] K. Yang, *Inhomogeneous superconducting state in quasi-one-dimensional systems*, Phys. Rev. **B63**, 140511(R) (2001).

[76] G. G. Batrouni, M. H. Huntley, V. G. Rousseau and R. T. Scalettar, *Exact Numerical Study of Pair Formation with Imbalanced Fermion Populations*, Phys. Rev. Lett. **100**, 116405 (2008).

[77] M. Casula, D. M. Ceperley, and E. J. Mueller, *Quantum Monte Carlo study of one-dimensional trapped fermions with attractive contact interaction*, Phys. Rev. **A78**, 033607 (2008).

[78] A. E. Feiguin and F. Heidrich-Meisner, *Pairing states of a polarized Fermi gas trapped in a one-dimensional optical lattice*, Phys. Rev. **B76**, 220508(R) (2007).

[79] M. Rizzi, M. Polini, M. A. Cazalilla, M. R. Bakhtiari, M. P. Tosi and R. Fazio, *Fulde-Ferrell-Larkin-Ovchinnikov pairing in one-dimensional optical lattices*, Phys. Rev. **B77**, 245105 (2008).

[80] M. Tezuka and M. Ueda, *Density-Matrix Renormalization Group Study of Trapped Imbalanced Fermi Condensates*, Phys. Rev. Lett. **100**, 110403 (2008).

[81] F. Heidrich-Meisner, A. E. Feiguin, U. Schollwöck and W. Zwerger, *BCS-BEC crossover and the disappearance of Fulde-Ferrell-Larkin-Ovchinnikov correlations in a spin-imbalanced one-dimensional Fermi gas*, Phys. Rev. **A 81**, 023629 (2010).

[82] J.C. Pei, J. Dukelsky and W. Nazarewicz, *Competition between normal superfluidity and Larkin-Ovchinnikov phases of polarized Fermi gases in elongated traps*, Phys. Rev. **A82**, 021603(R) (2010).

[83] M. M. Parish, S. K. Baur, E. J. Mueller and D. A. Huse, Phys. Rev. Lett. **106**, 095301 (2011).

[84] D. H. Kim, J. J. Kinunen, J.-P. Martikainen and P. Törmä, *Exotic Superfluid States of Lattice Fermions in Elongated Traps*, Phys. Rev. Lett. **106** 095301 (2011).

[85] M. J. Wolak, V. G. Rousseau, and G. G. Batrouni, *Pairing in population imbalanced Fermion systems*, Computer Physics Communications **182**, 2021 (2011).

[86] X. J. Liu, H. Hu, P. D. Drummond, *Finite-temperature phase diagram of a spin-polarized ultracold Fermi gas in a highly elongated harmonic trap*, Phys. Rev. **A78**, 023601 (2008).

[87] A. M. Clogston, *Upper Limit for the Critical Field in Hard Superconductors*, Phys. Rev. Lett. **9**, 266 (1962).

[88] B. S. Chandrasekhar, *A note on the Maximum Critical Field of High-Field Superconductors*, Appl. Phys. Lett. **1**, 7 (1962).

[89] F. Heidrich-Meisner, G. Orso, A. E. Feiguin, *Phase separation of trapped spin-imbalanced Fermi gases in one-dimensional optical lattices*, Phys. Rev. **A 81**, 053602 (2010).

[90] M. Tezuka and M. Ueda, *Ground states and dynamics of population-imbalanced Fermi condensates in one dimension*, New J. Phys. **12**, 055029 (2010).

[91] T. K. Koponen, T.Paananen, J.-P. Martikainen, M. R.Bakhtiari and P. Törmä, *FFLO state in 1-, 2- and 3-dimensional optical lattices combined with a non-uniform background potential*, New J. Phys. **10**, 045014 (2008).

[92] P. Kakashvili and C. J. Bolech, *Paired states in spin-imbalanced atomic Fermi gases in one dimension*, Phys. Rev. **A79**, 041603(R) (2009).

[93] W. V. Liu, F. Wilczek, *Interior Gap Superfluidity*, Phys. Rev. Lett. **90**, 047002 (2003).

[94] E. Gubankova, W. V. Liu, F. Wilczek, *Breached Pairing Superfluidity: Possible Realization in QCD*, Phys. Rev. Lett. **91**, 032001 (2003).

[95] G. Orso, L. P. Pitaevskii and S. Stringari, *Equilibrium and dynamics of a trapped superfluid Fermi gas with unequal masses*, Phys. Rev. **A77**, 033611 (2008).

[96] G. Orso, E. Burovski and T. Jolicoeur, *Luttinger liquid of trimers in Fermi gases with unequal masses*, Phys. Rev. Lett. **104**, 065301 (2010).

[97] D. E. Sheehy and L. Radzihovsky, *BEC-BCS crossover, phase transitions and phase separation in polarized resonantly-paired superfluids*, Annals of Physics **322**, 1790-1924 (2007).

[98] A. Bulgac and M. M. Forbes, *Unitary Fermi Supersolid: The Larkin-Ovchinnikov Phase*, Phys. Rev. Lett. **101**, 215301 (2008).

[99] L. He and P. Zhuang, *Phase diagram of a cold polarized Fermi gas in two dimensions*, Phys. Rev. **A78**, 033613 (2008).

[100] B. Van Schaeybroeck, A. Lazarides, S. Klimin, J. Tempere, *Trapped Two-Dimensional Fermi Gases with Population Imbalance*, arXiv:0911.0984.

[101] S. M. A. Rombouts, *Unconventional pairing phases in the two-dimensional attractive Hubbard model with population imbalance*, arXiv:0902.1450.

[102] T. N. De Silva, *Population imbalanced Fermi gases in quasi two dimensions*, J. Phys. B: At. Mol. Opt. Phys. **42** 165301 (2009).

[103] Z. Cai, Y. Wang, C. Wu, *Stable Fulde-Ferrell-Larkin-Ovchinnikov pairing states in two-dimensional and three-dimensional optical lattices*, Phys. Rev. **A83**, 063621(2011).

[104] A. E Feiguin and F. Heidrich-Meisner, *Pair Correlations of a Spin-Imbalanced Fermi Gas on Two-Leg Ladders*, Phys. Rev. Lett. **102**, 076403 (2009).

[105] V. J. Emery, *Theory of the quasi-one-dimensional electron gas with strong "on-site" interactions*, Phys. Rev. **B14**, 2989 (1976).

[106] A. Moreo and D. J. Scalapino, *Cold Attractive Spin Polarized Fermi Lattice Gases and the Doped Positive U Hubbard Model*, Phys. Rev. Lett. **98**, 216402 (2007).

[107] M. Iskin, and C. J. Williams, *Population-imbalanced fermions in harmonically trapped optical lattices*, Phys. Rev. **A78**, 011603(R) (2008).

[108] Y. Fujihara, A. Koga, and N. Kawakami, *Superfluid properties of ultracold fermionic atoms in two-dimensional optical lattices*, Phys. Rev. **A81**, 063627 (2010).

[109] B. Grémaud, *Pairing properties of cold fermions in a honeycomb lattice*, Europhys. Lett. **98**, 47003 (2012).

[110] T. Paiva, R. R. dos Santos, R. T. Scalettar and P. J. H. Denteneer, *Critical temperature for the two-dimensional attractive Hubbard model*, Phys. Rev. **B69**, 184501 (2004).

[111] J. Tempere, S. N. Klimin and J. T. Devreese, *Effect of population imbalance on the Berezinskii-Kosterlitz-Thouless phase transition in a superfluid Fermi gas*, Phys. Rev. **A79**, 053637 (2009).

[112] B.-G. Englert, *Lectures on Quantum Mechanics Volume 2: simple systems* (p.129), World Scientific (2006).

[113] M. Rigol, G. G. Batrouni, V. G. Rousseau and R. T. Scalettar, *State diagrams for harmonically trapped bosons in optical lattices*, Physical Review **A79**, 053605 (2009).

[114] G. M. Brunn and K.Burnett, *Interacting Fermi gas in a harmonic trap*, Physical Review **A58**(3), 2427-2434 (1998).

[115] M. Iskin and C. A. R. Sá de Melo, *Mixtures of ultracold fermions with unequal masses*, Phys. Rev. **A76**, 013601 (2007).

[116] Y. Chen, Z. D. Wang, F. C. Zhang, C. S. Ting, *Exploring exotic superfluidity of polarized ultracold fermions in optical lattices*, Phys. Rev. **B79**, 054512 (2009).

[117] J. R. Engelbrecht, M. Randeria, and C.A.R. Sá de Melo, *BCS to Bose crossover: Broken-symmetry state*, Phys. Rev. **B55**, 15153 (1997).

[118] J. Tempere, S. N. Klimin, and J. T. Devreese, *Phase separation in imbalanced fermion superfluids beyond the mean-field approximation*, Phys. Rev. **A78**, 023626 (2008).

[119] A. E. Feiguin, *Spectral properties of a partially spin-polarized one-dimensional Hubbard/Luttinger superfluid*, Phys. Rev. **B79**, 100507 (2009).

[120] A. E. Feiguin and M. P. A. Fisher, *Exotic Paired States with Anisotropic Spin-Dependent Fermi Surfaces*, Phys. Rev. Lett. **103**, 025303 (2009).